Wave-Current Interaction Effects on Large-Volume Bodies in Water of Finite Depth

Dr.ing. Thesis

by

Anne Katrine Bratland
Division of Marine Hydrodynamics
The Norwegian Institute of Technology

December 21, 1995

TH-Trykk 1996

Abstract

A wave-current-body problem is considered. The computer program MULDIF (Zhao and Faltinsen [1989]), which calculates loads and responses on large-volume structures, is extended to include the effect of finite water depth.

A Green's function, satisfying a free surface condition with wave-current interaction and the bottom condition, is developed. Two alternative expressions are established, with satisfactory agreement in a broad range of parameter variations.

The present theory applies to arbitrary bodies. However, to verify our calculations only a restricted, half-immersed sphere is considered. In that case it is possible to compare with existing results (Grue and Biberg [1993]). The agreement is rather good.

To make programs like MULDIF more user-friendly, additional check-routines are necessary. A new way of calculating horizontal wave exciting forces is implemented. When a current is present, this is found to represent an improved check-routine, compared to existing routines which come from calculating wave exciting forces by a generalized Haskind relation, or finding damping coefficients by conservation of energy.

Acknowledgement

My supervisor Professor Odd M. Faltinsen has guided me patiently towards this thesis. He has introduced me to a fascinating field of research, and always encouraged me to overcome unproductive stages. Dr. Rong Zhao has also given invaluable supervision. Especially, he has helped me out on my numerous problems with the computer program MULDIF.

I also thank all my colleagues at NTH and MARINTEK, in particular Dr. Jan Roger Hoff and Dr. Jørgen Krokstad for help regarding numerical computations and MULDIF, respectively.

I am grateful to Dr. Finn Faye Knudsen for explaining to me how to find one of the Green's functions.

Espen Husstad has kindly corrected my English, and managed to stick out with me over these years. Thank you!

The first years of this study were financed by the Norwegian Institute of Technology. The Department of Marine Technology financed large parts of the concluding period of my work. This is most appreciated as the concluding period lasted for a long time.

Contents

Abstract i

Acknowledgement ii

Nomenclature v

1 Introduction 1

2 The Boundary Value Problem 7
- 2.1 Panel method . . . 9
- 2.2 Steady potential . . . 14

3 Wave-current Green's Function and its Multipoles 20
- 3.1 Analytical evaluation of the Green's function . . . 21
  - 3.1.1 Green's function - alternative 1 . . . 21
  - 3.1.2 Green's function - alternative 2 . . . 26
  - 3.1.3 Limiting values for the Green's function . . . 31
- 3.2 Numerical evaluation of the Green's function . . . 35
  - 3.2.1 Alternative 1 . . . 36
  - 3.2.2 Alternative 2 . . . 42
  - 3.2.3 Verification of the Green's function calculations . . . 44

4 Hydrodynamic Forces 53
- 4.1 Linear forces . . . 55
  - 4.1.1 Wave exciting forces . . . 55
  - 4.1.2 Added mass and damping coefficients . . . 65
- 4.2 Mean second order potential . . . 70
- 4.3 Drift forces . . . 71

5 Concluding Remarks 78

Bibliography 80

A Approximating the outer potential by a sum of multipoles inside the body 83

B Details from Chapter 3 86
B.1 Location of the poles far from origo 86
B.2 Residues 88
B.3 Convergence of the infinite series 88
B.4 Integration of the remaining integral 90
B.5 Derivatives 91
B.6 Green's function in terms of non dimensional parameters 94

Nomenclature

$\vec{a}$	Source point, $\vec{a}$ =(a, b, c)
A_{mk}	Added mass coefficients
B_{mk}	Damping coefficients
$\overline{B}_1$	Wave drift damping coefficient in surge
C_c	Water line curve of S_{C_0}
C_{mk}	Restoring matrix
$E(t)$	Time dependent total energy
$factor$	Factor that relates lengths of elements, $\frac{length_{elem.n}}{length_{elem.n+1}} = factor$
$\vec{FF}i$	Multiplication factors of an elements diagonal along the normal vector, $\vec{FF}i = (FF1, FF2, FF3)$
$\mathcal{F}_i$, $i \in \{1,..,6\}$	Linear force in six degrees of freedom, $\mathcal{F}_i = \Re\{F_i e^{i\omega t}\}$
F_i, $i \in \{1,..,6\}$	Complex linear force amplitude in six degrees of freedom, see $\mathcal{F}_i$
$\overline{F}_i$, $i \in \{1,..,6\}$	Drift force in six degrees of freedom
F_n	Froude number, $F_n = \frac{U}{\sqrt{gL}}$ (here $F_n = \frac{U}{\sqrt{gR}}$)
G	Wave/current Green's function, satisfying the bottom condition and the free surface condition far from the body
G_{ST}	Green's function for a steady problem, satisfying the zero-normal-flow condition through both the mean free surface and bottom surface
g	Acceleration of gravity
h	Water depth
i	Imaginary unit, $i = \sqrt{-1}$
$\Im\{z\}$	Imaginary part of z
K	Wave number for incident waves, $\omega_0^2 = Kg \tanh Kh$
L	Characteristic length
l_{elemSc}	Horizontal length of elements on control surface
m_j	Correction terms, see eq. 2.16 and 2.17
M_{mk}	Mass matrix

MULDIF	Computer program developed by Zhao et.al. [1988], and extended to handle the present problem
N_{eff}	Number of elements on the whole wet body surface
$\vec{n}$	Normal vector, pointing out of the fluid
p	Pressure
R	1. Radius of cylinder or sphere 2. Horizontal radius from origo, $x = R\cos v$, $y = R\sin v$
r	Horizontal radius from source point, $x - a = r\cos u$, $y - b = r\sin u$
R_C	Horizontal radius from origo to control surface
$\Re\{z\}$	Real part of z
S	Surface
S_0	Bottom surface in domain I, see figure 2.3
S_B	Body surface
$S_{\overline{B}}$	Mean body surface
S_C	Control surface, see figure 2.3
S_{C_0}	Control surface up to mean free surface
S_F	Free surface between the control surface and body surface, see figure 2.3
$S_{\overline{F}}$	Mean free surface between the control surface and body surface
T	Draught of body
U	Forward speed, current velocity
$\vec{U}$	Current vector
u	Angle, see r
$\vec{V}_B$	Local body velocity
v	Angle, see R
$\vec{X}$	(X, Y, Z) Space fixed coordinates
$\vec{x}$	(x, y, z) Translatory coordinates
z	Complex number
z^*	Complex conjugate of z
α	Current angle
β	Wave propagation angle
γ	Euler's constant, $\gamma = 0.577...$
ϵ	Small positive quantity
ζ	z-position of free surface
ζ_a	Amplitude of the incident wave
$\eta_k, k \in \{1,..,6\}$	Body motions in six degrees of freedom: surge, sway, heave, roll, pitch and yaw, see figure 2.2
λ	Wave length
ρ	Density of water
σ	Source density
τ	Brard number, $\tau = \frac{U\omega}{g}$
τ_{crit}	The largest Brard number when upstream waves exist
Φ	Total velocity potential

Φ_I	Velocity potential for the incident wave, $\Phi_I = \Re\{\phi_0 e^{i\omega t}\}$
Φ_1	First order velocity potential
$\overline{\Phi}_2$	Second order mean velocity potential
$\phi_0 e^{i\omega t}$	Complex velocity potential for the incident wave
$\phi_7 e^{i\omega t}$	Complex diffraction potential
$\phi_k \eta_k, k \in \{1, .., 6\}$	Complex radiation potential
$\phi_k^{II} \eta_k, k \in \{1, .., 7\}$	Complex diffraction and radiation potential in outer domain
ϕ_s	Total steady potential
ϕ_{sb}	Steady disturbance potential
ψ	Green's function for the inner problem, satisfying the bottom condition
$\psi_k \eta_k, k \in \{1, .., 6\}$	Complex radiation potential for reversed current
ω	Frequency of oscillation
ω_0	Frequency for the incident wave

Chapter 1

Introduction

Wave induced motions and loads on off-shore structures can be affected by current as well as finite water depth effects. Some off-shore fields are so shallow that the water depth can be of importance.

The analysis of large volume structures, like semi-submersible type platforms or tension leg platforms are based on a perturbation scheme, where the wave slope is assumed to be small. The lowest order (linear) approximation of an irregular sea is represented by a sum of sinusoidal waves of different amplitudes, periods, phases and propagation directions. Linear responses in irregular sea are obtained by simply adding responses for each wave component. A second order analysis includes non-linear interaction effects between the different frequency components in a linear analysis. This cause so-called sum and difference frequency effects.

The type of motion we want to examine, decide to what order the calculations have to be performed. The excited oscillations are usually divided into wave-frequency motion, high frequency motion and slow-drift motion. In addition the waves induce mean drift motions.

Wave-frequency motions are directly associated to the frequencies of the incident linear waves. Such motions can be described by linear theory. Mean drift forces are obtained by time-averaging body-forces correct to second order. Nevertheless, it turns out that we can use the principle of superposition also for this second order effect.

If we consider the combination of two (or more) incident waves, the sum of their frequencies will induce second order high-frequency motions. Similarly, the difference may induce second order slow-drift motions. If we want to examine slow, horizontal oscillations of moored structures, damping terms have to be calculated. The damping is due to both viscous effects and waves, where the latter is known as wave-drift damping. This is different from the so-called wave radiation damping that is included in a linear analysis. It is a second order effect associated with a structure's ability to create waves. When calculating wave-drift damping the slowly varying velocity of the body is usually interpreted as a quasi-steady speed. In the calculated mean horizontal forces the term proportional to this speed is regarded as damping. So, high-frequency motion and slow-drift motion are both second order quantities, and results in irregular sea include interaction effects.

Let us give some examples: Vertical motions are critical for drilling operations. When designing platforms one therefore tries to keep the resonance period in heave, as well as pitch and roll, far from the period of most waves in the sea. This has resulted in tension leg platforms (TLPs) and semi-submersibles, having very small and very large resonance periods in vertical motions, respectively. Thus, these marine structures are constructed to avoid linear resonance effects. Second order motion may, however, occur. For the TLP, sum-frequency resonance oscillations in heave, pitch and roll may be excited. This phenomenon is known as springing and may lead to fatigue. Slowly-varying and mean horizontal forces and yaw moments are important in design of mooring systems and thruster systems for positioning.

We will here study the effect of incident regular waves with one frequency. As mentioned before, this is sufficient for calculating linear responses, mean forces and wave-drift damping. By using the so-called Newman's relation [1974] we can also approximate slowly varying forces. Although wind may be important in some cases, we will consider loads due to water, only. Extensive discussions of all the above topics may be found in Faltinsen [1990]. Readers searching for more details and thorough explanations are referred to this book.

Even though regular harmonic waves are assumed we are still facing difficulties. The most necessary simplification to be made is given by the assumption of potential flow. For large-volume structures this usually gives good results. However, for bodies with sharp corners which make the flow separate, potential theory may be a limitation. An example of this is the slow-drift motion problem of moored structures. The damping due to viscous effects may then for some structures and conditions be more important than damping due to waves. There also occur important slow-drift viscous damping effects due to the anchor-lines (Huse [1986]).

Application of perturbation analysis, with wave slope as a small parameter, gives the next simplification. The zeroth order term in this series represents the steady flow field due to the forward speed. The steady potential does of course not satisfy the body boundary conditions at an oscillating body surface. Ogilvie and Tuck [1969] overcame this difficulty by introducing correction terms in the next order of the series, the so called m_j-terms.

Large-volume structures are more likely to be exposed to current than actually having forward speed. However, these problems can be considered equal if we assume the current to have constant direction and not to vary with depth.

Two important parameters appear in the wave-current-body problem: The Froude number, $F_n = \frac{U}{\sqrt{gL}}$, and the non-dimensional frequency of oscillation, $\omega\sqrt{\frac{L}{g}}$. Here, U is the steady current velocity, g the acceleration of gravity and L some characteristic length of the body. The product of these parameters gives the Brard number τ ($\tau = \frac{U\omega}{g}$). This number describes whether or not the problem may be solved as a small-speed problem. In this work we limit ourselves to small speed. For infinite water depth it is theoretically known that there are no unsteady wave systems upstream for τ larger than $1/4$. For finite water depth this bound on the Brard number is even less, expressing more clearly the fact that the Froude number should be a small quantity. Zhao and Faltinsen [1988] found in

the two-dimensional, infinite depth case that terms of order U^2 could be neglected in the free surface condition if F_n was less than ≈ 0.1. Physically, this corresponds to neglecting the steady wave systems. A consequence of considering a small Froude number is also that the steady flow problem can be solved as a double body flow problem.

One of the first works in the 3-D numerical boundary element method was carried out by Faltinsen and Michelsen [1974]. Here the Froude number was zero, but water depth was allowed to be finite. To obtain solutions they applied Green's second identity in the whole fluid domain. The Green's function satisfied the free surface condition, bottom condition and a radiation condition. Newman [1967] had earlier presented far field expressions for mean horizontal drift forces and mean yaw moment in the infinite depth case. These expressions were generalized to finite depth. However, only infinite water depth results were published. It should be noted that the drift forces and moments may also be obtained by integrating the pressure to second order over the body. However, this is often a difficult task from a numerical point of view.

Huijsmans and Herman [1985] made, in the slender body case, an early attempt in including the effect of a current. The Green's function was simplified by making a Taylor expansion in τ, and the waves did not interact with the near field steady flow.

For a submerged, 2-D body Grue and Palm [1985] included terms of order U^2 in the free surface condition, implying that their solution is valid for all speeds. The local steady flow does not have to interact with the waves in the case of submerged bodies situated sufficiently far from the free surface (Zhao [1994]).

A fully wave-current interaction solution was presented in Zhao and Faltinsen [1988]. A two-dimensional situation was considered. In the far field the velocity potential was approximated by multipoles inside the body. In the near-field description the flow was represented by Green's second identity and Rankine sources and dipoles. They gave the following conclusions for a 2-D floating body in combined current and waves:

- The waves should interact with the local steady flow around a 2-D surface piercing body.
- Current influences the wave excitation loads more than the added mass and damping coefficients.
- Current influences the mean wave-drift forces.
- Wave-drift damping is important for slow-drift motions for a moored structure, however; viscous effects cannot be neglected for the slow-drift damping.

Later, Zhao et.al. [1988] extended the method to 3-D problems, finding the above conclusions to hold also here. The 3-D solution was based on the same hybrid method. A vertical control surface at some finite distance from the body separated an inner and outer domain. In the outer domain the waves were superposed on the undisturbed current velocity, while in the near field the waves were superposed on the local flow. With this method it was

necessary to discretize three boundaries; the body surface, the control surface and the part of the free surface lying in between. This gives a numerical disadvantage due to the larger equation system of unknowns. However, the major part of the calculations was done with Rankine singularities, representing a numerical advantage compared to applying Green's functions that satisfy the far field boundary conditions. To verify their numerical results Zhao et.al. [1988] made experimental studies, with satisfactory agreement.

A more detailed description of this method was given in Zhao and Faltinsen [1989]. Here, the numerical difficulties concerning the m_j-terms were discussed, and a theoretical way of getting stable results was presented. They also showed that a Taylor expansion in τ of the Green's function could lead to large errors in the generated wave field far from the body.

Nossen et.al. [1991] developed further the idea of Huijsmans and Herman [1985] with power series expansion of τ. They considered a 3-D, infinite fluid volume, with a Kelvin-Havelock type of Green's function; only the body surface and the near field part of the free surface needed to be discretized. The Green's function was not expanded in a Taylor series in the far field. Results were published for the wave-drift damping and compared with Zhao and Faltinsen [1989]. The agreement was generally good. Due to their Taylor expanded Green's function an accurate picture of the wave field far from the body is difficult to achieve.

The study of Nossen et.al. [1991] has been the framework of several extensions. Grue and Palm [1993] developed the mean yaw moment correct to second order, and Grue and Biberg [1993] included finite water depth.

Clark et.al. [1992] presented an expression for wave drift damping as function of the drift force for zero current velocity. They considered a situation of one or several cylinders at infinite water depth. The results agreed remarkable well with existing results when the cylinders were restrained. However, it is interesting to note that they did not give a proof for this expression, and they did not know it's limitations. Later, Grue and Biberg [1993] also found excellent agreement for a restricted cylinder in finite water depth.

Eatock-Taylor and Teng [1993] studied, within potential theory, the effect of sharp corners on a surface piercing, truncated cylinder in waves and current. Their approach was based on Nossen et.al. [1991], but applied a higher order panel method. They discovered that the first order forces, the diagonal terms of added mass and damping coefficients, body motions and the mean drift forces and damping coefficients were rather insensitive to corner radii. On the contrary, the off-diagonal terms of added mass and damping coefficient changed significantly as the corner radius approached zero.

Recently, Prins [1995] attacked the wave-current problem by performing time-domain calculations. His results agreed rather well with existing frequency domain results. However, he seemed to have a problem with the double body flow. This difficulty is also present in our work.

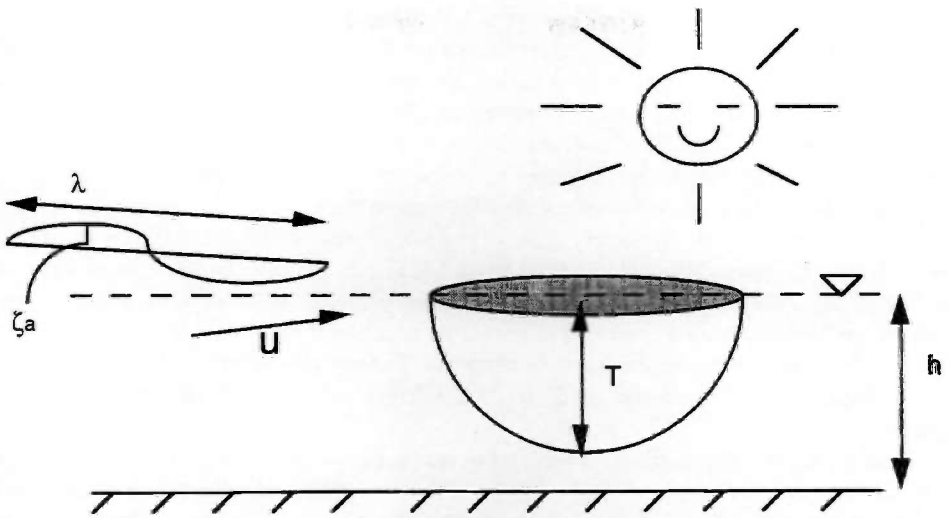

Figure 1.1: *Sketch of the model, which includes current and the incident, sinusoidal wave.*

This work

The scope of this study is to extend the work described in Zhao et.al.[1988] and Zhao and Faltinsen [1989] in order to include the effect of water depth. Two new, independent parameters appear as the water depth becomes finite (see fig. 1.1): body draught-depth ratio, T/h, and wave length-depth ratio, λ/h. The present problem (wave-current-body, finite depth) has so far been studied by Grue and Biberg [1993]. The special case of no current has interested several authors. They all agree on a general tendency that the horizontal drift forces increase as the water depth decreases. For infinite depth the authors find that the horizontal drift forces often increase, when waves and current propagate in the same direction. Thus, it is not surprising that Grue and Biberg [1993] find that the drift forces can increase considerably as the water depth decreases, and current is present. When operating in water of finite depth it is therefore important to achieve prediction of sea loads by finite depth calculations.

In **Chapter 2** the exact *boundary value problem* within potential theory will be formulated. The only difference from the infinite water depth case (Zhao and Faltinsen [1989]) is captured in the claim of no flow through the sea floor. The perturbation process is described and we show how to solve the problem by applying Green's second identity in a finite fluid volume. Outside this volume the flow is approximated by multipoles inside the body. The proof for this model is given in Appendix A. To apply this method the Brard number has to be below its critical value; when upstream waves no longer exist. We will here examine the effect water depth has on the critical Brard number.

In this chapter we also study the *steady potential*, which represents an independent

boundary value problem. We follow the procedure given by Hess and Smith [1962] with Green's function by Newman [1991]. The Hess and Smith procedure implies that the mean wetted body surface is approximated by plane quadrilateral elements and that quantities like source density, dipole and velocity potential are constant over each element. The Rankine sources will be integrated over an element based on Newman's [1986] expression. The convergence (with respect to number of elements) for this method is investigated by comparing the "added mass" coefficients of a sphere with results in Pettersen [1980]. Added mass here means zero frequency limit of the added mass coefficients for an unsteady problem. It can be shown that this added mass value can be calculated in terms of the steady potential. We are going to find that the convergence is slow, producing rather large errors for a reasonable amount of elements on the body. However, the errors do not increase considerably with decreasing water depth. The m_j-terms and the derivatives on the free surface will not be checked here, but we will get an indication of their accuracies in Chapter 4.

In **Chapter 3** the *Green's function* for a wave-current problem is studied. This function, together with its derivatives, represent an approximation of the velocity potential at some distance from the body. The Green's function is initially given as a double integral and the goal is to simplify as much as possible. We may freely choose in what direction to integrate first, and this opens for the opportunity of attacking the problem in two different ways. The development of the Green's function chosen for our purpose is based on a general idea of Knudsen [1992]. However, we first try another way around by developing a method which involves Mittag-Lefflers theorem from complex analysis. This theorem is used in order to increase speed of convergence. Although this method is not successful here, we hope that it might be applicable to other cases.

Explicit expressions for limiting values are also established, and the derivatives are calculated to sixth order. The details from the calculations in this chapter are put in Appendix B.

Resulting *sea loads* in finite water depth are discussed in **Chapter 4**. We present the expressions for wave exciting forces, added mass and damping coefficients, horizontal drift forces and wave-drift damping. A floating sphere is our test example. Then the difficulties concerning sharp corners are avoided. Besides, this was also one of the examples in Grue and Biberg [1993], so we can compare some of the results. We try to achieve the results in several ways, often by the aid of Green's theorem. In this way we both get a check of the computer code, and a better understanding of which parameters that cause problems. We will see that the m_j-terms represent a large problem and that the diagonal damping coefficients are too robust to be the only objects of check-routines for the program. A new way of writing the horizontal wave exciting forces, whithout including derivatives on the body surface, is implemented. In this way a check of the m_j-terms is performed. Errors due to m_j-terms are not detected by applying the generalized Haskind relation, nor by comparing damping terms for zero and non-zero speed.

Finally, we compare the formula of Clark et.al. [1992] with our wave-drift damping results. Although we do not find full agreement this simple formula represents a good estimate.

Chapter 2

The Boundary Value Problem

Consider a freely floating structure in horizontal, steady motion, exposed to incident waves. A right handed, space fixed coordinate system, denoted (X, Y, Z), has the positive Z-axis upwards, and origo at the mean free surface. The translatory coordinate system (having speed $\vec{U} = (U_x, U_y)$), with origo in the center of the structure, may then be written $(x, y, z) = (X + U_x t, Y + U_y t, Z)$. This is illustrated in figure 2.1.

A mathematically identical problem case arise from a structure located in waves and exposed to a current, only the current direction is opposite the velocity direction of the structure. For the present problem $\vec{U} = U(\cos\alpha\vec{i} + \sin\alpha\vec{j})$ is defined as the undisturbed current vector. Here, α is the angle between the current direction and the positive x-axis, and $\vec{i}$ and $\vec{j}$ are the unit vectors along the x an y direction, respectively.

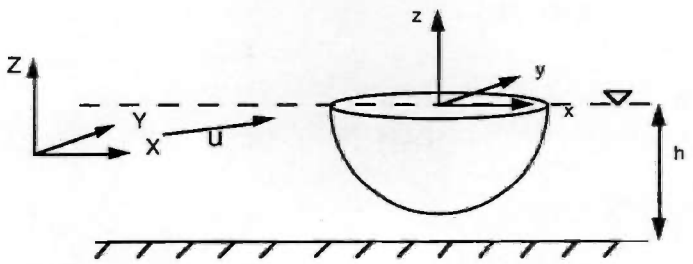

Figure 2.1: *Coordinate definitions.*

For large volume structures the natural assumptions are those of irrotational flow and incompressible fluid. Thus, a time dependent velocity potential, Φ, exists, satisfying the Laplace equation, $\nabla^2\Phi = 0$.

The incident wave potential refers to the translating coordinate system and may be written

$$\Phi_I = \Re\{\phi_0 e^{i\omega t}\} = \Re\{\frac{g\zeta_a}{\omega_0}\frac{\cosh K(z+h)}{\cosh Kh}e^{i[\omega t - K(x\cos\beta + y\sin\beta)]}\}. \tag{2.1}$$

The wave amplitude, ζ_a, the wave number K, and the circular frequency of oscillation, ω_0, refer to the space fixed coordinate system, while the wave propagation angle, β, is related to the positive x-axis. The imaginary unit is denoted i and t is a time unit. $\Re$ means the real part.

The wave number is related to the frequency of oscillation and water depth, h, by the dispersion relation for linear gravity waves:

$$\omega_0^2 = Kg \tanh Kh, \tag{2.2}$$

and the frequency of encounter, ω, is given by the equation

$$\omega = \omega_0 + UK \cos(\beta - \alpha). \tag{2.3}$$

Boundary conditions

By assuming a constant atmospheric pressure the combined kinematic and dynamic non-linear free surface condition can be written as

$$\frac{\partial^2 \Phi}{\partial t^2} + g\frac{\partial \Phi}{\partial z} + 2\nabla\Phi \cdot \frac{\partial}{\partial t}\nabla\Phi + \frac{1}{2}\nabla\Phi \cdot \nabla(\nabla\Phi \cdot \nabla\Phi) = 0, \tag{2.4}$$

on the free surface, ζ, given by

$$\zeta = -\frac{1}{g}\left(\frac{\partial \Phi}{\partial t} + \frac{1}{2}\nabla\Phi \cdot \nabla\Phi\right). \tag{2.5}$$

More details may for instance be found in Newman [1978].

At the instantaneous body surface the normal velocity of the body equals that of the adjacent fluid. This is expressed as

$$\vec{V}_B \cdot \vec{n} = \nabla\Phi \cdot \vec{n}, \tag{2.6}$$

where $\vec{V}_B$ is the local body velocity and $\vec{n}$ a time dependent normal vector.

In addition, a zero flow condition through the sea floor must be imposed. For horizontal sea bottom this is written as

$$\frac{\partial \Phi}{\partial z} = 0 \qquad \text{for } z = -h. \tag{2.7}$$

If the problem is solved in the time domain, initial conditions are needed. We are later going to operate in the frequency domain. Then, radiation conditions are needed.

2.1 Panel method

The following method is an extension of Zhao and Faltinsens [1989] work. They analyzed the combined current-wave interaction on large 3-D structures, floating in deep water. Here, the water depth is allowed to be finite, only introducing the depth as an additional parameter.

The body is restrained from drifting, but free to oscillate in six degrees of freedom. The (x, y, z)-coordinate system refers to a body at rest. The amplitudes of the incident wave and body motions are assumed small, relative to both body dimensions and wave length of the incident waves. Also the current velocity, U, is small, so that both the Brard number, $\tau = \frac{\omega U}{g}$, and the Froude number, $F_n = \frac{U}{\sqrt{gL}}$, can be considered small. Here, L is a characteristic length of the body.

Next, the potential flow solution will be written as a series expansion in wave amplitude:

$$\Phi = \underbrace{\phi_s}_{\sim(\zeta_a)^0} + \underbrace{\Phi_1}_{\sim(\zeta_a)^1} + \underbrace{\Phi_2}_{\sim(\zeta_a)^2} + \cdots \tag{2.8}$$

Here ϕ_s represents the steady state disturbed current potential. Far from the body, ϕ_s is asymptotically given as

$$\phi_s = U(x \cos\alpha + y \sin\alpha). \tag{2.9}$$

The object of this work is to solve the problem correct to $\mathcal{O}(U)$. A consequence of neglecting terms of $\mathcal{O}(U^2)$, is that the steady wave system is neglected.

Correct to first order in current velocity, the steady potential then satisfies the rigid wall condition, $\frac{\partial \phi_s}{\partial z} = 0$, at the mean free surface. In addition, the steady potential satisfies the zero flow condition through the mean body surface and - through the sea floor. This particular boundary value problem is discussed in the next section.

The first order potential, Φ_1, can be decomposed into potentials due to incident and reflected waves and wave systems created by body motions,

$$\Phi_1 = \Re\{\phi_0 e^{i\omega t} + \phi_7 e^{i\omega t} + \sum_{k=1}^{6} \phi_k \eta_k\}. \tag{2.10}$$

The body motions, η_k, are defined in figure 2.2. We have now assumed steady state solutions to the problem (we are in the frequency domain).

Writing the velocity potential as in 2.8 and 2.10, and keeping terms to first order both in wave amplitude and current velocity, the free surface condition 2.4 gives the following conditions for ϕ_k, $k \in \{1, .., 6\}$ and $(\phi_0 + \phi_7)$:

$$-\omega^2 \phi_k + 2i\omega \nabla\phi_s \cdot \nabla\phi_k + i\omega \left(\frac{\partial^2 \phi_s}{\partial x^2} + \frac{\partial^2 \phi_s}{\partial y^2} \right) \phi_k + g \frac{\partial \phi_k}{\partial z} = 0 \qquad z = 0. \tag{2.11}$$

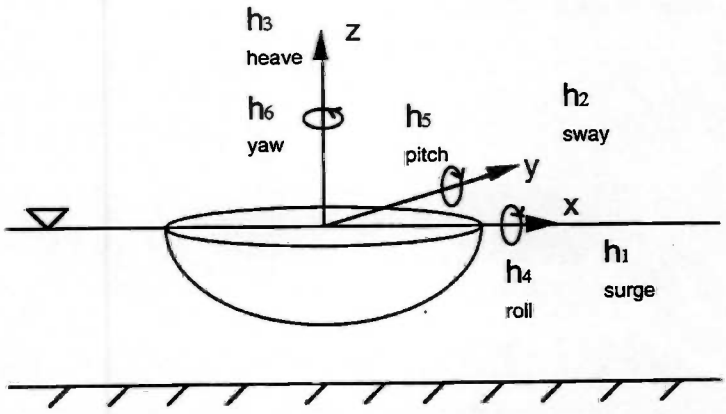

Figure 2.2: *Body motion definition*

Details can be found by using expressions presented by Newman [1978], and neglecting terms of order U^2.

Next, the fluid is separated into two domains, as illustrated in figure 2.3. In the inner domain, ϕ_k should satisfy the free surface condition 2.11, while in the outer domain, where the steady potential is assumed to be undisturbed by the body all ϕ_k may satisfy the simpler free surface condition

$$-\omega^2\phi_k + 2i\omega U(\cos\alpha\frac{\partial\phi_k}{\partial x} + \sin\alpha\frac{\partial\phi_k}{\partial y}) + g\frac{\partial\phi_k}{\partial z} = 0 \qquad z = 0. \tag{2.12}$$

Applied on the mean body surface, the linear body boundary conditions are written

$$\frac{\partial\phi_k}{\partial n} = \begin{cases} i\omega n_k + m_k & , k \in \{1,\ldots,6\} \\ -\frac{\partial\phi_0}{\partial n} & , k = 7. \end{cases} \tag{2.13}$$

The m_k-terms arise because the steady potential satisfies the zero normal flow condition at the mean body surface, producing an error of order ζ_a. The n_k- and m_k-components are according to Ogilvie and Tuck [1969] defined by

$$(n_1, n_2, n_3) = \vec{n} \tag{2.14}$$
$$(n_4, n_5, n_6) = \vec{r}\times\vec{n} \tag{2.15}$$
$$(m_1, m_2, m_3) = -\vec{n}\cdot\nabla\nabla\phi_s \tag{2.16}$$
$$(m_4, m_5, m_6) = -\vec{n}\cdot\nabla\vec{r}\times\nabla\phi_s, \tag{2.17}$$

where $\vec{r} = x\vec{i} + y\vec{j} + z\vec{k}$.

Each component should also satisfy the zero-normal-flow condition through the sea bottom;

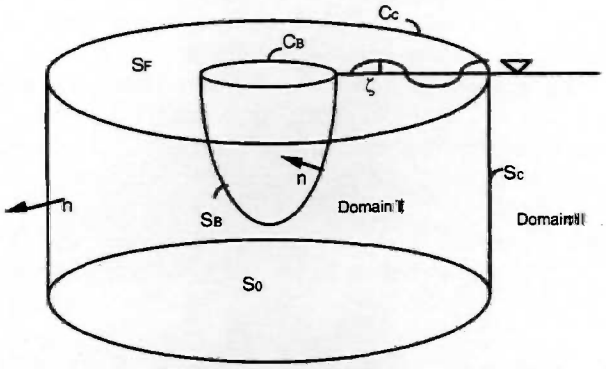

Figure 2.3: *Surface and domain definition. The inner domain is enclosed by a control surface, S_C, the body surface, S_B, and the part of the free surface and bottom surface that are inside the control surface, S_F and S_0. The normal vector, $\vec{n}$, is pointing out of this fluid volume.*

$$\frac{\partial \phi_k}{\partial z} = 0 \qquad \text{for } z = -h. \tag{2.18}$$

In order to get unique solutions, radiation conditions for the body-generated wave system has to be imposed. This can mathematically be done by introducing a fictitious Rayleigh viscosity (see Ogilvie and Tuck [1969]), which implies in our problem that there exists no incident wave system generated by the body.

In the outer domain, ϕ_k may be written as a sum of multipoles, with singularities inside the body (see appendix A),

$$\phi_k^{II} = \sum_{l=1}^{L} \sum_{m=1}^{M} A_{lm} G^l(\vec{x}; \vec{a}_m), \qquad k \in \{1, .., 7\} \tag{2.19}$$

where $G(\vec{x}; \vec{a}_m)$ is the Green's function evaluated in chapter 3. $G^l(\vec{x}; \vec{a}_m)$ denotes all possible combinations of derivatives of l'th order with respect to the three source point coordinates, $\vec{a}_m = (a, b, c)_m$. A_{lm} are constants and M denotes number of singularities inside the body. ϕ_k^{II} satisfies the free surface condition 2.12, the bottom condition and a radiation condition.

A solution to the boundary value problems can be found by applying Green's second identity to ϕ_k and a Green's function, ψ, to a fluid domain enclosed by the surface $S = S_F \cup S_B \cup S_C \cup S_0$ (See fig. 2.3). To linear theory this looks like

$$4\pi \phi_k(x_0, y_0, z_0) = \iint_{S_{\overline{F}} + S_{\overline{B}} + S_{C_o}} (\phi_k \frac{\partial \psi}{\partial n} - \psi \frac{\partial \phi_k}{\partial n}) ds, \tag{2.20}$$

where $S_{\overline{F}}$ denotes the mean free surface between the mean body surface, $S_{\overline{B}}$, and the control surface. S_{C_o} is the control surface up to the mean free surface. The Green's

function for the inner problem is chosen as $\psi = [(x-x_0)^2+(y-y_0)^2+(z-z_0)^2]^{-1/2} + [(x-x_0)^2+(y-y_0)^2+(2h+z+z_0)^2]^{-1/2}$. In this way, the integral over the sea floor, S_0, vanishes. In the numerical solution $S_{\overline{F}}$, $S_{\overline{B}}$ and S_{C_0} are divided into plane quadrilateral elements and the velocity potential and its normal derivative are assumed to be constant over each element. Letting $\vec{x}_0$ in equation 2.20 approach the midpoint of every element on the surfaces, a Fredholm integral equation is established. Matching the inner and outer solution at the control surface, a sufficient number of equations are established for solving the ϕ_k-problem.

Having obtained ϕ_k, we can find the wave exciting loads and the added mass and damping coefficients. The wave exciting forces are $\mathcal{F}_m = \Re\{F_m e^{i\omega t}\}$, where F_m are given by

$$F_m = -\rho \iint_{S_{\overline{B}}} [i\omega(\phi_0+\phi_7) + \nabla\phi_s \cdot \nabla(\phi_0+\phi_7)] n_m ds \qquad m \in \{1,..,6\} \tag{2.21}$$

and the added mass and damping coefficients are written

$$A_{mk} = \Re\{F_{mk}\}/\omega^2 \tag{2.22}$$

$$B_{mk} = -\Im\{F_{mk}\}/\omega, \tag{2.23}$$

where

$$F_{mk} = -\rho \iint_{S_{\overline{B}}} (i\omega\phi_k + \nabla\phi_s \cdot \nabla\phi_k) n_m ds. \tag{2.24}$$

Finally, we find the first order motions by solving the equations of motion,

$$\sum_{k=1}^{6} [(M_{mk}+A_{mk})\ddot{\eta}_k + B_{mk}\dot{\eta}_k + C_{mk}\eta_k] = F_m e^{i\omega t}, \tag{2.25}$$

and the first order potential is determined.
In the above equation M_{mk} and C_{mk} is the mass matrix and the restoring matrix, respectively. The restoring matrix follows from hydrostatic - and mass considerations. Expressions for M_{mk} and C_{mk} may be found in Faltinsen and Michelsen [1974].

The parameter $\tau = \frac{U\omega}{g}$, which is the product of the non-dimensional frequency, $\omega\sqrt{\frac{L}{g}}$, and the Froude number, is a common parameter to use in the wave-current-body interaction problems. For infinite water depth it is known that important changes occur at $\tau = \frac{1}{4}$. For τ larger than $\frac{1}{4}$ there are no body-generated upstream wave systems. Our solution procedure does not apply when $\tau > \frac{1}{4}$ because we have implicitly assumed body-generated waves all around the body. For finite water depth the critical τ-value is not as easy to give.

The following way of establishing τ_{crit} for finite water depth was suggested by Børresen [1984]:
$\phi_k \sim \frac{\cosh k(z+h)}{\cosh kh} e^{i[\omega t - k(x\cos(\alpha+\pi)+y\sin(\alpha+\pi))]}$ is assumed to represent body-generated waves far from the body, propagating along the negative current axis. By linearizing the free surface condition 2.4 to the mean free surface and keeping terms to first order in wave amplitude,

we get a free surface condition valid for all current velocities. We insert the assumed potential in order to decide the wave numbers k. This means there exist body-generated waves upstream as long as

$$-\omega^2 - 2k\omega U - U^2k^2 + gk \tanh kh = 0 \tag{2.26}$$

has real, positive solutions. The reason why they have to be real and positive lies in the formulation of the assumed potential.

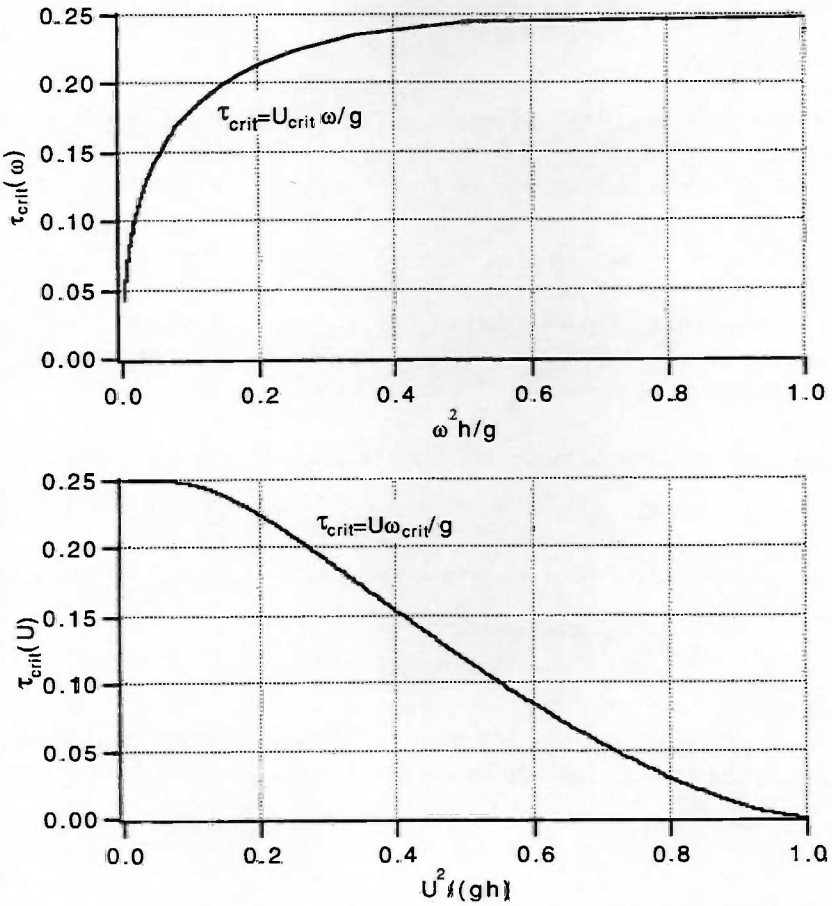

Figure 2.4: *Critical τ-value for finite water depth.*

The dependency of water depth for the critical τ-value is shown in figure 2.4. The figures are obtained by numerically increasing the current velocity and frequency, respectively,

until eq. 2.26 fails to give solution. We have ensured that the two wave numbers tend to the same limit before vanishing, thus producing the same curves for τ_{crit}, and that the two curves agree. We have also ensured, as pointed out by Børresen [1984], that the non-dimensional magnitude of $\frac{d}{dk}\left(\tanh kh - \frac{1}{gk}(\omega + Uk)^2\right)$ is close to zero at the point where the wave numbers coincide.

2.2 Steady potential

The steady potential will be written as a sum of disturbed and undisturbed potential,

$$\phi_s = U(x\cos\alpha + y\sin\alpha) + \phi_{sb}. \tag{2.27}$$

Here ϕ_{sb} satisfies the Laplace equation, and correct to $\mathcal{O}(U)$, ϕ_{sb} also fulfills the following boundary conditions:

The flow through the free surface and the sea floor is zero,

$$\frac{\partial \phi_{sb}}{\partial z} = 0, \qquad z = 0 \text{ and } z = -h, \tag{2.28}$$

there is no total velocity through the body surface,

$$\frac{\partial \phi_{sb}}{\partial n} = -U(n_1\cos\alpha + n_2\sin\alpha) = -\vec{U}\cdot\vec{n}, \tag{2.29}$$

and the disturbance potential should vanish far from the body

$$\phi_{sb} \to 0, \qquad \text{as } x^2 + y^2 \to \infty. \tag{2.30}$$

The solution to this boundary value problem is found by distributing sources on the body surface,

$$\phi_{sb} = \iint_{S_B} \sigma G_{ST}\, ds. \tag{2.31}$$

Here, σ is the source strength and G_{ST} is a Green's function satisfying the boundary conditions, except at the body surface. Newman [1991] calculated the Green's function according to

$$G_{ST} = L(r, z - z_0) + L(r, z + z_0) \tag{2.32}$$

where $r = \sqrt{(x - x_0)^2 + (y - y_0)^2}$ and

$$L(r,z) = \frac{1}{\sqrt{r^2 + z^2}} + \sum_{n=1}^{\infty}\left[\frac{1}{\sqrt{r^2 + (2nh - z)^2}} + \frac{1}{\sqrt{r^2 + (2nh + z)^2}} - \frac{1}{nh}\right]. \tag{2.33}$$

Since the above infinite sum is known to converge slowly, he actually rewrote equation 2.33 in two alternative ways, procedures which are also used in this work.

In the numerical procedure the surface is divided into plane quadrilateral surfaces with constant source strength over each element. The six first terms in the Green's function are integrated exactly over an element (according to Newman [1986]), whereas for the remaining part the mid point approximation has been applied. This means that the boundary condition 2.29 is written

$$\sum_{j=1}^{N_B} \sigma_j \left(\iint_{S_{\overline{B}_j}} G_{CL}^{ij} \cdot \vec{n}^i ds + S_{\overline{B}_j} (G_{ST}^{ij} - G_{CL}^{ij}) \cdot \vec{n}^i \right) = \vec{V}_s \cdot \vec{n}^i, \quad i = 1, N_B, \tag{2.34}$$

where N_B is the number of elements on the body,

$$G_{CL}^{ij} = \sum_{\substack{z = z_i - z_j \\ z = z_i + z_j}} \frac{1}{\sqrt{r_{ij}^2 + z^2}} + \frac{1}{\sqrt{r_{ij}^2 + (z - 2h)^2}} + \frac{1}{\sqrt{r_{ij}^2 + (z + 2h)^2}} \tag{2.35}$$

and $r_{ij} = \sqrt{(x_i - x_j)^2 + (y_i - y_j)^2}$ where $\vec{x}_i = (x_i, y_i, z_i)$ denotes the midpoint of element i.

In addition to the steady potential itself, it is important to achieve its derivatives up to second order both on the free surface and on the body surface. At the free surface the derivatives are obtained by applying potentials at adjacent elements. The second order derivatives at the body surface are needed in the so called m_j-terms. These terms are known to be difficult to compute numerically (discussed in Zhao and Faltinsen [1989]). Because the potential is constant over an element the tangential velocities are implicitly said to be zero. Thus, the derivatives cannot be found directly at or in the vicinity of the surfaces. In MULDIF, the m_j-terms are calculated by first evaluating the potential at three distinct points along the normal vector. To achieve second order derivatives here, the steady potential is also evaluated at some small distances around these points. The derived values are then extrapolated back to the body surface (see fig. 2.5).

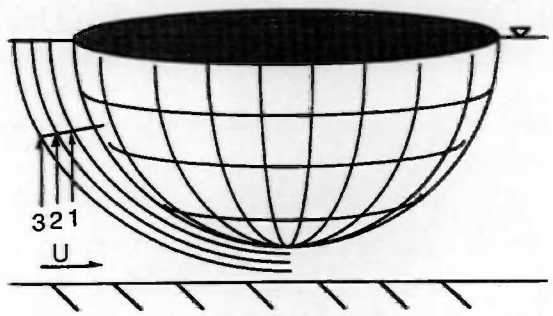

Figure 2.5: *Explanation of m_j-calculation.*

To achieve reasonable results, the differentiation has to be carried out at approximately twice the length of the element. We choose to differentiate at 2.0, 2.2 and 2.4 times the element diagonal length, respectively ($\vec{FFi} = (2.0, 2.2, 2.4)$). For the part of the body surface that is close to the sea floor, we therefore have to distribute small elements. This is because the current varies rapidly here, and because we want to avoid differentiating far below the sea floor. Examples of successful and unsuccessful m_j-calculation are illustrated in figure 2.6. We have tried to show that it might be all right to differentiate below the sea floor in some cases, and that rapid variation of the derivatives implies larger sensitivity to both $\vec{FFi}$ and length of elements.

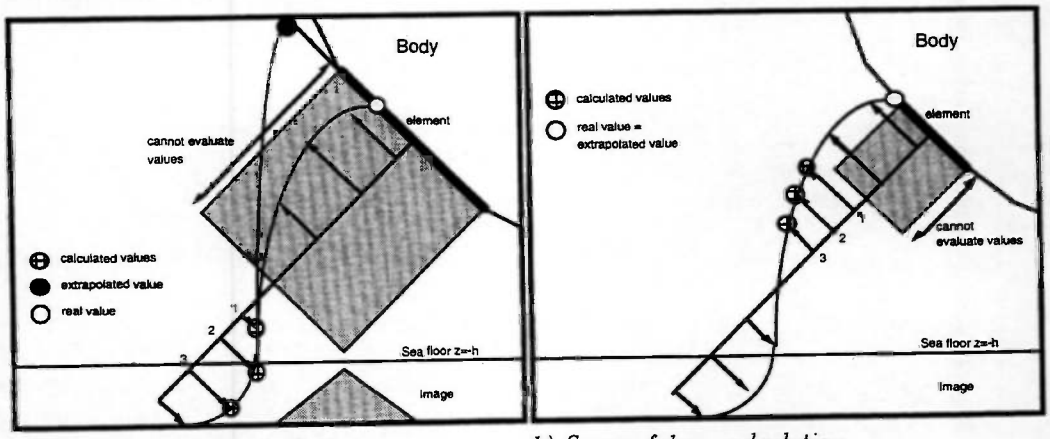

a) Unsuccessful m_j-calculation; too large element or too large $\vec{FFi}$.

b) Successful m_j-calculation.

Figure 2.6: *Possible difficulties when calculating m_j-terms. Note that the drawn m_j-values are only speculations.*

Similar problems of course also appear in infinite water depth, for instance when two cylinders are close to each other.

At sharp corners the m_j-terms are singular. The difficulties associated with corners are discussed in Zhao and Faltinsen [1989].

We will here do a check of the potential only, represented by the limit of the zero current added mass coefficients for an unsteady problem as the frequency tends to zero. It can be shown that this can be written in terms of the steady potential. Following Pettersen [1980] these added mass coefficients are given as

$$A_{ij} = \rho \frac{1}{U^2} \iint_{S_B} \phi^i_{sb} \frac{\partial \phi^j_{sb}}{\partial n} ds. \tag{2.36}$$

The convergence as a function of number of elements on the body is rather slow. This is demonstrated in figure 2.7. N_{eff} here means number of elements on the body surface (half the sphere). We have investigated two different element distributions, one with small

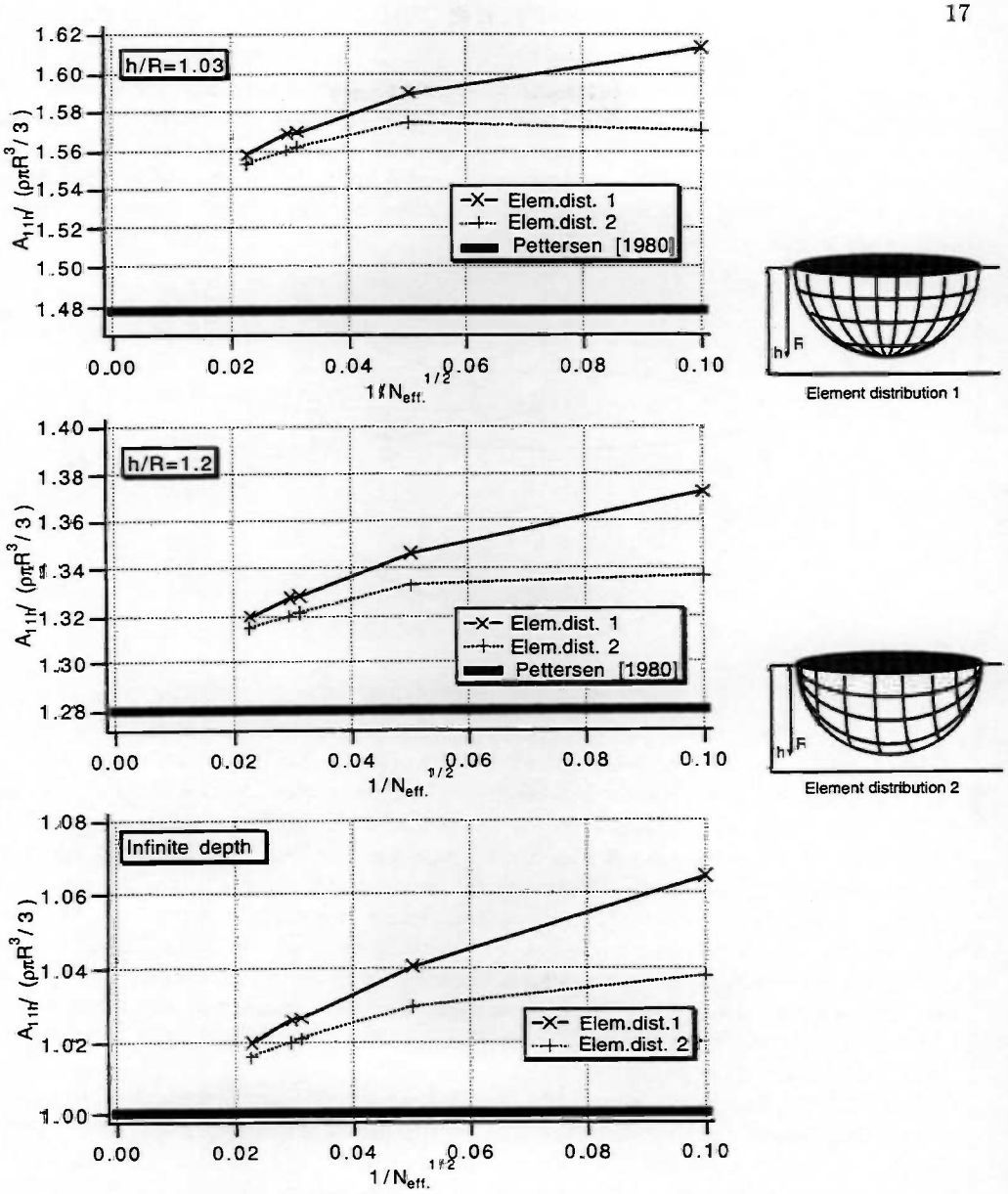

Figure 2.7: *Convergence of surge added mass in finite water vs. effective elements on a half-sphere. The thick lines (finite-depth results from Pettersen [1980] or the well known infinite depth result) are not functions of elements.*

elements against the current and the other with small elements against the sea floor. In both cases we have drawn the lines surrounding the elements with constant and equal angular spacing, both horizontally and vertically. The angles are explained in figure 2.8. These distributions give results tending to the same limit, but if the highest number of tested elements is used ($N_{eff} = 1936$) the error relative to the converged values by Pettersen [1980] is up to 5%.

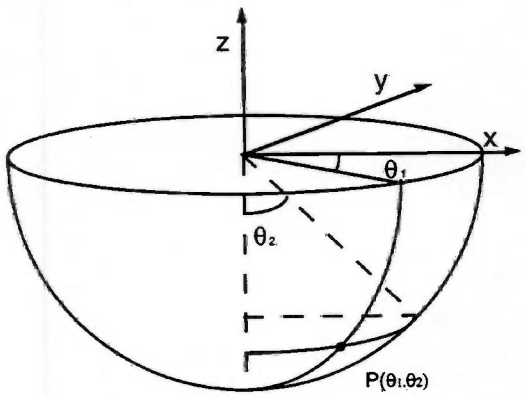

Figure 2.8: *Angle definition.*

Hess and Smith [1962] presented results for the velocity distribution on a sphere in deep water. The agreement with analytical results seemed perfect for 2160 elements on the body surface. They used "element distribution 1" (which causes faster convergence, see fig 2.7) with the small elements against the current axis and they satisfied the body boundary condition on the null point of each element (as opposed to our geometrical mid point). By null point means the point on the quadrilateral element where the distribution of constant sources induces zero tangential velocity. For practical purposes we cannot afford to apply this amount of elements, and we will have to choose "element distribution 2" with smaller elements against the sea floor. Thus, we expect inaccurate results caused by this routine. It should also be noted that the error in calculating the m_j-terms is likely to be larger than in the calculation of the added mass.

In section 4.1.2 we are going to find the added mass coefficients for an unsteady problem by applying Green's second identity. The results presented in figure 4.11 indicate that distributing both sources and dipoles over the body surface may produce faster convergence than just sources. We assume that the results from Pettersen [1980] and Mavrakos [1981] represent correct values (the infinite depth result in fig. 2.7 is indeed correct). Then, for 1156 elements the errors in fig. 2.7 are approximately 2.5%, 4% and 6% for $h/R = \infty$, 1.2 and 1.03, respectively, while the error presented in fig. 4.11 is approximately 2% for $h/R = 1.5$. Due to additional error sources in an unsteady problem we expected this added mass coefficient to be less accurate. For the infinite depth results we have used a standard routine, so the possibility for bugs in our computer code is small.

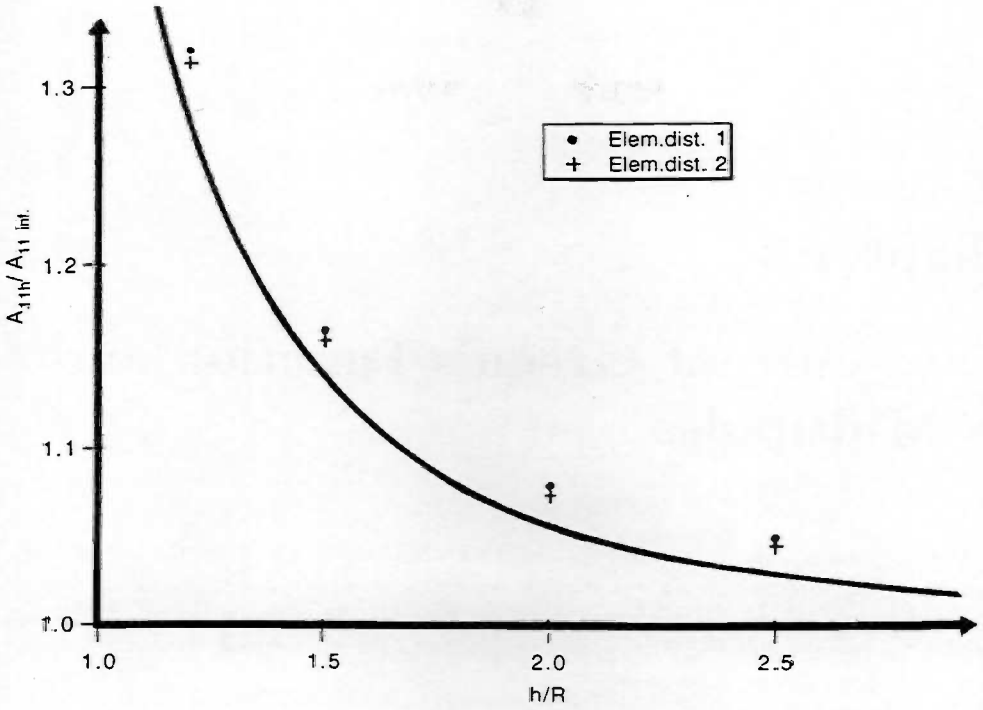

Figure 2.9: *Surge added mass in finite water for a half immersed sphere. 1936 effective elements on the body. The solid line is due to Pettersen [1980] ($N_{eff} = N_B$ =number of elements on the wet body surface).*

In figure 2.9 the same added mass coefficients are shown as function of water depth. Compared to the results from Pettersen [1980] it seems like a systematic error occurs.

We may have to look for improved methods to calculate the steady potential. Hiren [1995] has recently presented a higher order panel method that looks promising.

Chapter 3

Wave-current Green's Function and its Multipoles

The velocity potential of a harmonically pulsating source, traveling beneath the free surface with speed $\vec{V} = -U(\cos\alpha\vec{i} + \sin\alpha\vec{j})$, may be written $\phi = \Re\{AG(\vec{x},\vec{a})e^{i\omega t}\}$. Here, A is a constant, t a time unit, ω the frequency of pulsation and G the so called Green's function. $\vec{a}$ denotes the source point and $\vec{x}$ the point of evaluation. For small speed, terms containing U^2 are neglected in all calculations.

Thus, G should satisfy

(i) the Laplace equation outside the singular point,

$$\nabla^2 G = 0 \qquad (x,y,z) \neq (a,b,c), \tag{3.1}$$

(ii) the free surface condition (z=0):

$$\omega^2 G - g\frac{\partial G}{\partial z} - 2i\omega U(\cos\alpha\frac{\partial G}{\partial x} + \sin\alpha\frac{\partial G}{\partial y}) - \mu\left[i\omega G + U(\cos\alpha\frac{\partial G}{\partial x} + \sin\alpha\frac{\partial G}{\partial y})\right] = 0 \tag{3.2}$$

and

(iii) the bottom condition:

$$\frac{\partial G}{\partial z} = 0 \qquad z = -h. \tag{3.3}$$

The radiation condition is here implemented in the free surface condition by introducing an artificial viscosity, μ (often called the Rayleigh viscosity). Now the complex conjugate of the Green's function that we seek no longer satisfies the above equations. Having fulfilled its mission μ is set to zero. Equation 3.2 results from starting the development of the free surface calculations from Eulers equation rather than from Bernoullis equation. In Eulers equation an artificial pressure variation term is included, $\mu\rho\nabla[Ux\cos\alpha + Uy\sin\alpha y + AG(\vec{x},\vec{a})e^{i\omega t}]$. A proof for this device, in a steady case, is presented in Lamb [1945]. Although widely used, other authors are not too thrilled about it, as expressed by Ogilvie and Tuck [1969]: "This device is extremely convenient, which is about all that justifies its use".

Now, writing G as

$$G = \frac{1}{\sqrt{r^2+(z-c)^2}} + \frac{1}{\sqrt{r^2+(z+c+2h)^2}} + G_1,$$

G_1 is, after Fourier transforming the above equations, found to satisfy

$$G_1 = \frac{1}{\pi}\int_0^{2\pi}\int_0^{\infty} \frac{e^{ikr\cos(\theta-u+\alpha)}e^{-kh}\cosh k(z+h)\cosh k(c+h)[k(1+2\tau\cos\theta)+\nu]}{k\sinh kh - [\nu+2\tau\cos\theta k - \overline{\mu}i(\nu+\tau k\cos\theta)]\cosh kh} dk d\theta. \quad (3.4)$$

Here $x-a = r\cos u$ and $y-b = r\sin u$. The parameters $\tau = \frac{U\omega}{g}$ and $\nu = \frac{\omega^2}{g}$ have been introduced. $\overline{\mu} = \frac{\mu}{\omega}$ is the non-dimensional Rayleigh viscosity.

3.1 Analytical evaluation of the Green's function

In this section the Green's function will be evaluated analytically in two different ways: First we integrate eq. 3.4 in k-direction, leaving us with a θ-integral. Quite naturally, in the second approach, we merely reverse the order of integration. Eventually the limiting expressions are established.

3.1.1 Green's function - alternative 1

As a first alternative we will evaluate G_1 by first integrating in k. A similar technique as John [1950] used in the zero speed case will be applied. We write G_1 (eq. 3.4) as

$$G_1 = \frac{1}{2\pi}\int_0^{2\pi}\int_0^{\infty}[e^{kc}+e^{-k(2h+c)}]e^{ikr\cos(\theta-u+\alpha)}p(k,\theta)dkd\theta, \quad (3.5)$$

where

$$p(k,\theta) = \frac{\cosh k(z+h)[k(1+2\tau\cos\theta)+\nu]}{k\sinh kh - [\nu+2\tau k\cos\theta - \overline{\mu}i(1+\tau k\cos\theta)]\cosh kh}. \quad (3.6)$$

We will regard k as a complex parameter. Then $p(k,\theta)$ has an infinite number of simple poles, c_n, in the complex plane, all given by the equation

$$[\nu+2\tau\cos\theta c_n - \overline{\mu}i(1+\tau\cos\theta c_n)]\cosh c_n h = c_n \sinh c_n h. \quad (3.7)$$

Figure 3.1 shows the location of the poles for $\theta = 0$ and $\theta = \frac{\pi}{2}$ for a special case. The real positive and negative pole is called c_{0+} and c_{0-}, respectively. By applying the Rayleigh viscosity, c_{0+} is found to tend to the real axis from below, and c_{0-} from above ($c_{0+} = \lim_{\epsilon\to 0}(c_{0+} - i\epsilon)$ and $c_{0-} = \lim_{\epsilon\to 0}(c_{0-} + i\epsilon)$). The complex poles are numbered $n = 1,-1,2,-2,...$ with $|n|$ growing with larger $|c_n|$, and positive n denotes the poles with positive imaginary part.
From equation 3.7, c_{-n} is found to be the complex conjugate of c_n, and c_n has the asymptotic behavior $c_n \to \frac{1}{2h}\ln\left[\frac{1+2\tau\cos\theta}{1-2\tau\cos\theta}\right] + \frac{in\pi}{h}$ (see appendix B.1).

Now we rewrite $p(k,\theta)$ as the sum of its principal parts and an analytic function;

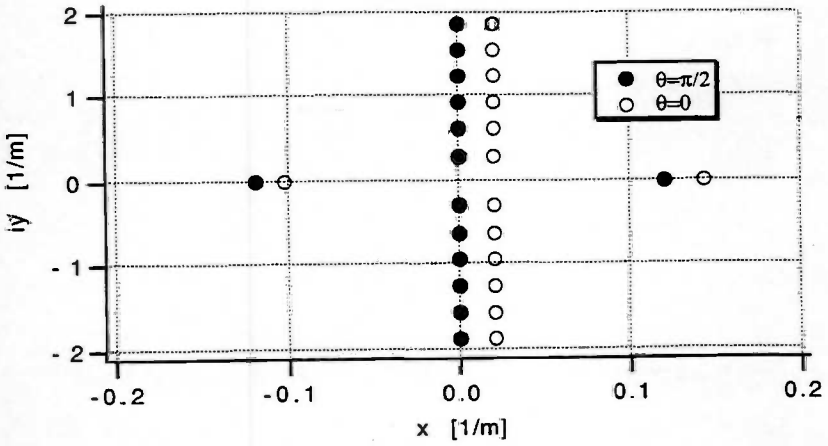

Figure 3.1: *Zeros in the complex plane* $x + iy$ *of* $[\nu + 2\tau\cos\theta c_n]\cosh c_n h - c_n \sinh c_n h$ *(*$\nu = 0.1\frac{1}{m}$, $\tau = 0.1$ *and* $h = 10m$*).*

$$p(k,\theta) = g(k,\theta) + \sum_{n=-\infty}^{\infty} \frac{b_n}{k - c_n}. \tag{3.8}$$

Here, $g(k,\theta)$ is the analytic function and the residues satisfy (for details see appendix B.2)

$$b_n = \frac{c_n^2 e^{c_n h}\cosh c_n(z+h)}{c_n^2 h + \nu\cosh^2 c_n h}. \tag{3.9}$$

Since c_n is of order n, b_n is of order $\mathbb{1}$, and a thorough study of the infinite series is needed in order to decide whether or not it converges. In appendix B.3 the series is found to converge uniformly in all closed intervals on the real axis. It converges like $\sum_{n=1}^{\infty} \frac{\sin\frac{n\pi z}{h}}{n}$, which has a very slow convergence. Nevertheless, we will take advantage of Mittag-Leffler's theorem (for results in complex analysis see for instance Henrici [1974]) concerning non-convergent series in order to make our series converge faster.

Mittag-Leffler's theorem states that a meromorph function, f, can be written as

$$f(z) = \sum_m [s_m(z) - r_m(z)] + g(z) \tag{3.10}$$

when f has poles in $z = z_m$, $|z_0| < |z_1| < |z_2| \cdots$. Here s_m is the part of the Laurent series about the m'th pole not representing an analytical function (in our case $\frac{b_n}{k-c_n}$). The infinite sum $\sum_m s_m(z)$ does not exist. r_m is a convergence generating polynomial and g is some analytical function. This makes the series converge uniformly on all bounded regions of the complex plane, with the exception of the poles. Assuming origo not being a pole, r_m is the Taylor expansion of s_m around 0 to a suitable degree.

It is difficult to determine the optimal number of terms to use in the Taylor expansion, so we will start out by considering the first term only. Then,

$$p(k,\theta) = g_1(k,\theta) + \sum_{n=-\infty}^{\infty} \frac{b_n}{k-c_n} + \frac{b_n}{c_n}, \tag{3.11}$$

where $g_1(k,\theta)$ is a new analytic function (since the sum converges: $g_1(k,\theta) = g(k,\theta) - \sum \frac{b_n}{c_n}$).

From equation 3.6 we see that $p(k,\theta)$ is finite in the whole complex plane away from the poles. Furthermore, Liouville's theorem states that if an analytic function is bounded in the whole complex plane, then it must be a constant. So, $g_1(k,\theta)$ is a constant, and by comparing equation 3.6 and equation 3.11 for $k = 0$, we see that the constant equals -1. Hence,

$$p(k,\theta) = -1 + \sum_{n=-\infty}^{\infty} \frac{b_n k}{c_n(k-c_n)}. \tag{3.12}$$

The sum now converges as $\frac{1}{n^2}$. In fact, adding L terms in the Taylor series would imply a convergence like $\sum \frac{A(L)}{n^{L+1}} - B(L)$. This series may converge faster or slower depending on the magnitude of A and B. A closer study of the number of terms to add will be done after the final expression has been established.

Remembering that c_{0+} only tends to the real axis, the infinite sum converges uniformly on $0 \le k \le \kappa$, $\kappa \to \infty$, and since $\int_0^\infty \equiv \lim_{\kappa\to\infty} \int_0^\kappa$, this is sufficient. Uniform convergence allows us to integrate term by term. Thus, writing G_1 as

$$G_1 = \frac{1}{2\pi} \int_0^{2\pi} \int_0^\infty [e^{kc} + e^{-k(2h+c)}] e^{ikr\cos(\theta+u-\alpha)} \left(-1 + \sum_{n=-\infty}^{\infty} \frac{b_n k}{c_n(k-c_n)} \right) dk d\theta, \tag{3.13}$$

we find

$$\begin{aligned} G_1 &= -\frac{1}{\sqrt{c^2+r^2}} - \frac{1}{\sqrt{(2h+c)^2+r^2}} \\ &\quad + \frac{1}{2\pi} \int_0^{2\pi} \sum_{n=-\infty}^{\infty} b_n \sum_{i=1}^{2} \left\{ \frac{1}{c_n \beta_i} + e^{-\beta_i c_n} \int_{-\beta_i c_n}^{\infty} \frac{e^{-t}}{t} dt \right\} d\theta, \end{aligned} \tag{3.14}$$

where

$$\beta_1 = -c - ir\cos(\theta - u + \alpha)$$

$$\beta_2 = 2h + c - ir\cos(\theta - u + \alpha).$$

The term $\int_{-\beta c_n}^{\infty} \frac{e^{-t}}{t} dt$ is according to Abramowitz and Stegun [1970, eq. 5.1.1] equal to the exponential integral $E_1(-\beta c_n)$ if $|\arg(-\beta c_n)| < \pi$. What does that imply in our case? It is impossible to say from this expression. We have to go back to the exact formulation $\lim_{A\to\infty} \int_0^A \frac{e^{-\beta k}}{k-c_n} dk$ and substitute $t = \beta(k - c_n)$. So, we look at $\lim_{A\to\infty} e^{-\beta c_n} \int_{-\beta c_n}^{\beta(A-c_n)} \frac{e^{-t}}{t} dt$. e^{-t} may be approximated by the series $\sum_{n=0}^{\infty} \frac{(-t)^n}{n!}$. Inserting this in the integral we see that the first term in the series gives an ln-function, $\int_{-\beta c_n}^{-\beta(A-c_n)} \frac{1}{t} dt = [\ln|t| + i\arg(t)]_{-\beta c_n}^{\beta(A-c_n)}$. The ln function is not defined at the negative real axis, and for complex arguments it is

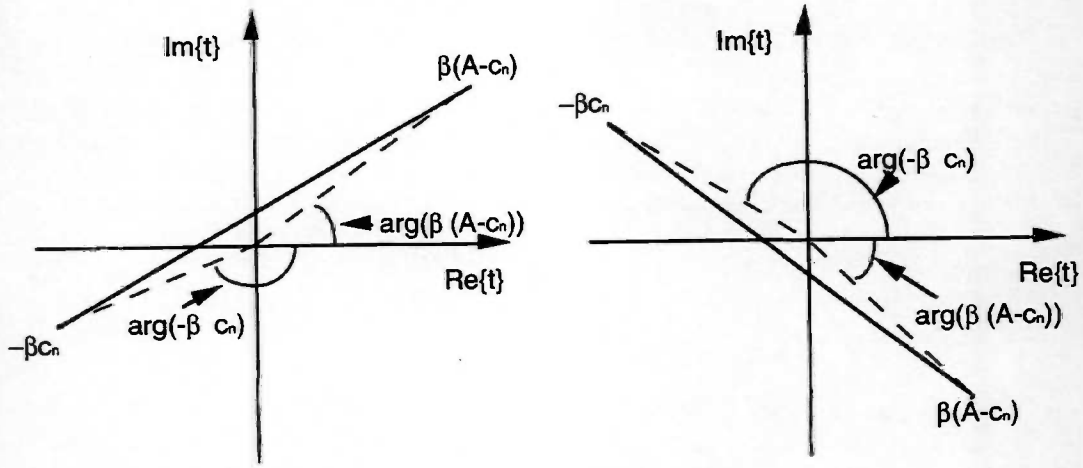

Figure 3.2: *Integration path for* $\int_{-\beta c_n}^{\beta(A-c_n)} \frac{e^{-t}}{t} dt$

not unique. This is why the exponential integral jumps when crossing the negative real axis.

Figure 3.2 shows two cases where $\int_{-\beta c_n}^{\infty} \frac{e^{-t}}{t} dt \neq E_1(-\beta c_n)$. That is if $\Re\{-\beta c_n\} < 0$ and $\Im\{\beta(k - c_n)\} \cdot \Im\{-\beta c_n\} < 0$ for k satisfying $\Re\{\beta(k - c_n)\} = 0$.
Since the real part of β is always larger than zero, these are the only cases where the negative real axis is crossed.
We require all arguments to lie in the interval $(-\pi, \pi)$. In the first case $[i \arg(t)]_{-\beta c_n}^{\beta(A-c_n)} > \pi i$.
Hence we have to subtract $2\pi i$. In the second case we have to add $2\pi i$. Thus,

$$\int_{-\beta c_n}^{\infty} \frac{e^{-t}}{t} dt = \begin{cases} E_1(-\beta c_n) - 2\pi i & \text{if} \quad \Re\{-\beta c_n\} < 0 \text{ and } \Im\{-\beta c_n\} < 0 \text{ and } \Im\{c_n\} < 0 \\ E_1(-\beta c_n) + 2\pi i & \text{if} \quad \Re\{-\beta c_n\} < 0 \text{ and } \Im\{-\beta c_n\} > 0 \text{ and } \Im\{c_n\} > 0 \\ E_1(-\beta c_n) & \text{else.} \end{cases}$$

The derivatives of the integral parts of G_1 (equation 3.14) , G_{1_B}, are

$$\frac{\partial^M G_{1_B}}{\partial a^{M_1} \partial b^{M_2} \partial c^{M_3}} = \frac{1}{2\pi} \int_0^{2\pi} \sum_{n=-\infty}^{\infty} b_n c_n^M \sum_{i=1}^{2} \left\{ \sum_{m=0}^{M} \frac{m!}{(\beta_i c_n)^{m+1}} + e^{-\beta_i c_n} \int_{-\beta_i c_n}^{\infty} \frac{e^{-t}}{t} dt \right\} \times \frac{\partial^{M_1} \beta i}{\partial a^{M_1}} \frac{\partial^{M_2} \beta i}{\partial b^{M_2}} \frac{\partial^{M_3} \beta i}{\partial c^{M_3}} d\theta. \quad (3.15)$$

where $M = M_1 + M_2 + M_3$.

We will rewrite equation 3.15 in order to speed up the convergence.
The asymptotic expansion of the exponential integral is given by Abramowitz and Stegun [1970, eq. 5.1.51];

$$E_1(z) = \frac{e^{-z}}{z}(1 - \frac{1}{z} + \frac{2!}{z^2} - \frac{3!}{z^3} + \frac{4!}{z^4} \cdots) \qquad (|\arg(z)| < \pi). \tag{3.16}$$

Since we seek a function that is continuous crossing the negative real axis, the approximation

$$e^{-\beta_i c_n} \int_{-\beta_i c_n}^{\infty} \frac{e^{-t}}{t} dt \approx -\sum_{l=0}^{L} \frac{l!}{(\beta_i c_n)^{l+1}} \tag{3.17}$$

is valid for all large $|\beta_i c_n|$.
This is a series that does not converge. Hence it is important to know how many terms to include; i.e. which L should be chosen.

Now we single out a part of equation 3.15 called T:

$$T = \sum_{n=-\infty}^{\infty} b_n c_n^M \left\{ \sum_{m=0}^{M} \frac{m!}{(\beta_i c_n)^{m+1}} + e^{-\beta_i c_n} \int_{-\beta_i c_n}^{\infty} \frac{e^{-t}}{t} dt \right\}. \tag{3.18}$$

For all $|n| > N(\theta)$ $|\beta_i c_n|$ is large enough to use the approximation in equation 3.17. Equation 3.18 then looks like

$$\begin{aligned} T = & \sum_{n=-N(\theta)}^{N(\theta)} b_n c_n^M \left\{ \sum_{m=0}^{M} \frac{m!}{(\beta_i c_n)^{m+1}} + e^{-\beta_i c_n} \int_{-\beta_i c_n}^{\infty} \frac{e^{-t}}{t} dt \right\} \\ & - \left(\sum_{n=-\infty}^{-N(\theta)-1} + \sum_{n=N(\theta)+1}^{\infty} \right) \sum_{j=1}^{L-M} \frac{b_n (M+j)!}{\beta_i^{M+j+1} c_n^{j+1}}. \end{aligned} \tag{3.19}$$

We see from equation 3.12 that

$$\frac{\partial^j p(k,\theta)}{\partial k^j}_{|k=0} = -\sum_{n=-\infty}^{\infty} \frac{j! b_n}{c_n^{j+1}}. \tag{3.20}$$

$\frac{\partial^j p(k,\theta)}{\partial k^j}_{|k=0}$ is found from equation 3.6 (for instance $\frac{\partial p(k,\theta)}{\partial k}_{|k=0} = -1$, $\frac{\partial^2 p(k,\theta)}{\partial k^2}_{|k=0} = -z^2 - 2hz + 2h - 4\tau\cos\theta$ ...) and we may write

$$\begin{aligned} T = & \sum_{n=-N(\theta)}^{N(\theta)} b_n c_n^M \left\{ \sum_{m=0}^{M} \frac{m!}{(\beta_i c_n)^{m+1}} + e^{-\beta_i c_n} \int_{-\beta_i c_n}^{\infty} \frac{e^{-t}}{t} dt \right\} \\ & + \sum_{j=1}^{L-M} \left[\left(\sum_{n=-N(\theta)}^{N(\theta)} \frac{b_n}{c_n^{j+1}} \right) - \frac{1}{j!} \frac{\partial^j p(k,\theta)}{\partial k^j}_{|k=0} \right] \frac{(M+j)!}{\beta_i^{M+j+1}}. \end{aligned} \tag{3.21}$$

The total Green's function evaluated in this section is then

$$G_{Alt.1} = \frac{1}{\sqrt{r^2+(z-c)^2}}+\frac{1}{\sqrt{r^2+(z+c+2h)^2}}-\frac{1}{\sqrt{c^2+r^2}}-\frac{1}{\sqrt{(2h+c)^2+r^2}} \tag{3.22}$$
$$+\frac{1}{2\pi}\int_0^{2\pi}\sum_{i=1}^{2}\left\{\sum_{n=-N(\theta)}^{N(\theta)} b_n\left[\frac{1}{(\beta_i c_n)}+e^{-\beta_i c_n}\int_{-\beta_i c_n}^{\infty}\frac{e^{-t}}{t}dt\right]\right.$$
$$\left.+\sum_{j=1}^{L}\left[\left(\sum_{n=-N(\theta)}^{N(\theta)}\frac{b_n}{c_n^{j+1}}\right)-\frac{1}{j!}\frac{\partial^j p(k,\theta)}{\partial k^j}_{|k=0}\right]\frac{j!}{\beta_i^{j+1}}\right\}d\theta.$$

The derivatives of the integral part are given in appendix B.5.

We would get the same result if we added more terms in the Taylor series applying Mittag-Leffler's theorem (and of course withdraw them). Now, however, it is immediately seen that the error done by ending the summation at N terms, may be related to the accuracy of the approximation of the exponential integral:

$$\Delta_n(\theta) \sim \sum_{n=N(\theta)+1}^{\infty}\ \sum_{\substack{z=-\beta_1 c_n\\ z=-\beta_1 c_{-n}\\ z=-\beta_2 c_n\\ z=-\beta_2 c_{-n}}}\left\{e^z\int_z^{\infty}\frac{e^{-t}}{t}dt-\left[e^z\int_z^{\infty}\frac{e^{-t}}{t}dt\right]_{asmp}(L)\right\}. \tag{3.23}$$

This shows that different number of terms are needed to get a constant error in θ and that L must not be chosen too large. Hopefully the series converges much faster than indicated above, but with a convergence related to the magnitude of $[\frac{c}{h}+i\frac{r}{h}\cos(\theta+u-\alpha)]$.

We notice that the integrand becomes singular as the source point tends to the free surface. However, unless the evaluation point is at the free surface as well, the integral exists. To circumvent this problem an extra routine should be made, differentiating the Green's function with respect to the vertical evaluation point. Since

$$\frac{\partial^M G(r,Z_1,Z_2)}{\partial Z_2^M}\Big|_{\substack{Z_1=z\\ Z_2=c}} = \frac{\partial^M G(r,Z_1,Z_2)}{\partial Z_1^M}\Big|_{\substack{Z_1=c\\ Z_2=z}} \tag{3.24}$$

we simply choose the routine where $\min(|z|,|c|)$ is to be included in $p(k,\theta)$.

3.1.2 Green's function - alternative 2

The second method, integrating first in θ, will be based on a general idea from Knudsen [1992]. In this approach it is convenient to write terms in equation 3.4 not containing θ as just some functions of k;

$$G_1 = \frac{1}{\pi}\int_0^{\infty} A\int_0^{2\pi}\frac{B+C\cos\theta}{D+E\cos\theta}e^{ikr\cos(\theta-u+\alpha)}d\theta dk, \tag{3.25}$$

where

$$A = A(k) = \cosh k(z+h)\cosh k(c+h)e^{-kh}$$

$$B = B(k) = k + \nu$$

$$C = C(k) = 2\tau k$$

$$D = D(k) = k\sinh kh - \nu(1-\overline{\mu}i)\cosh kh$$

$$E = E(k) = -2\tau k\cosh kh(1-\frac{\overline{\mu}}{2}i).$$

Now we will substitute $t = e^{i\theta}$. Equation 3.25 then looks like

$$G_1 = \frac{1}{\pi i}\int_0^\infty A(k)\int_{|t|=1}\frac{1}{t}Q(k,t)e^{\frac{ikr}{2}(\gamma t+\frac{1}{\gamma t})}dtdk, \tag{3.26}$$

where $\gamma = e^{i(\alpha-u)}$ and $Q(k,t) = \frac{A+B\frac{1}{2}(t+\frac{\gamma}{t})}{D+E\frac{1}{2}(t+\frac{1}{t})}$.

Assume for a moment that $\tau \neq 0$. Then $E \neq 0$ and $Q(k,t)$ has two roots in the t-plane, $\rho_1 = \frac{-D-\sqrt{D^2-E^2}}{E}$ and $\rho_2 = \frac{-D+\sqrt{D^2-E^2}}{E}$. Since $\rho_1\rho_2 = 1$, they are either both on the unit circle, or one of them must be inside- and the other one outside the unit circle.

Denoting the root with the smallest absolute value ρ_s and the other one ρ_l, simple calculations give (see also figure 3.3)

$$\rho_s = \begin{cases} \rho_1 & k < \sigma_1 \\ \rho_2 & k > \sigma_1 \end{cases}$$

where σ_1 and σ_2 (in the interval (σ_1,σ_2) the roots are complex) are given by the equations

$$\begin{aligned} \sigma_1\tanh\sigma_1 h - \nu &= -2\tau\sigma_1 \\ \sigma_2\tanh\sigma_2 h - \nu &= 2\tau\sigma_2. \end{aligned} \tag{3.27}$$

There will always be one k that gives $|\rho_1| \equiv |\rho_2| \equiv 1$. However, one point does not affect the result as long as exactly that point is avoided as an integrand value in the following numerical integration.

Now, as we know more about the roots, we make a partial fraction expansion of $Q(k,t)$:

$$Q(k,t) = \kappa - 2\kappa_1 + \kappa_1(\frac{1}{1-\frac{\rho_s}{t}} + \frac{1}{1-\frac{t}{\rho_l}}), \tag{3.28}$$

where $\kappa_1 = \kappa_1(k) = \frac{CD-BE}{E(\rho_l E+D)}$ and $\kappa = \kappa(k) = \frac{C}{E} + \kappa_1$.

$Q(k,t)$ may be further rewritten by applying $\frac{1}{1-x} = \sum_{n=0}^\infty x^n$, $|x| < 1$;

$$Q(k,t) = \kappa + \kappa_1\sum_{n=1}^\infty\left[(\frac{\rho_s}{t})^n + (\frac{t}{\rho_l})^n\right]. \tag{3.29}$$

The remaining expression in equation 3.26 may also be rewritten in powers in t (See Whittaker and Watson [1950] page 358);

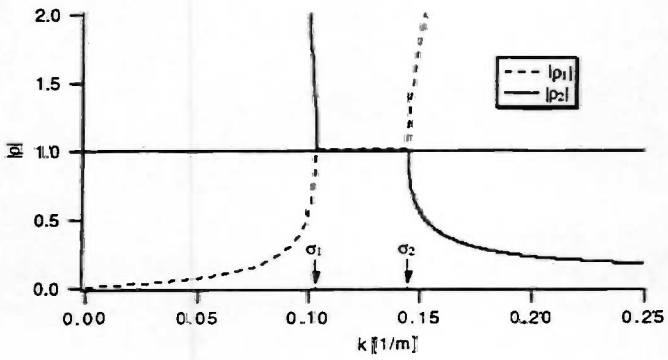

a)

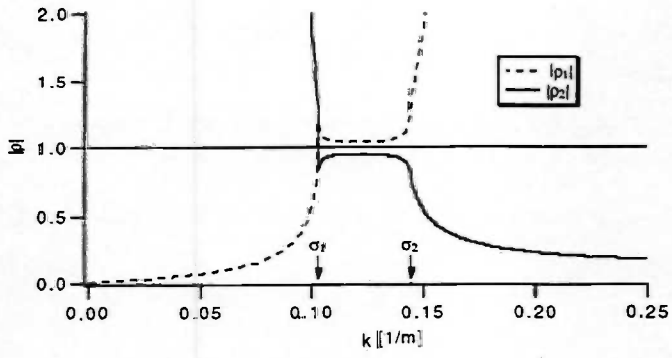

b)

Figure 3.3: *Absolute value of the roots of $Q(k,t)$ as a function of k (τ=0.1, $\nu = 0.1\frac{1}{m}$ and $h = 10m$). a) $\overline{\mu} = 0.0$ b) $\overline{\mu} = 0.01$.*

$$e^{\frac{ikr}{2}(\gamma t+\frac{1}{\gamma t})} = \sum_{n=-\infty}^{\infty} (\gamma i)^n J_n(kr) t^n. \tag{3.30}$$

Inserting the new expressions in equation 3.26 and integrating by the method of residues, we are left with the integral

$$G_1 = 2\int_0^\infty A(k)[\kappa(k)J_0(kr) + \kappa_1(k)\sum_{n=1}^{\infty}(i\rho_s)^n J_n(kr)(\gamma^n + \frac{1}{\gamma^n})]dk, \tag{3.31}$$

or fully written:

$$\begin{aligned} G_1 &= -2\int_0^\infty \frac{\cosh k(z+h)\cosh k(c+h)e^{-kh}}{\cosh kh} J_0(kr)dk \\ &\quad -2\int_0^{\sigma_1} f(k)[J_0(kr) + 2\sum_{n=1}^{\infty}(i\rho_{s_1})^n J_n(kr)\cos n(\alpha-u)]dk \\ &\quad +2\int_{\sigma_1}^\infty f(k)[J_0(kr) + 2\sum_{n=1}^{\infty}(i\rho_{s_2})^n J_n(kr)\cos n(\alpha-u)]dk, \end{aligned} \tag{3.32}$$

where

$$\begin{aligned} f(k) &= \frac{k\cosh k(z+h)\cosh k(c+h)}{\cosh^2 kh\sqrt{(k\tanh kh-\nu)^2 - 4\tau^2k^2}} \\ \rho_{s_1} &= \frac{k\tanh kh - \nu + \sqrt{(k\tanh kh-\nu)^2 - 4\tau^2k^2}}{2\tau k} \\ \rho_{s_2} &= \frac{k\tanh kh - \nu - \sqrt{(k\tanh kh-\nu)^2 - 4\tau^2k^2}}{2\tau k} \end{aligned}$$

and J_n are Bessel functions of the first kind.

It seems hard to integrate further in k. The exception is the first integral in equation 3.32 which is not time consuming to evaluate numerically anyway since most expressions involved are already calculated. However, we can not get too many ways of checking the code.

So, we will look at the term

$$\begin{aligned} T &= \frac{1}{\sqrt{r^2+(z-c)^2}} + \frac{1}{\sqrt{r^2+(z+c+2h)^2}} \\ &\quad -2\int_0^\infty \frac{\cosh k(z+h)\cosh k(c+h)e^{-kh}}{\cosh kh} J_0(kr)dk. \end{aligned} \tag{3.33}$$

To simplify we follow the same method as in section 3.1.1, writing T as

$$T = -2\int_0^\infty p(k)J_0(kr)dk \tag{3.34}$$

where

$$p(k) = \begin{cases} \frac{\cosh k(z+h)\sinh kc}{\cosh kh} & \text{if } |z| \geq |c| \\ \frac{\cosh k(c+h)\sinh kz}{\cosh kh} & \text{if } |c| \geq |z|. \end{cases} \tag{3.35}$$

Regard k a complex parameter. Then $p(k)$ has poles of order one in $k = \frac{(2n+1)\pi i}{2h}$, where n is any integer, including 0. As in section 3.1.1 we write $p(k)$ as a sum of the principal parts and an analytical function;

$$p(k) = g(k) - \frac{2}{h}\sum_{n=0}^{\infty} \frac{k \sin\left[\frac{(2n+1)\pi}{2}\frac{z}{h}\right] \sin\left[\frac{(2n+1)\pi}{2}\frac{c}{h}\right]}{k^2 + \left(\frac{(2n+1)\pi}{2h}\right)^2} \tag{3.36}$$

Here terms of positive and negative poles are added and $g(k)$ is the analytic function. We see that the infinite sum converges. Then, applying Liouville's theorem and comparing equation 3.35 and equation 3.36, $g(k)$ is found to be zero.
By inserting the new p(k) in equation 3.34 and integrating (see Abramowitz and Stegun [1970] eq.11.4.44) we get

$$T = \frac{2}{h}\sum_{n=0}^{\infty} \sin\left[\frac{(2n+1)\pi}{2}\frac{z}{h}\right] \sin\left[\frac{(2n+1)\pi}{2}\frac{c}{h}\right] K_0\left(\frac{(2n+1)\pi}{2}\frac{r}{h}\right). \tag{3.37}$$

Here K_0 is a modified Bessel function of the second kind. We are later (section 3.1.3) going to find that this term represents the infinite frequency Green's function.

If $|z+c|$ is small, the integrals in equation 3.32 with infinite integration limit decay slowly with increasing k. To avoid difficulties regarding when to stop integrating we follow the same technique as Faltinsen and Michelsen [1974] used for zero Froude number. That is: integrate up to a certain $k = \sigma_3$, which for $k > \sigma_3$ satisfies $1 - \tanh kh < \epsilon$. σ_3 should also be chosen larger than σ_2. The remaining integral may then be written

$$RI^A = \frac{1}{2\pi}\int_0^{2\pi}\int_{\sigma_3}^{\infty} e^{k(z+c+ir\cos(\theta-u+\alpha))} \frac{k(1+2\tau\cos\theta)+\nu}{k(1-2\tau\cos\theta)-\nu} dk d\theta \tag{3.38}$$

if we do not apply equation 3.37 and

$$RI^B = \frac{1}{2\pi}\int_0^{2\pi}\int_{\sigma_3}^{\infty} e^{k(z+c+ir\cos(\theta-u+\alpha))} \frac{2k}{k(1-2\tau\cos\theta)-\nu} dk d\theta \tag{3.39}$$

if we do. The integration variables are now changed.

Integrating in k (for details, see appendix B.4) gives the total Green's function without applying equation 3.37 as

$$\begin{aligned} G^A_{Alt.2}(\vec{x},\vec{a}) &= \frac{1}{\sqrt{r^2+(z-c)^2}} + \frac{1}{\sqrt{r^2+(z+c+2h)^2}} \\ &\quad -2\int_0^{\sigma_3} \frac{\cosh k(z+h)\cosh k(c+h)e^{-kh}}{\cosh kh} J_0(kr)dk \end{aligned} \tag{3.40}$$

$$-2\int_0^{\sigma_1} f(k)[J_0(kr)+2\sum_{n=1}^{\infty}(i\rho_{s_1})^n J_n(kr)\cos n(\alpha-u)]dk$$
$$+2\int_{\sigma_1}^{\sigma_3} f(k)[J_0(kr)+2\sum_{n=1}^{\infty}(i\rho_{s_2})^n J_n(kr)\cos n(\alpha-u)]dk$$
$$+\frac{1}{2\pi}\int_0^{2\pi} e^{-\beta\sigma_3}\left[\frac{1}{\beta}\frac{1+2\tau\cos\theta}{1-2\tau\cos\theta}+\frac{2\nu}{(1-2\tau\cos\theta)^2}G[\beta(\sigma_3-\frac{\nu}{1-2\tau\cos\theta})]\right]d\theta,$$

and with equation 3.37:

$$\begin{aligned}G^B_{Alt.2}(\vec{x},\vec{a}) &= \frac{2}{h}\sum_{n=0}^{\infty}\sin\left[\frac{(2n+1)\pi}{2}\frac{z}{h}\right]\sin\left[\frac{(2n+1)\pi}{2}\frac{c}{h}\right]K_0\left(\frac{(2n+1)\pi}{2}\frac{r}{h}\right)\\ &-2\int_0^{\sigma_1} f(k)[J_0(kr)+2\sum_{n=1}^{\infty}(i\rho_{s_1})^n J_n(kr)\cos n(\alpha-u)]dk \qquad (3.41)\\ &+2\int_{\sigma_1}^{\sigma_3} f(k)[J_0(kr)+2\sum_{n=1}^{\infty}(i\rho_{s_2})^n J_n(kr)\cos n(\alpha-u)]dk\\ &+\frac{1}{2\pi}\int_0^{2\pi} e^{-\beta\sigma_3}\left[\frac{1}{\beta}\frac{2}{1-2\tau\cos\theta}+\frac{1+2\tau\cos\theta}{(1-2\tau\cos\theta)^2}G[\beta(\sigma_3-\frac{\nu}{1-2\tau\cos\theta})]\right]d\theta.\end{aligned}$$

Here $\beta=-[z+c+ir\cos(\theta-u+\alpha)]$ and $G[\beta(\sigma_3-\frac{\nu}{1-2\tau\cos\theta})]$ is $e^{[\beta(\sigma_3-\frac{\nu}{1-2\tau\cos\theta})]}E_1[\beta(\sigma_3-\frac{\nu}{1-2\tau\cos\theta})]$. E_1 is the exponential integral. The derivatives of the integral parts of equation 3.40 are listed in appendix B.5.

3.1.3 Limiting values for the Green's function

Infinite frequency limit

Let us go back to equation 3.32 and see what happens if $\nu=\frac{\omega^2}{g}$ and $\tau=\frac{U\omega}{g}$ tend to infinity. We see that σ_1 and σ_2 both tend to infinity and $f(k)$ and ρ_{s_1} tend to zero. Thus, the three last terms vanish, and the infinite frequency Green's function is

$$\begin{aligned}G_{\omega\to\infty} &= \frac{1}{\sqrt{r^2+(z-c)^2}}+\frac{1}{\sqrt{r^2+(z+c+2h)^2}} \qquad (3.42)\\ &-2\int_0^{\infty}\frac{\cosh k(z+h)\cosh k(c+h)e^{-kh}}{\cosh kh}J_0(kr)dk.\end{aligned}$$

Inserting $z=0$ and recalling that $\int_0^{\infty}e^{-ax}J_0(bx)dx=\frac{1}{\sqrt{a^2+b^2}}$ (Abramowitz and Stegun [1970] eq. 11.4.39), we find that this G fulfills the free surface condition for infinite frequency; $G_{\omega\to\infty}=0$. For large r/h we use the expression given earlier

$$G_{\omega\to\infty}=\frac{2}{h}\sum_{n=0}^{\infty}\sin\left[\frac{(2n+1)\pi}{2}\frac{z}{h}\right]\sin\left[\frac{(2n+1)\pi}{2}\frac{c}{h}\right]K_0\left(\frac{(2n+1)\pi}{2}\frac{r}{h}\right). \qquad (3.43)$$

τ tends to zero

$\tau = \frac{\omega U}{g}$ may tend to zero in two ways. Either by $\omega \to 0$ or by $U \to 0$.

We first look at the case $U \to 0$. Then the well known solution by John [1950] gives the limiting value;

$$G^*_{U=0} = 2\pi i \sum_{k=0}^{\infty} \frac{c_k^2 - \nu^2}{hc_k^2 - h\nu^2 + \nu} H_0^{(1)}(c_k r) \cosh c_k(z+h) \cosh c_k(c+h), \tag{3.44}$$

where the c_k's are given by

$$c_k \sinh c_k h - \nu \cosh c_k h = 0. \tag{3.45}$$

The star denotes complex conjugate, and is due to the way he writes the velocity potential; $\phi = \Re\{AGe^{-i\omega t}\}$, while we chose $\phi = \Re\{AGe^{i\omega t}\}$. These two potentials represent incoming and outgoing waves, the sign of the Rayleigh viscosity multiplied by the frequency, decides which is which.

$H_0^{(1)}$ is the Hankel function (or Bessel function of the third kind) and is related to the modified Bessel function of the second kind, $K_0(z)$, as (Abramowitz and Stegun eq. 9.6.4) $K_0(z) = \frac{\pi i}{2} H_0^{(1)}(ze^{\frac{\pi i}{2}})$ if $-\pi < \arg z \leq \frac{\pi}{2}$.

John [1950] also found the Green's function for the limit $\omega \to 0$. Then the real part of equation 3.44 tends to infinity while the imaginary part tends to $\Im\{G_{U=0}\} = -\frac{\pi}{h}$. John gave the Green's function for a steady problem as $G_{STEADY} = \lim_{\nu \to 0} \left(G_{U=0} + \frac{\ln \nu h}{h} \right)$ when $G_{U=0}$ is expressed as above.

Asymptotic formulation far from the source

To get an idea of how the Green's function behaves far from the source point we could make an asymptotic expansion in r. However, for the proof in appendix A it is convenient to write the Green's function as $G(\vec{x}, \vec{a}) = f(\vec{x})g(\vec{a})$. Thus we introduce $(x, y) = (R\cos v, R \sin v)$ and make an asymptotic expansion in R. The simplest way to do this seems to go all the way back to equation 3.4. From this point we will follow the same technique as Grue and Biberg [1993] used for finite water depth, only they had current along the negative $x-$axis only.

G may be written

$$G = \frac{1}{\pi} \int_0^{2\pi} \int_0^{\infty} e^{ikR\cos(\theta - v + \alpha)} p(k, \theta) dk d\theta \tag{3.46}$$

where

$$p(k,\theta) = \left[\frac{e^{-kh} \cosh k(z+h) \cosh k(c+h)[k(1+2\tau\cos\theta)+\nu]}{k \sinh kh - [\nu + 2\tau \cos\theta k] \cosh kh} + \frac{1}{2}\left(e^{-k|z-c|} + e^{-k(z+c+2h)} \right) \right] \times e^{-ik[a\cos(\theta+\alpha) + b\sin(\theta+\alpha)]}. \tag{3.47}$$

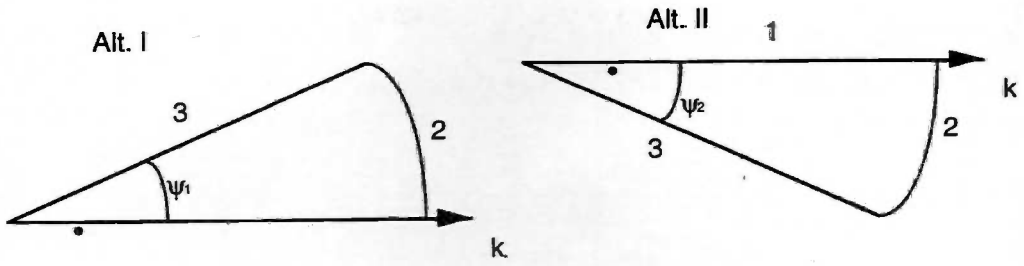

Figure 3.4: *Path alternatives*

Now we will integrate in the complex plane according to figure 3.4; substitute $k = le^{i\psi}$ and choose ψ so as to make the integral over arc 2 to vanish. The Green's function is then

$$G = \frac{1}{\pi}\int_{\frac{-\pi}{2}-\alpha+v}^{\frac{\pi}{2}-\alpha+v}\int_0^\infty e^{(-l\sin\psi_1+il\cos\psi_1)R\cos(\theta-v+\alpha)}p(le^{i\psi_1},\theta)e^{i\psi_1}dld\theta$$
$$+\frac{1}{\pi}\int_{\frac{\pi}{2}-\alpha+v}^{\frac{3\pi}{2}-\alpha+v}\left[\int_0^\infty e^{(-l\sin\psi_2+il\cos\psi_2)R\cos(\theta-v+\alpha)}p(le^{i\psi_2},\theta)e^{i\psi_2}dl+2\pi iRes\right]d\theta, \quad (3.48)$$

where Res is the residue of the integrand at $k = c_0$. By integration by parts, the integrals in l are found to be of order $\frac{1}{R^2}$. Thus

$$G_{R\to\infty} = 2i\int_{\frac{\pi}{2}-\alpha+v}^{\frac{3\pi}{2}-\alpha+v}\frac{c_0^2\cosh c_0(z+h)\cosh c_0(c+h)}{c_0^2h+\nu\cosh^2 c_0h}e^{-ic_0[a\cos(\theta+\alpha)+b\sin(\theta+\alpha)]} \quad (3.49)$$
$$\times e^{iRc_0\cos(\theta-v+\alpha)}d\theta+\mathcal{O}(\frac{1}{R^2}),$$

where $c_0 = c_0(\theta)$ is implicitly given by

$$c_0\sinh c_0h-[\nu+2\tau\cos\theta c_0]\cosh c_0h=0. \quad (3.50)$$

This integral is on the form $I = \int_a^b f(\theta)e^{iRg(\theta)}d\theta$. Hence, for large R the method of stationary phase may be applied. In that case the solution satisfies $I \approx f(\theta_0)\sqrt{\frac{2\pi}{|Rg''(\theta_0)|}}e^{i(Rg(\theta_0)\pm\frac{\pi}{4})}$ (as given e.g. in Newman [1977]) if θ_0 is in the open range of integration and $g''(\theta_0)\neq 0$. The sign ahead of $\frac{\pi}{4}$ is equal to the sign of $g''(\theta_0)$. Here $g(\theta) = c_0\cos(\theta-v+\alpha)$ and the equation for stationary phase is $g'(\theta) = c_0'\cos(\theta-v+\alpha)-c_0\sin(\theta-v+\alpha) = 0$. Together with the requirement $\theta_0\in(\frac{\pi}{2}-v+\alpha,\frac{3\pi}{2}+v-\alpha)$ this leads to the following solution:

$$\sin(\theta_0-v+\alpha) = -\frac{2\tau}{F(c_0)}\sin(v-\alpha),\quad \cos(\theta_0-v+\alpha) = -\sqrt{1-\frac{4\tau^2}{F(c_0)^2}\sin^2(v-\alpha)} \quad (3.51)$$

where $F(c_0) = \tanh c_0h+\frac{c_0h}{\cosh^2 c_0h}$. The two times derivative of g is given by

$$g''(\theta_0) = \frac{c_0}{F(c_0)-2\tau\cos\theta_0}\{4\tau\sin\theta_0\cos(\theta_0-v+\alpha)$$
$$+\left[\frac{8\tau^2c_0h\sin^2\theta_0(\frac{\nu}{c_0}+c_0^2h^2\tanh c_0h)}{\cosh^2 c_0h[F(c_0)-2\tau\cos\theta_0]^2}-F(c_0)\right]\cos(\theta_0-v+\alpha)\} \quad (3.52)$$

where θ_0 may be eliminated by applying $\begin{matrix}\sin\\ \cos\end{matrix}[\theta_0] = \begin{matrix}\sin\\ \cos\end{matrix}[(\theta_0 - v + \alpha) + (v - \alpha)]$ and equation 3.51. When Taylor expanding in τ we see that $g''(\theta_0)$ is positive, thus the asymptotic Green's function reads

$$\begin{aligned} G_{R\to\infty} &= i\sqrt{\frac{8\pi}{R|g''(\theta_0)|}}\frac{c_0^2\cosh c_0(z+h)\cosh c_0(c+h)}{c_0^2 h+\nu\cosh^2 c_0 h}e^{-ic_0R\sqrt{1-\frac{4\tau^2}{F(c_0)^2}\sin^2(v-\alpha)}} \\ &\times e^{ic_0a\left(\sqrt{1-\frac{4\tau^2}{F(c_0)^2}\sin^2(v-\alpha)}\cos v-\frac{2\tau}{F(c_0)}\sin(v-\alpha)\sin v\right)} \\ &\times e^{ic_0b\left(\frac{2\tau}{F(c_0)}\sin(v-\alpha)\cos v+\sqrt{1-\frac{4\tau^2}{F(c_0)^2}\sin^2(v-\alpha)}\sin v\right)}e^{\frac{i\pi}{4}}+\mathcal{O}(\frac{1}{R}). \end{aligned} \tag{3.53}$$

For the proof in appendix A an explicit expression of c_0 as a function of α is needed. Taylor expanding equation 3.50 in τ gives

$$c_0 = K - \frac{2\tau K\cos(v-\alpha)}{\tanh Kh+\frac{Kh}{\cosh^2 Kh}} + \text{higher order of } \tau \tag{3.54}$$

where K is the wave number for the incident wave given by the equation $Kg\tanh Kh = \omega_0^2$, and c_0 is assumed to be the wave number for the outgoing waves at large distance from the source point.

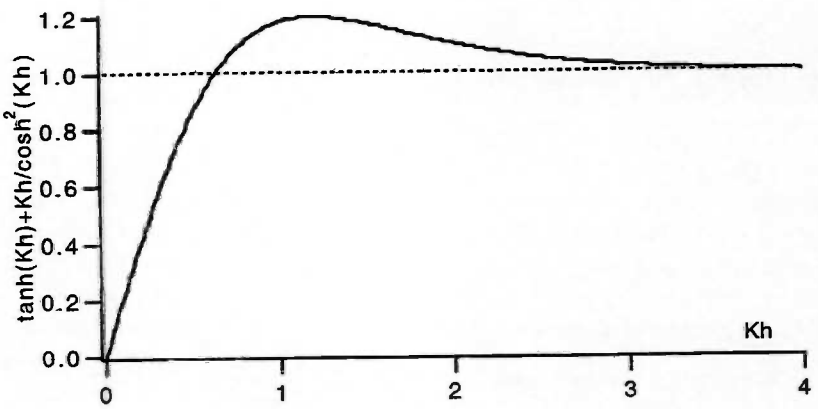

Figure 3.5: Denominator of the second term in equation 3.54.

Equation 3.54 and figure 3.5 show how the wave number c_0 is affected by the sea floor and the current.

3.2 Numerical evaluation of the Green's function

In this section we will look at the numerical evaluation of the Green's function as expressed in section 3.1.1 and 3.1.2. Inputs and outputs are in single precision and the calculations are in double precision. We will first look at some numerical aspects common for the alternative Green's functions. Both methods need an integration routine for arrays of complex integrands. Also a routine for evaluation of the exponential integral is needed in both cases. Hoff [1990] did an extensive study of integration routines and of the exponential integral in his work regarding the Green's function with arbitrary speed and infinite water depth. He kindly gave us the computer code for the methods he found most efficient for our type of Green's function. These methods are described in Hoff [1990]. Only a brief description will be given here.

Integration scheme

In the QUADPACK-library Hoff found a scheme of the Gauss-Kronrod type (QNG). These schemes are suitable for iterative algorithms. If the integral with $n = m$ abscissae does not satisfy the desired accuracy, then an $n = 2m + 1$ point formula, which includes the m original integrand values, will be used. All the weights are changed, however.
Hoff modified the routine to cope with complex functions, and we modified to arrays of complex functions.

The exponential integral

Daubisse [1981] gave a formula for approximation of the complex exponential integral by a series of exponential functions. Writing for $|\arg z| < \pi$

$$e^z E_1(z) = \begin{cases} \int_0^\infty \frac{e^{-zt}}{t+1} dt & \text{if } \Re z > 0 \\ \int_0^\infty \frac{e^{izt}}{t+i} dt & \text{if } \Re z \leq 0 \text{ and } \Im z > 0 \\ \left(\int_0^\infty \frac{e^{iz^* t}}{t+i} dt \right)^* & \text{if } \Re z \leq 0 \text{ and } \Im z < 0 \end{cases} \tag{3.55}$$

(the star denotes complex conjugate), and approximating the term $\frac{1}{t+1}$ or $\frac{1}{t+i}$ by exponential functions, the evaluation of the integral is quite straight forward. If the magnitude of z is less than 1, the power series (Abramowitz and Stegun [1970] eq. 5.1.11)

$$E_1(z) = -\gamma - \ln z - \sum_{n=1}^{\infty} \frac{(-1)^n z^n}{n! n} \qquad |\arg z| < \pi \tag{3.56}$$

gives better results. Hoff [1990] found this procedure to be significantly faster than other formulas (such as local formulas). The accuracy is of 5-6 decimals.

Location of zeros

We want to solve the equation $f(x) = 0$ numerically. Håvie [1991] recommends Newton-Raphsons method when analytic differentiation of f is possible: We assume x_{k-1} to be

an approximate solution of $f(x) = 0$, and let the next iteration be defined by $x_k = x_{k-1} + \Delta x_{k-1}$. The two first terms in the Taylor series of $f(x)$ around x_{k-1} satisfy

$$f(x_k) \approx f(x_{k-1}) + f'(x_{k-1})\Delta x_{k-1} = 0, \tag{3.57}$$

producing the iteration scheme

$$x_k = x_{k-1} - \frac{f(x_{k-1})}{f'(x_{k-1})}. \tag{3.58}$$

The iteration terminates when $|f(x_{k-1})|$ and $|\Delta x_{k-1}|$ are both less than some ϵ.

Newton-Raphsons method has quadratic convergence and the scheme is applicable for functions of real and complex arguments.

3.2.1 Alternative 1

The Green's function for infinite water depth, as expressed by Grekas [1981], contains one evaluation of the exponential integral for each θ. In the original MULDIF program this Green's function is used, with evaluation of the exponential integral by local formulas. Here, for each θ, it is necessary to calculate $2+4\cdot N(\theta)$ exponential integrals, find $2+N(\theta)$ poles numerically, and evaluate additional terms compared to Grekas' formulation. $N(\theta)$ denotes number of terms in the infinite series.

We demand the Green's function for finite water depth not to be considerable slower than in the infinite depth case. But, since Hoff [1990] found the exponential integral evaluated in terms of local formulas to be approximately eight times slower than by the formula of Daubisse [1981], we will give this method a chance.

Location of the poles

We wish to find the solutions of equation 3.7 numerically. Here, we can save some computer time, using the fact that $c_n(-\theta) = -c_n(\theta - \pi) = -c_n(\theta + \pi) = c_n(\theta)$, which means it is sufficient to find the poles in an interval of length $\pi/2$. The poles will be found by Newton-Raphsons method. In order to ensure that the expected solution is the one we get, the estimated value has to be close to the solution. The estimates for the real poles will be separated into deep and shallow water estimates. If νh is large (See appendix B.6; Green's function in terms of non-dimensional parameters) $\tanh c_{0\pm}h$ may be approximated by ± 1. Thus the approximation of the real poles become

$$\begin{aligned} c_{0+} &= \frac{\nu}{1 - 2\tau\cos\theta} \\ c_{0-} &= -\frac{\nu}{1 + 2\tau\cos\theta}. \end{aligned} \tag{3.59}$$

If νh is small, the terms $c_{0\pm}h$ are small, and may be used as approximations of $\tanh c_{0\pm}h$. We then get the estimates

$$\begin{aligned} c_{0+} &= \max[\tau\cos\theta \pm \sqrt{\tau^2\cos\theta^2 + h\nu}]/h \\ c_{0-} &= \min[\tau\cos\theta \pm \sqrt{\tau^2\cos\theta^2 + h\nu}]/h. \end{aligned} \tag{3.60}$$

Equation 3.59 will be used if νh is less than 0.7, and equation 3.60 if νh is larger than 0.7.

Figure 3.1 indicates that the difficulty of finding the complex poles is very much concentrated to the first pole, c_1. Since the real part seems to vary very little with n we may apply the asymptotic solution as an estimate. The imaginary part lies in the interval $(\frac{\pi}{2h}, \frac{\pi}{h})$. By empiric considerations we have reached the following estimates:

$$c_1 = (a_1, b_1) = \left(\frac{1}{2h}\ln\left[\frac{1+2\tau\cos\theta}{1-2\tau\cos\theta}\right], \frac{\pi}{2h}(1+e^{-0.3\nu h})\right) \tag{3.61}$$

$$c_n = (a_n, b_n) = \left(a_{n-1}, b_{n-1} + \frac{\pi}{h}\right). \tag{3.62}$$

The iteration terminates when 10 decimal places are reached for both the real and imaginary part.

Number of terms in the infinite series

The technique of applying convergence accelerating polynomials is very successful, as may be viewed in table 3.1. We remember from section 3.1.1 that L represents *extra* convergence accelerating terms. In order to determine the constant term we already added one term. So, $L = 0$ represents a convergence of order $\frac{1}{n^2}$, compared to the original $\frac{\sin nz}{n}$.

In table 3.1 and 3.2 we have set number of terms to be independent of θ. For $r/h = 1$ this Green's function agrees with the second alternative method to five decimal places when $L = 3$ and $N = 2$. There is a tendency for slower convergence and larger error when $|\frac{c}{h}|$ is small, which is more visible for $\frac{\partial G}{\partial a}$ in table 3.2. For the higher order derivatives $\frac{r}{h}$ and $|\frac{c}{h}|$ have to be large in order to give reasonable results. Examples of bad results are given in table 3.4. Somewhat better results for increasing $\frac{r}{h}$ are shown in table 3.5. We here notice that too many terms in the infinite series causes inaccuracies.

We will try to explain this sensitivity to the different parameters. For each n we get a contribution to the sum, dependent of n, the degree of derivative, M, the number of convergence accelerating terms $L - M$ and the parameter $-\beta c_n$ $(= zn)$. Let us say we denote the n'th contribution $\Delta(n, z, M, L)$ and for simplicity write this as

$$\Delta(n, z, M, L) = n^M e^{nz} E_1(nz) + \left(\frac{1}{n^{L-M+1}} - A\right)\frac{L!}{z^{L+1}}. \tag{3.63}$$

We know that the relative error of $e^{nz}E_1(nz)$ may be as large as $\epsilon_{E_1} \sim 10^{-5}$ when calculated as we do. z has double precision accuracy and the poles are found with an accuracy of approximately 10 decimals. If we exclude other error sources and assume that $A = A(n, z, M, L)$ is found exactly, the calculated contribution may be written

$$\begin{aligned}\Delta(n, z, M, L)_{calc} &= \Delta(n, z, M, L) - \epsilon_{E_1}\left[n^M e^{nz} E_1(nz)\right] \\ &-\epsilon_z\left[\left(A - \frac{1}{n^{L-M+1}}\right)\frac{(L+1)!}{z^{L+1}}\right] - \epsilon_n\left[n^M M e^{nz} E_1(nz) - \frac{(L-M+1)L!}{z^{L+1}n^{L-M+1}}\right]\end{aligned} \tag{3.64}$$

The total relative error then satisfies

$$\epsilon = \frac{\Delta(n,z,M,L) - \Delta(n,z,M,L)_{calc}}{\Delta(n,z,M,L)} = \epsilon_{E_1}\left[\frac{n^M e^{nz} E_1(nz)}{\Delta(n,z,M,L)}\right] + \epsilon_z\left[\frac{\left(A - \frac{1}{n^{L-M+1}}\right)\frac{(L+1)!}{z^{L+1}}}{\Delta(n,z,M,L)}\right] + \epsilon_n\left[\frac{n^M M e^{nz} E_1(nz) - \frac{(L-M+1)L!}{z^{L+1}n^{L-M+1}}}{\Delta(n,z,M,L)}\right]. \quad (3.65)$$

In words: If the argument is small and we have chosen too many convergence accelerating terms we expect inaccurate results due to ϵ_z and ϵ_n. On the other hand, if fewer terms are chosen the sum converges slowly and we get bad results for the higher order derivative due to ϵ_{E_1}.

	$G \cdot 10\ [1/m]$	$\frac{c}{h} = -1.0$		
	L			
N	0	1	2	3
1	-0.30542, -1.68096	-0.33631, -1.68757	-0.33582, -1.68785	-0.33659, -1.68737
2	-0.34338, -1.68920	-0.33611, -1.68751	-0.33616, -1.68726	-0.33611, -1.68729
3	-0.34250, -1.68856	-0.33613, -1.68725	-0.33615, -1.68727	-0.33611, -1.68729
4	-0.33335, -1.68665	-0.33612, -1.68725	-0.33611, -1.68730	-0.33612, -1.68729
5	-0.33353, -1.68678	-0.33611, -1.68730	-0.33611, -1.68730	-0.33612, -1.68729
6	-0.33756, -1.68710	-0.33612, -1.68731	-0.33612, -1.68729	-0.33612, -1.68729
Alt. 2	-0.33612, -1.68729			
	$G \cdot 10\ [1/m]$	$\frac{c}{h} = -0.5$		
	L			
N	0	1	2	3
1	-0.33729, -1.93994	-0.36400, -1.94820	-0.36412, -1.94822	-0.36640, -1.94839
2	-0.37251, -1.95060	-0.36627, -1.94850	-0.36631, -1.94822	-0.36617, -1.94824
3	-0.37177, -1.94983	-0.36630, -1.94820	-0.36628, -1.94822	-0.36617, -1.94822
4	-0.36376, -1.94741	-0.36614, -1.94818	-0.36614, -1.94822	-0.36616, -1.94822
5	-0.36391, -1.94758	-0.36613, -1.94824	-0.36614, -1.94822	-0.36616, -1.94822
6	-0.36741, -1.94863	-0.36617, -1.94824	-0.36617, -1.94822	-0.36616, -1.94822
7	-0.36735, -1.94857	-0.36617, -1.94822	-0.36617, -1.94822	-0.36616, -1.94822
Alt. 2	-0.36616, -1.94822			
	$G \cdot 10\ [1/m]$	$\frac{c}{h} = -0.1$		
	L			
N	0	1	2	3
1	-0.41996, -2.54286	-0.41996, -2.55289	-0.42106, -2.55300	-0.42210, -2.55384
2	-0.42737, -2.55700	-0.42461, -2.55444	-0.42462, -2.55436	-0.42455, -2.55432
3	-0.42711, -2.55431	-0.42469, -2.55431	-0.42461, -2.55432	-0.42455, -2.55429
4	-0.42347, -2.55424	-0.42453, -2.55424	-0.42452, -2.55426	-0.42452, -2.55428
5	-0.42352, -2.55346	-0.42451, -2.55426	-0.42452, -2.55426	-0.42452, -2.55428
6	-0.42510, -2.55475	-0.42454, -2.55428	-0.42454, -2.55427	-0.42452, -2.55428
7	-0.42507, -2.55470	-0.42455, -2.55427	-0.42454, -2.55427	-0.42452, -2.55428
8	-0.42507, -2.55398	-0.42454, -2.55427	-0.42454, -2.55427	-0.42452, -2.55428
9	-0.42520, -2.55400	-0.42453, -2.55427	-0.42454, -2.55427	-0.42452 ,-2.55428
10	-0.42521, -2.55446	-0.42453, -2.55427	-0.42454, -2.55427	-0.42452, -2.55428
11	-0.42577, -2.55444	-0.42454, -2.55427	-0.42454, -2.55427	-0.42452, -2.55428
Alt. 2	-0.42454, -2.55427			

Table 3.1: *Green's function as function of number of terms in the infinite series, N, and extra convergence accelerating terms, L. ($\omega = 1s^{-1}$, $h = 10m$, $r = 10m$, $z = -5m$, $u = \alpha = 0$ and $U = 1m/s$). Alt.2 denotes G as calculated in section 3.1.2.*

	$\frac{\partial G}{\partial a} \cdot 10^2\ [1/m^2]$ $\frac{c}{h} = -1.0$			
	$L-1$			
N	0	1	2	3
1	1.78366, -1.10025	1.73655, -1.10358	1.73874, -1.10400	1.74049, -1.10245
2	1.73091, -1.10350	1.74191, -1.10266	1.74180, -1.10226	1.74170, -1.10236
3	1.73225, -1.10295	1.74190, -1.10230	1.74179, -1.10232	1.74170, -1.10239
4	1.74584, -1.10202	1.74164, -1.10233	1.74166, -1.10240	1.74168, -1.10239
5	1.74555, -1.10215	1.74164, -1.10241	1.74166, -1.10240	1.74168, -1.10239
6	1.74395, -1.10257	1.74168, -1.10239	1.74168, -1.10241	1.74167, -1.10239
Alt. 2	1.74168, -1.10238			

	$\frac{\partial G}{\partial a} \cdot 10^2\ [1/m^2]$ $\frac{c}{h} = -0.5$			
	$L-1$			
N	0	1	2	3
1	2.04313, -1.28106	1.99492, -1.28903	1.99548, -1.29103	1.98863, -1.29005
2	1.98034, -1.29200	1.99160, -1.28896	1.99150, -1.28898	1.99191, -1.28905
3	1.98171, -1.29075	1.99159, -1.28893	1.99157, -1.28998	1.99192, -1.28902
4	1.99625, -1.28805	1.99195, -1.28890	1.99197, -1.28902	1.99191, -1.28902
5	1.99597, -1.28832	1.99197, -1.28905	1.99197, -1.28903	1.99191, -1.28902
6	1.98966, -1.28961	1.99191, -1.28907	1.99190, -1.28903	1.99191, -1.28903
7	1.98976, -1.28941	1.99190, -1.28902	1.99190, -1.28903	1.99191, -1.28903
8	1.99327, -1.28874	1.99190, -1.28900	1.99191, -1.28902	1.99190, -1.28902
9	1.99323, -1.28879	1.99191, -1.28903	1.99191, -1.28902	1.99190, -1.28902
10	1.99099, -1.28922	1.99192, -1.28904	1.99191, -1.28903	1.99190, -1.28903
Alt. 2	1.99192, -1.28902			

	$\frac{\partial G}{\partial a} \cdot 10^2\ [1/m^2]$ $\frac{c}{h} = -0.1$			
	$L-1$			
N	0	1	2	3
1	2.56961, -1.66084	2.55296, -1.67846	2.54948, -1.67876	2.54408, -1.68220
2	2.52715, -1.68822	2.53310, -1.68374	2.53100, -1.68349	2.53137, -1.68326
3	2.52743, -1.68669	2.53085, -1.68321	2.53106, -1.68323	2.53138, -1.68306
4	2.53303, -1.68131	2.53154, -1.68292	2.53156, -1.68297	2.53154, -1.68299
5	2.53299, -1.68159	2.53160, -1.68299	2.53156, -1.68299	2.53155, -1.68300
6	2.53075, -1.68388	2.53153, -1.68306	2.53152, -1.68304	2.53157, -1.68302
7	2.53076, -1.68378	2.53150, -1.68304	2.53152, -1.68304	2.53157, -1.68302
8	2.53195, -1.68251	2.53148, -1.68301	2.53148, -1.68302	2.53151, -1.68301
9	2.53195, -1.68255	2.53149, -1.68302	2.53148, -1.68301	2.53152, -1.68301
10	2.53122, -1.68337	2.53154, -1.68303	2.53154, -1.68303	2.53158, -1.68302
11	2.53122, -1.68334	2.53153, -1.68302	2.53154, -1.68303	2.53158, -1.68302
Alt. 2	2.53152, -1.68302			

Table 3.2: $\frac{\partial G}{\partial a}$ *as function of number of terms in the infinite series,* N*, and extra convergence accelerating terms,* $L-1$ *(*$\omega = 1s^{-1}$*,* $h = 10m$*,* $r = 10m$*,* $z = -5m$*,* $u = \alpha = 0$ *and* $U = 1m/s$*). Alt.2 denotes* $\frac{\partial G}{\partial a}$ *as calculated in section 3.1.2.*

	$(\Re\{\frac{\partial G}{\partial a}\}, \Im\{\frac{\partial G}{\partial a}\}) \cdot 10^2\ [1/m^2]$			
	h			
N	5m	10m	20m	40m
1	3.40392, -3.52176	1.98863, -1.29005	1.71183, -0.84320	1.91974, -0.85487
2	3.40384, -3.52174	1.99191, -1.28905	1.73038, -0.83524	1.74150, -0.81451
3	3.40391, -3.52178	1.99192, -1.28902	1.73782, -0.83353	1.76384, -0.80439
4	3.40383, -3.52175	1.99191, -1.28901	1.73941, -0.83311	1.75480, -0.80083
5	3.40392, -3.52178	1.99191, -1.28902	1.73966, -0.83301	1.76466, -0.79929
Alt. 2	3.40390, -3.52176	1.99192, -1.28902	1.73966, -0.83299	1.76123, -0.79781

Table 3.3: $\frac{\partial G}{\partial a}$ *for increasing depth.* ($U = 1m/s$, $r = 1m$, $z = c = -5m$, $\omega = 1s^{-1}$, $\alpha = u = 0$ *and* $L - 1 = 3$.) *Alt.2 denotes* $\frac{\partial G}{\partial a}$ *as calculated in sec.3.1.2.*

	$\frac{\partial^4 G}{\partial a^4} \cdot 10^5\ [1/m^5]$			
	$L-4$			
N	0	1	2	3
1	5.31529, -2.42884	3.92881, -3.43403	3.47366, -3.50473	0.92882, -4.32982
2	0.30358, -3.47754	0.62802, -3.22217	0.62072, -3.15927	0.77646, -3.10674
3	0.35729, -3.27478	0.64187, -3.07665	0.66949, -3.08052	0.80070, -3.04333
4	1.05689, -2.91166	0.93303, -3.00369	0.93495, -3.01525	0.91139, -3.02481
5	1.05742, -2.93513	0.94198, -3.01518	0.93607, -3.01286	0.91434, -3.02130
6	0.88523, -3.13084	0.94198, -3.08383	0.94889, -3.08003	0.95726, -3.07949
7	0.87345, -3.15517	0.93497, -3.11249	0.93694, -3.11369	0.94497, -3.11336
8	0.69812, -2.98418	0.65868, -3.01260	0.65907, -3.01427	0.65763, -3.01675
9	0.71954, -2.90751	0.68152, -2.93391	0.68056, -2.93323	0.67922, -2.93565
10	1.29814, -3.07582	1.13247, -3.05682	1.32434, -3.05595	1.13255, -3.05731
Alt. 2	0.87641, -3.04361			

Table 3.4: $\frac{\partial^4 G}{\partial a^4}$ *as function of number of terms in the infinite series,* N*, and extra convergence accelerating terms,* $L - 4$ ($\omega = 1s^{-1}$, $h = 10m$, $r = 10m$, $z = -5m$, $c = -1m$, $u = \alpha = 0$ *and* $U = 1m/s$). *Alt.2 denotes* $\frac{\partial^4 G}{\partial a^4}$ *as calculated in section 3.1.2.*

	$(\Re\{\frac{\partial^4 G}{\partial a^4}\}, \Im\{\frac{\partial^4 G}{\partial a^4}\})\ [1/m^5]$			
	r			
N	$15m$	$50m$	$100m$	$200m$
0	0.58910, -0.43481	9.68294, -0.58609	2.59879, 6.86393	-4.97457, -1.74530
1	0.97403, -0.26405	9.68254, -0.58634	2.59893, 6.86404	-4.97450, -1.74527
2	1.03189, -0.25273	9.69015, -0.59282	2.60521, 6.86285	-4.97294, -1.74587
3	1.03214, -0.25350	9.69015, -0.60094	2.60432, 6.86012	-4.97314, -1.74659
Alt. 2	1.03797, -0.25236	9.68281, -0.58608	2.59870, 6.86400	-4.97461, -1.74527
	$\times 10^{-5}$	$\times 10^{-6}$	$\times 10^{-6}$	$\times 10^{-6}$

Table 3.5: $\frac{\partial^4 G}{\partial a^4}$ *for increasing distance from source point,* r. ($U = 1m/s$, $h = 10m$, $z = c = -5m$, $\omega = 1s^{-1}$ *and* $\alpha = u = 0$. $L - 4 = 3$.) *Alt.2 den.* $\frac{\partial^4 G}{\partial a^4}$ *as calc. in 3.1.2*

3.2.2 Alternative 2

In this section the Green's function as expressed in equation 3.32 will be evaluated numerically. We see that the integrand has square root singularities at $k = \sigma_1$ and σ_2. This means the integration scheme needs to be modified. In addition σ_1 and σ_2 have to be found numerically. We will find the location of σ_3 (that is; when to change the integration variables), and decide how many terms are needed in the infinite series. The Bessel functions are calculated in the NAG-library.

Location of singularities

By Newton-Raphsons method we will find the solutions to

$$k \tanh kh - \nu = \pm 2\tau k \tag{3.66}$$

for k on the positive real axis. We will have the same kinds of estimates as in the previous section: That is, if νh is large,

$$\sigma_1 = \frac{\nu}{1+2\tau} \qquad \sigma_2 = \frac{\nu}{1-2\tau} \tag{3.67}$$

are good guesses. And if νh is small, the terms $\sigma_{1,2}h$ are small, and may be used as approximations for $\tanh \sigma_{1,2}h$. We then get the estimates

$$\sigma_1 = (\sqrt{\tau^2 + \nu h} - \tau)/h \qquad \sigma_2 = (\sqrt{\tau^2 + \nu h} + \tau)/h. \tag{3.68}$$

Using equation 3.67 to find σ_1 and σ_2 for $\nu h > 0.5$ and $\nu h > 1.0$, respectively, and equation 3.68 else, we find the solutions correct to 10 decimal places after at most 4-5 iterations.

Integration routine

The k-integral part of the Green's function, G_1^k, may be written

$$G_1^k = \int_0^{\sigma_1} F_1(k)dk + \int_{\sigma_1}^{\sigma_2} F_1(k)dk + \int_{\sigma_2}^{\sigma_3} F_2(k)dk, \tag{3.69}$$

where the integrand has square root singularities at σ_1 and σ_2. A method to circumvent this problem is given in Press et. al. [1989]: If the integrand contains a square root singularity in the lower end point, a, the identity

$$\int_a^b F(k)dk = \int_0^{\sqrt{b-a}} 2tF(a+t^2)dt \tag{3.70}$$

is used, and

$$\int_a^b F(k)dk = \int_0^{\sqrt{b-a}} 2tF(b-t^2)dt \tag{3.71}$$

for a singularity at the upper limit. For singularities at both endpoints the integral is divided into two parts. Thus, we write

$$G_1^k = \int_0^{\sigma_1} F_1(k)dk + \int_{\sigma_1}^{\frac{\sigma_1+\sigma_2}{2}} F_1(k)dk + \int_{\frac{\sigma_1+\sigma_2}{2}}^{\sigma_2} F_1(k)dk + \int_{\sigma_2}^{\sigma_3} F_2(k)dk, \tag{3.72}$$

which after change of variables gives

$$G_1^k = \int_0^{\sqrt{\sigma_1}} 2tF_1(\sigma_1 - t^2)dt + \int_0^{\sqrt{\frac{\sigma_1+\sigma_2}{2}}} 2t[F_1(\sigma_1 + t^2) + F_1(\sigma_2 - t^2)]dt + \int_0^{\sqrt{\sigma_3-\sigma_2}} 2tF_2(\sigma_2 + t^2)dt. \tag{3.73}$$

There are still numerical problems (due to overflow) if the integration scheme includes the endpoints. This is however not the case for the Gauss-Kronrod scheme.

Number of terms in the infinite series

There are two factors deciding the numbers of terms needed; the magnitude of kr and ρ_s. We know that $1 = \sum_{n=-\infty}^{\infty} J_n(kr)$ (eq.3.30 with $\gamma t = i$), and since $J_n(kr)$ decreases for larger kr, this indicates that the series converges slower for larger r. In an interval around $k = \nu$ the absolute value of ρ_s is close to one and thus has no convergence generating effect, and we conclude that the number of terms needed may be written $N = f(r\nu)$ when N is constant in k.

Table 3.6 shows number of terms vs. increasing $r\nu$. It seems like a good guess to set N equal to $f(r\nu) = 2 + 7\ln(1 + r\nu)$. The derivatives need more terms to obtain the same accuracy, this may be viewed in table 3.7. Approximately two extra terms for each degree of derivative seems to be sufficient, giving $N = 2(1 + M) + 7\ln(1 + r\nu)$. However, there is no harm done by adding too many terms.

Location of σ_3

To achieve good results for the c-derivatives of the Green's function we find that $\sigma_3 h >\approx 50$ and $\sigma_3 >\approx 20\sigma_2$. Since $1 - \tanh 50 \approx 10^{-43}$ this is most likely due to inaccurate calculation of the last integral in equation 3.40, which includes the exponential integral. We have integrated straight forward while Faltinsen and Michelsen [1974], who considered a similar problem for zero speed, used some "mid-point-rule". Then, they could change the integration variables already when $kh = 4.5$.

	$(\Re\{G\}, \Im\{G\})[1/m]$			
	$r\nu$			
N	1.	4.	16.	64.
1	-0.335750, -1.993804			
2	-0.326534, -1.972564	0.110696, 1.028420		
3	-0.327867, -1.972577	0.131969, 1.013368		
4	-0.327845, -1.972575	0.132801, 1.016799		
5	-0.327843, -1.972575	0.132377, 1.016717		
6	-0.327843, -1.972575	0.132406, 1.016678	-0.963482, 5.091100	
7	$\boxed{-0.327845, -1.972576}^{*}$	0.132409, 1.016683	-1.000300, 5.042377	
8	$\times 10^{-1}$	0.132408, 1.016682	-0.986222, 5.037272	
9		0.132408, 1.016682	-0.986169, 5.040611	-2.695217, -0.474791
12		$\boxed{0.132417, 1.016681}^{*}$	-0.986183, 5.040301	-3.150304, 0.702767
13		$\times 10^{-1}$	-0.986722, 5.040301	-2.972010, -0.366580
14			-0.986722, 5.040301	-2.265113 , -0.136883
27			$\boxed{-0.986647, 5.040299}^{*}$	-2.567074, 0.079640
28			$\times 10^{-2}$	-2.567073, 0.079641
29				-2.567073, 0.079641
				$\boxed{-2.566987, 0.079674}^{*}$
				$\times 10^{-2}$

Table 3.6: *Greeen's function for increasing $r\nu$ as functions of terms in the infinite series ($\omega = 1s^{-1}$, $h = 10m$, $z = c = -5m$, $u = \alpha = 0$ and $U = 1m/s$).* * *The numbers in the boxes are due to the Green's function calculated by the first alternative, with $N = 4$ and $L = 3$.*

3.2.3 Verification of the Green's function calculations

In the previous sections we have evaluated the Green's function in two ways. The first, G_{Alt1}, is expected to give give good results for moderate and large r/h-ratio. It's higher order derivatives, however, need a large r/h-ratio in order to produce correct values. The other one, G_{Alt2}, and its multipoles are expected to be more accurate, except for very small τ. For $\tau = 0$, G_{Alt2} fails completely when written as we do.

Since we want to evaluate the Green's function and its derivatives on the control surface, which represents a moderate ratio r/h, we have no choice but to choose the Green's function evaluated analytically in section 3.1.2 and numerically in 3.2.2; G_{Alt2}.

The accuracy of the Green's function and its derivatives should be approximately of the same order of magnitude as in the infinite depth case programmed by Zhao and used in the original MULDIF program (Zhao and Faltinsen [1989]). Since the relation

$$\left.\frac{\partial^M G(\vec{A},\vec{B};\alpha)}{\partial B_j^M}\right|_{\substack{\vec{A}=\vec{x}\\ \vec{B}=\vec{a}}} = \left.\frac{\partial^M G(\vec{A},\vec{B};\alpha+\pi)}{\partial A_j^M}\right|_{\substack{\vec{A}=\vec{a}\\ \vec{B}=\vec{x}}} \qquad \begin{matrix} x_j \in (x,y,z) = \vec{x} \\ a_j \in (a,b,c) = \vec{a} \end{matrix} \tag{3.74}$$

	$(\Re\{\frac{\partial^6 G}{\partial a^6}\}, \Im\{\frac{\partial^6 G}{\partial a^6}\})[1/m^7]$			
	$r\nu$			
N	1.	4.	16.	64.
13	8.171931, 0.131364			
14	8.183994, 0.131351	-6.259366, -6.472850		
15	8.182447, 0.132384	-6.259366, -7.963828		
16	8.182623, 0.132273	-5.310369, -7.963828		
17	8.182611, 0.132292	-5.310369, -7.416958	0.006527, -6.876846	
18	8.182612, 0.132291	-5.593000, -7.416958	0.012527, -6.876844	
19	8.182612, 0.132291	-5.593000, -7.536915	0.012527, -6.303612	
20		-5.593909, -7.536915	0.075354, -6.303616	
21	$\times 10^{-5}$	-5.593909, -7.536915	0.075355, -6.303614	
23			0.075355, -6.303614	3.215049, -0.248420
24		$\times 10^{-8}$	0.075355, -6.303614	3.213112, -0.246853
33				3.213111, -0.247818
34			$\times 10^{-8}$	3.213110, -0.247818
35				3.213110, -0.247818
				$\times 10^{-8}$

Table 3.7: $\frac{\partial^6 G}{\partial a^6}$ *for increasing* $r\nu$ *as functions of terms in the infinite series* ($\omega = 1s^{-1}$, $h = 10m$, $z = c = -5m$, $u = \alpha = 0$ *and* $U = 1m/s$).

is valid, we may relate the accuracy to the Laplace equation and the free surface condition given in the beginning of this chapter.

The free surface condition is valid in the two-dimensional plane $z = 0$, and we may differentiate in x and y and still get a zero right hand side. In table 3.8 some of the derivatives are listed for decreasing depth. We see that the accuracy is not dependent of depth and comparable to infinite depth results.

As the source point tends to the free surface the results gets poorer. This is illustated in table 3.9. But, since the accuracy of the multipoles still is comparable to those due to infinite depth, we are satisfied. It shows, however, that the singularity points inside the body (see Chapter 4) must not be situated too close to the free surface.

The Laplace equation is valid in the whole fluid domain, except from the source point. We may therefore differentiate the equation with respect to the three evaluation point coordinates. An example is given in table 3.10.

Figure 3.6 shows a contour plot[1] of the Green's function for various depth. At a water depth of 50 meters and frequency equal one, the Green's function should approximately agree with the infinite depth Green's function: The frequency and depth correspond to a wave length of $\approx 62m$. We know that the sea floor has little effect upon the wave if the water depth exceeds half the wave length. Here $\lambda/(2h) \approx 0.6$ and there should be

[1]We have used an UNIRAS plotting program

no visible difference due to the wave part of the Green's function, between infinite water depth and a depth of $50m$. A closer view of the difference along the current axis can be seen in figure 3.7. The curves agree rather well, indicating that the plotting procedure may be inaccurate. However, it illustrates the basic patterns: The wave lengths get shorter for more shallow water, and is shortest upstream (left side).

As the current velocity tends to zero the errors in the Green's function increase. For $\tau = \frac{U\omega}{g}$ less than 0.0001, the zero current Green's function is assumed to give better results. This is illustrated in figure 3.8, where a comparison with the Green's function G_{Alt1} (which has nearly a constant error as U varies), has been made. In our previous calculations it is assumed that U is always positive. If anybody insists on a negative current value as input, we take the absolute value and add π to the current angle.

At last we check whether the Green's function satisfies the frequency limits given in section 3.1.3. It may be seen from figure 3.9 that the results are reasonable . However, we bear in mind that $\tau = \frac{\omega U}{g}$ is a small quantity in this context so that the high frequency results are really unimportant when a current is present.

	$h=\infty$	$h=100m$	$h=10m$	$h=6m$
$\left(\nu G - \frac{\partial G}{\partial z} - 2i\tau(\cos\alpha\frac{\partial G}{\partial x} + \sin\alpha\frac{\partial G}{\partial y})\right)^{\bullet}$	$3.5\cdot10^{-7}$	$1.2\cdot10^{-8}$	$2.0\cdot10^{-8}$	$6.5\cdot10^{-8}$
$\frac{\partial}{\partial x}\left(\nu G - \frac{\partial G}{\partial z} - 2i\tau(\cos\alpha\frac{\partial G}{\partial x} + \sin\alpha\frac{\partial G}{\partial y})\right)^{\bullet}$	$1.4\cdot10^{-7}$	$8.1\cdot10^{-8}$	$4.7\cdot10^{-8}$	$4.7\cdot10^{-8}$
$\frac{\partial}{\partial y}\left(\nu G - \frac{\partial G}{\partial z} - 2i\tau(\cos\alpha\frac{\partial G}{\partial x} + \sin\alpha\frac{\partial G}{\partial y})\right)^{\bullet}$	$4.8\cdot10^{-7}$	$5.4\cdot10^{-8}$	$6.5\cdot10^{-8}$	$8.2\cdot10^{-8}$
$\frac{\partial^2}{\partial x\partial y}\left(\nu G - \frac{\partial G}{\partial z} - 2i\tau(\cos\alpha\frac{\partial G}{\partial x} + \sin\alpha\frac{\partial G}{\partial y})\right)^{\bullet}$	$6.2\cdot10^{-7}$	$1.2\cdot10^{-7}$	$1.1\cdot10^{-7}$	$8.2\cdot10^{-9}$
$\frac{\partial^2}{\partial x^2}\left(\nu G - \frac{\partial G}{\partial z} - 2i\tau(\cos\alpha\frac{\partial G}{\partial x} + \sin\alpha\frac{\partial G}{\partial y})\right)^{\bullet}$	$4.7\cdot10^{-7}$	$2.5\cdot10^{-8}$	$4.2\cdot10^{-8}$	$2.7\cdot10^{-8}$
$\frac{\partial^2}{\partial y^2}\left(\nu G - \frac{\partial G}{\partial z} - 2i\tau(\cos\alpha\frac{\partial G}{\partial x} + \sin\alpha\frac{\partial G}{\partial y})\right)^{\bullet}$	$2.0\cdot10^{-6}$	$1.3\cdot10^{-7}$	$8.8\cdot10^{-8}$	$1.1\cdot10^{-7}$
$\frac{\partial^3}{\partial x^3}\left(\nu G - \frac{\partial G}{\partial z} - 2i\tau(\cos\alpha\frac{\partial G}{\partial x} + \sin\alpha\frac{\partial G}{\partial y})\right)^{\bullet}$	$2.3\cdot10^{-6}$	$6.0\cdot10^{-8}$	$1.4\cdot10^{-7}$	$1.2\cdot10^{-7}$
$\frac{\partial^5}{\partial x^5}\left(\nu G - \frac{\partial G}{\partial z} - 2i\tau(\cos\alpha\frac{\partial G}{\partial x} + \sin\alpha\frac{\partial G}{\partial y})\right)^{\bullet}$	$1.4\cdot10^{-5}$	$8.3\cdot10^{-7}$	$1.8\cdot10^{-7}$	$3.0\cdot10^{-7}$

Table 3.8: *Free surface equation for Green's function and some derivatives. Comparison of present method and infinite depth Green's function in the original MULDIF program. The expressions are non-dimensionalized by* $\frac{\partial^{(M_1+M_2)}}{\partial x^{M_1}\partial y^{M_2}}\left(\nu G - \frac{\partial G}{\partial z} - 2i\tau(\cos\alpha\frac{\partial G}{\partial x} + \sin\alpha\frac{\partial G}{\partial y})\right)^{\bullet} = \left|\frac{\partial^{(M_1+M_2)}}{\partial x^{M_1}\partial y^{M_2}}\left(\nu G - \frac{\partial G}{\partial z} - 2i\tau(\cos\alpha\frac{\partial G}{\partial x} + \sin\alpha\frac{\partial G}{\partial y})\right)\right| / \max\left(\left|\frac{\partial^{(M_1+M_2+1)}G}{\partial x^{M_1+1}\partial y^{M_2}}\right|, \left|\frac{\partial^{(M_1+M_2+1)}G}{\partial x^{M_1}\partial y^{M_2+1}}\right|, \left|\frac{\partial^{(M_1+M_2+1)}G}{\partial x^{M_1}\partial y^{M_2}\partial z}\right|\right)$ *($U = 1m/s$, $r = 10m$, $z = 0m$, $c = -5m$, $\omega = 1s^{-1}$, $\alpha = -\frac{\pi}{4}$ and $u = 0$).*

	$\lvert\frac{c}{\tau}\rvert = 0.2$	$\lvert\frac{c}{\tau}\rvert = 0.1$	$\lvert\frac{c}{\tau}\rvert = 0.05$	$\lvert\frac{c}{\tau}\rvert = 0.01$
$\left(\nu G - \frac{\partial G}{\partial z} - 2i\tau(\cos\alpha\frac{\partial G}{\partial x} + \sin\alpha\frac{\partial G}{\partial y})\right)^{\bullet}$	$1.1 \cdot 10^{-7}$	$5.8 \cdot 10^{-7}$	$2.6 \cdot 10^{-6}$	$4.1 \cdot 10^{-5}$
$\frac{\partial}{\partial x}\left(\nu G - \frac{\partial G}{\partial z} - 2i\tau(\cos\alpha\frac{\partial G}{\partial x} + \sin\alpha\frac{\partial G}{\partial y})\right)^{\bullet}$	$1.3 \cdot 10^{-6}$	$9.4 \cdot 10^{-6}$	$5.2 \cdot 10^{-5}$	$1.1 \cdot 10^{-2}$
$\frac{\partial}{\partial y}\left(\nu G - \frac{\partial G}{\partial z} - 2i\tau(\cos\alpha\frac{\partial G}{\partial x} + \sin\alpha\frac{\partial G}{\partial y})\right)^{\bullet}$	$1.3 \cdot 10^{-6}$	$9.6 \cdot 10^{-6}$	$4.6 \cdot 10^{-5}$	$9.4 \cdot 10^{-3}$
$\frac{\partial^2}{\partial x \partial y}\left(\nu G - \frac{\partial G}{\partial z} - 2i\tau(\cos\alpha\frac{\partial G}{\partial x} + \sin\alpha\frac{\partial G}{\partial y})\right)^{\bullet}$	$1.0 \cdot 10^{-5}$	$2.7 \cdot 10^{-5}$	$1.3 \cdot 10^{-3}$	$4.8 \cdot 10^{-1}$
$\frac{\partial^2}{\partial x^2}\left(\nu G - \frac{\partial G}{\partial z} - 2i\tau(\cos\alpha\frac{\partial G}{\partial x} + \sin\alpha\frac{\partial G}{\partial y})\right)^{\bullet}$	$3.5 \cdot 10^{-5}$	$5.2 \cdot 10^{-5}$	$4.5 \cdot 10^{-3}$	$8.9 \cdot 10^{-1}$
$\frac{\partial^2}{\partial y^2}\left(\nu G - \frac{\partial G}{\partial z} - 2i\tau(\cos\alpha\frac{\partial G}{\partial x} + \sin\alpha\frac{\partial G}{\partial y})\right)^{\bullet}$	$1.8 \cdot 10^{-5}$	$3.7 \cdot 10^{-5}$	$1.9 \cdot 10^{-3}$	$6.8 \cdot 10^{-1}$
$\frac{\partial^3}{\partial x^3}\left(\nu G - \frac{\partial G}{\partial z} - 2i\tau(\cos\alpha\frac{\partial G}{\partial x} + \sin\alpha\frac{\partial G}{\partial y})\right)^{\bullet}$	$8.0 \cdot 10^{-5}$	$1.3 \cdot 10^{-3}$	$9.2 \cdot 10^{-2}$	$8.7 \cdot 10^{-1}$
$\frac{\partial^5}{\partial x^5}\left(\nu G - \frac{\partial G}{\partial z} - 2i\tau(\cos\alpha\frac{\partial G}{\partial x} + \sin\alpha\frac{\partial G}{\partial y})\right)^{\bullet}$	$2.2 \cdot 10^{-3}$	$1.4 \cdot 10^{-1}$	1.1	1.1

a) $h = \infty$.

	$\lvert\frac{c}{\tau}\rvert = 0.2$	$\lvert\frac{c}{\tau}\rvert = 0.1$	$\lvert\frac{c}{\tau}\rvert = 0.05$	$\lvert\frac{c}{\tau}\rvert = 0.01$
$\left(\nu G - \frac{\partial G}{\partial z} - 2i\tau(\cos\alpha\frac{\partial G}{\partial x} + \sin\alpha\frac{\partial G}{\partial y})\right)^{\bullet}$	$2.6 \cdot 10^{-8}$	$4.9 \cdot 10^{-8}$	$5.9 \cdot 10^{-8}$	$6.4 \cdot 10^{-4}$
$\frac{\partial}{\partial x}\left(\nu G - \frac{\partial G}{\partial z} - 2i\tau(\cos\alpha\frac{\partial G}{\partial x} + \sin\alpha\frac{\partial G}{\partial y})\right)^{\bullet}$	$5.4 \cdot 10^{-8}$	$1.4 \cdot 10^{-7}$	$2.0 \cdot 10^{-7}$	$4.8 \cdot 10^{-2}$
$\frac{\partial}{\partial y}\left(\nu G - \frac{\partial G}{\partial z} - 2i\tau(\cos\alpha\frac{\partial G}{\partial x} + \sin\alpha\frac{\partial G}{\partial y})\right)^{\bullet}$	$3.8 \cdot 10^{-8}$	$1.1 \cdot 10^{-7}$	$1.7 \cdot 10^{-7}$	$4.1 \cdot 10^{-3}$
$\frac{\partial^2}{\partial x \partial y}\left(\nu G - \frac{\partial G}{\partial z} - 2i\tau(\cos\alpha\frac{\partial G}{\partial x} + \sin\alpha\frac{\partial G}{\partial y})\right)^{\bullet}$	$6.4 \cdot 10^{-8}$	$8.2 \cdot 10^{-7}$	$4.8 \cdot 10^{-5}$	1.2
$\frac{\partial^2}{\partial x^2}\left(\nu G - \frac{\partial G}{\partial z} - 2i\tau(\cos\alpha\frac{\partial G}{\partial x} + \sin\alpha\frac{\partial G}{\partial y})\right)^{\bullet}$	$9.7 \cdot 10^{-8}$	$2.6 \cdot 10^{-6}$	$2.5 \cdot 10^{-4}$	$9.5 \cdot 10^{-1}$
$\frac{\partial^2}{\partial y^2}\left(\nu G - \frac{\partial G}{\partial z} - 2i\tau(\cos\alpha\frac{\partial G}{\partial x} + \sin\alpha\frac{\partial G}{\partial y})\right)^{\bullet}$	$4.7 \cdot 10^{-8}$	$8.3 \cdot 10^{-7}$	$8.4 \cdot 10^{-5}$	$9.7 \cdot 10^{-1}$
$\frac{\partial^3}{\partial x^3}\left(\nu G - \frac{\partial G}{\partial z} - 2i\tau(\cos\alpha\frac{\partial G}{\partial x} + \sin\alpha\frac{\partial G}{\partial y})\right)^{\bullet}$	$1.6 \cdot 10^{-7}$	$4.3 \cdot 10^{-5}$	$6.1 \cdot 10^{-4}$	$5.0 \cdot 10^{-1}$
$\frac{\partial^5}{\partial x^5}\left(\nu G - \frac{\partial G}{\partial z} - 2i\tau(\cos\alpha\frac{\partial G}{\partial x} + \sin\alpha\frac{\partial G}{\partial y})\right)^{\bullet}$	$1.0 \cdot 10^{-2}$	$7.4 \cdot 10^{-1}$	$9.6 \cdot 10^{-1}$	$4.9 \cdot 10^{-1}$

b) $h = 10m$.

Table 3.9: *Free surface equation for Green's function and some derivatives for source point close to the free surface. Comparison of present method and infinite depth Green's function in the original MULDIF program. The expressions are non-dimensionalized in the same way as in the previous table.* ($U = 1m/s$, $r = 10m$, $z = 0m$, $\omega = 1s^{-1}$, $\alpha = -\frac{\pi}{4}$ *and* $u = 0$).

	$h=\infty$	$h=1000.$		$h=\infty$	$h=1000.$
$\nabla^2 G^\bullet$	$3.4\cdot10^{-7}$	$1.1\cdot10^{-7}$	$\frac{\partial^3\nabla^2 G^\bullet}{\partial x^2\partial y}$	$1.4\cdot10^{-7}$	$1.4\cdot10^{-7}$
$\frac{\partial\nabla^2 G^\bullet}{\partial x}$	$6.2\cdot10^{-8}$	$4.1\cdot10^{-9}$	$\frac{\partial^3\nabla^2 G^\bullet}{\partial y^2\partial z}$	$3.6\cdot10^{-8}$	$1.8\cdot10^{-7}$
$\frac{\partial\nabla^2 G^\bullet}{\partial y}$	$1.8\cdot10^{-7}$	$1.6\cdot10^{-8}$	$\frac{\partial^3\nabla^2 G^\bullet}{\partial x\partial y\partial z}$	$3.8\cdot10^{-7}$	$4.8\cdot10^{-8}$
$\frac{\partial\nabla^2 G^\bullet}{\partial z}$	$7.3\cdot10^{-7}$	$3.1\cdot10^{-8}$	$\frac{\partial^3\nabla^2 G^\bullet}{\partial x\partial y^2}$	$2.1\cdot10^{-7}$	$1.4\cdot10^{-7}$
$\frac{\partial^2\nabla^2 G^\bullet}{\partial x^2}$	$1.7\cdot10^{-7}$	$2.4\cdot10^{-8}$	$\frac{\partial^4\nabla^2 G^\bullet}{\partial y^4}$	$1.6\cdot10^{-6}$	$9.4\cdot10^{-7}$
$\frac{\partial^2\nabla^2 G^\bullet}{\partial y^2}$	$1.7\cdot10^{-7}$	$5.8\cdot10^{-9}$	$\frac{\partial^4\nabla^2 G^\bullet}{\partial x^4}$	$3.6\cdot10^{-8}$	$4.5\cdot10^{-9}$
$\frac{\partial^2\nabla^2 G^\bullet}{\partial z^2}$	$4.0\cdot10^{-8}$	$4.6\cdot10^{-8}$	$\frac{\partial^4\nabla^2 G^\bullet}{\partial x^4}$	$1.5\cdot10^{-6}$	$9.4\cdot10^{-7}$
$\frac{\partial^2\nabla^2 G^\bullet}{\partial x\partial y}$	$1.0\cdot10^{-6}$	$1.5\cdot10^{-7}$	$\frac{\partial^4\nabla^2 G^\bullet}{\partial x^3\partial y}$	$2.0\cdot10^{-7}$	$1.0\cdot10^{-7}$
$\frac{\partial^2\nabla^2 G^\bullet}{\partial x\partial y}$	$3.6\cdot10^{-8}$	$4.7\cdot10^{-8}$	$\frac{\partial^4\nabla^2 G^\bullet}{\partial y^3\partial x}$	$2.3\cdot10^{-7}$	$1.0\cdot10^{-7}$
$\frac{\partial^2\nabla^2 G^\bullet}{\partial x\partial z}$	$5.1\cdot10^{-8}$	$4.8\cdot10^{-8}$	$\frac{\partial^4\nabla^2 G^\bullet}{\partial x^3\partial y}$	$4.7\cdot10^{-7}$	$2.2\cdot10^{-7}$
$\frac{\partial^3\nabla^2 G^\bullet}{\partial x^3}$	$2.9\cdot10^{-7}$	$1.1\cdot10^{-7}$	$\frac{\partial^4\nabla^2 G^\bullet}{\partial x^3\partial x}$	$4.4\cdot10^{-7}$	$1.8\cdot10^{-7}$
$\frac{\partial^3\nabla^2 G^\bullet}{\partial y^3}$	$2.5\cdot10^{-7}$	$1.1\cdot10^{-7}$	$\frac{\partial^4\nabla^2 G^\bullet}{\partial x^3\partial z}$	$2.6\cdot10^{-6}$	$3.8\cdot10^{-7}$
$\frac{\partial^3\nabla^2 G^\bullet}{\partial z^3}$	$1.4\cdot10^{-7}$	$9.8\cdot10^{-8}$	$\frac{\partial^4\nabla^2 G^\bullet}{\partial y^3\partial z}$	$9.9\cdot10^{-7}$	$2.5\cdot10^{-7}$
$\frac{\partial^3\nabla^2 G^\bullet}{\partial x^2\partial z}$	$3.8\cdot10^{-7}$	$6.0\cdot10^{-8}$	$\frac{\partial^4\nabla^2 G^\bullet}{\partial z\partial x^2\partial y}$	$1.3\cdot10^{-7}$	$1.0\cdot10^{-7}$
$\frac{\partial^3\nabla^2 G^\bullet}{\partial y^2\partial z}$	$1.8\cdot10^{-7}$	$3.6\cdot10^{-8}$	$\frac{\partial^4\nabla^2 G^\bullet}{\partial z^2\partial x\partial y}$	$1.5\cdot10^{-7}$	$1.0\cdot10^{-7}$
$\frac{\partial^3\nabla^2 G^\bullet}{\partial z^2\partial y}$	$1.6\cdot10^{-7}$	$6.1\cdot10^{-8}$	$\frac{\partial^4\nabla^2 G^\bullet}{\partial z\partial x\partial y^2}$	$2.4\cdot10^{-7}$	$8.4\cdot10^{-8}$
$\frac{\partial^3\nabla^2 G^\bullet}{\partial z^2\partial x}$	$1.7\cdot10^{-9}$	$5.8\cdot10^{-8}$	$\frac{\partial^4\nabla^2 G^\bullet}{\partial y^2\partial x^2}$	$3.1\cdot10^{-7}$	$2.1\cdot10^{-7}$

Table 3.10: *Laplace equation for Green's function and its derivatives. Comparison of present method and infinite depth Green's function in the original MULDIF program. The Laplace equation and the derivatives are non-dimensionalized by* $\frac{\partial^{(M_1+M_2+M_3)}\nabla^2 G^\bullet}{\partial x^{M_1}\partial y^{M_2}\partial z^{M_3}} = \left|\frac{\partial^{(M_1+M_2+M_3)}\nabla^2 G}{\partial x^{M_1}\partial y^{M_2}\partial z^{M_3}}\right| / \max\left(\left|\frac{\partial^{(M_1+M_2+M_3+2)}G}{\partial x^{2+M_1}\partial y^{M_2}\partial z^{M_3}}\right|, \left|\frac{\partial^{(M_1+M_2+M_3+2)}G}{\partial x^{M_1}\partial y^{2+M_2}\partial z^{M_3}}\right|, \left|\frac{\partial^{(M_1+M_2+M_3+2)}G}{\partial x^{M_1}\partial y^{M_2}\partial z^{2+M_3}}\right|\right)$ *($U = 1m/s$, $r = 10m$, $z = c = -5m$, $\omega = 1s^{-1}$, $\alpha = -\frac{\pi}{4}$ and $u = 0$).*

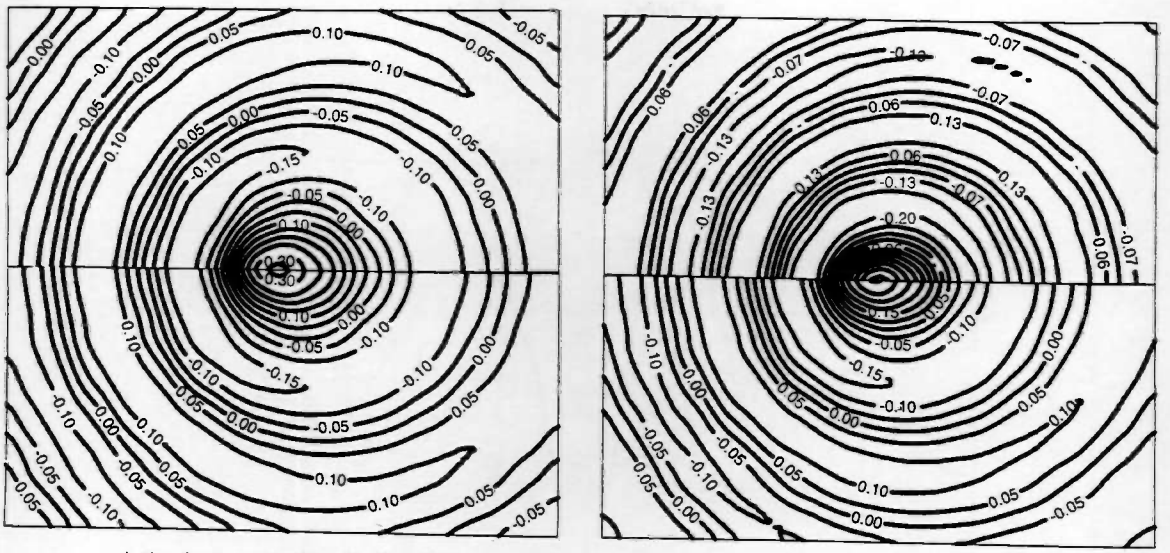

a) Real part of Green's function.

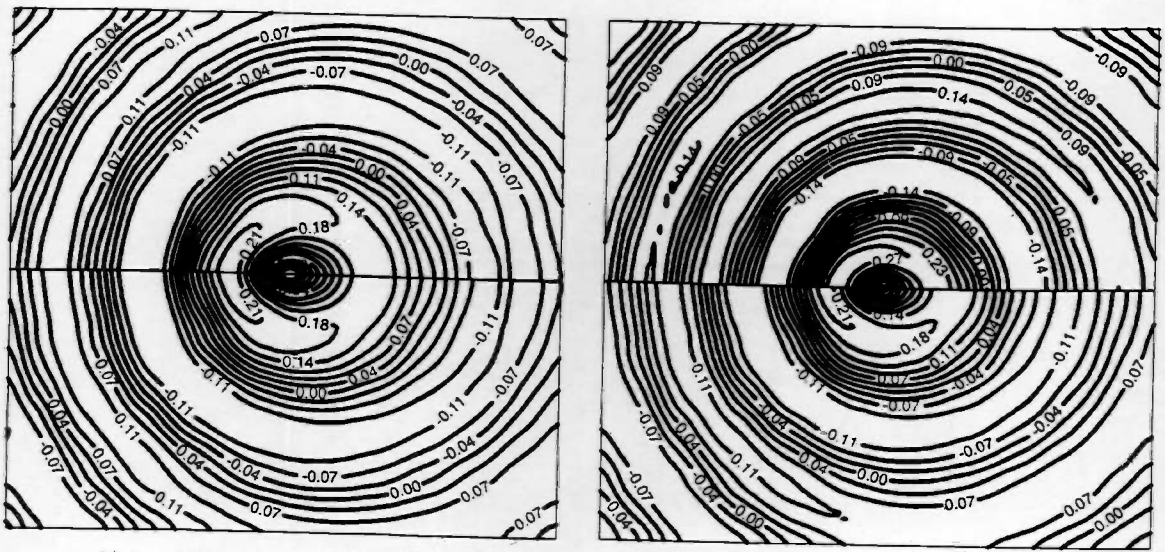

b) Imaginary part of Green's function.

Figure 3.6: *Green's function* $[1/m]$ *for various depth. The left side shows infinite water depth in the lower half plane vs.* $h = 50m$ *in the upper half plane. The right side shows* $h = 6m$ *in the upper half plane vs.* $h = 12m$ *in the lower.* $x - a$ *and* $y - b$ *vary between -80m and 80m. (*$U = 1m/s$, $z = 0m$, $c = -5m$, $\omega = 1s^{-1}$ *and* $\alpha = 0$*).*

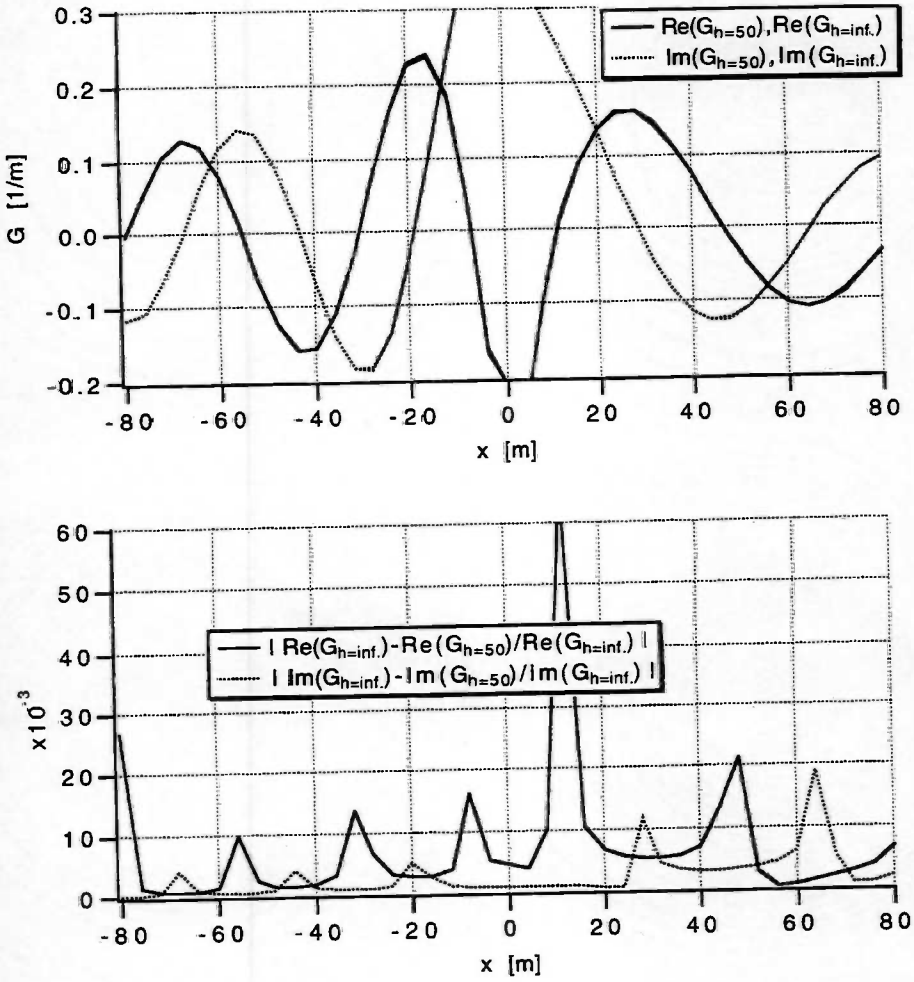

Figure 3.7: *Comparison of the Green's function for* $h = 50m$ *and* $h = \infty$ *along the current axis* ($U = 1m/s$, $z = 0m$, $c = -5m$, $\omega = 1s^{-1}$ *and* $\alpha = 0$).

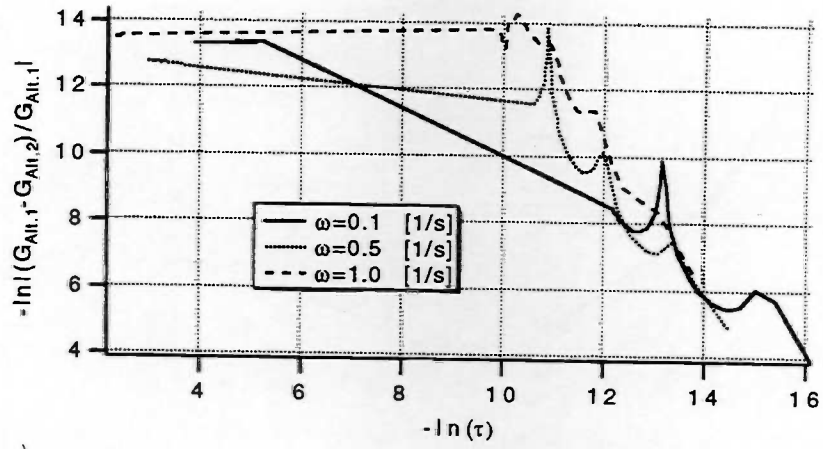

a)

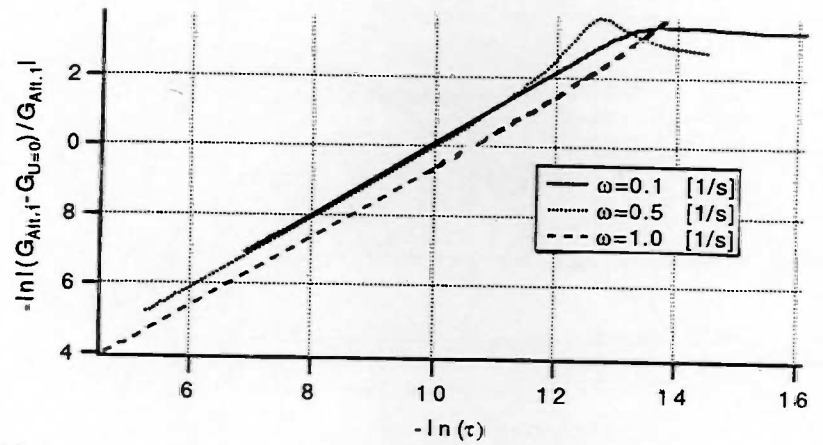

b)

Figure 3.8: *a) Difference between the Green's function evaluated in section 3.1.1 (G_{alt1}) and in section 3.1.2, (G_{alt2}), for decreasing current velocity. b) Difference between the Green's function evaluated in section 3.1.1 (G_{alt1}) and the zero current Green's function ($G_{U=0}$) by John [1950] for decreasing current velocity ($r = 10m$, $h = 10m$, $z = c = -5m$ and $\alpha = u = 0$).*

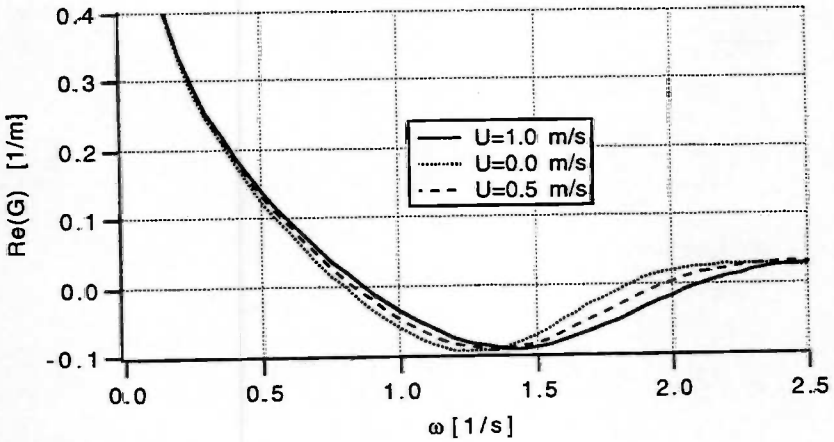

a) Real part.

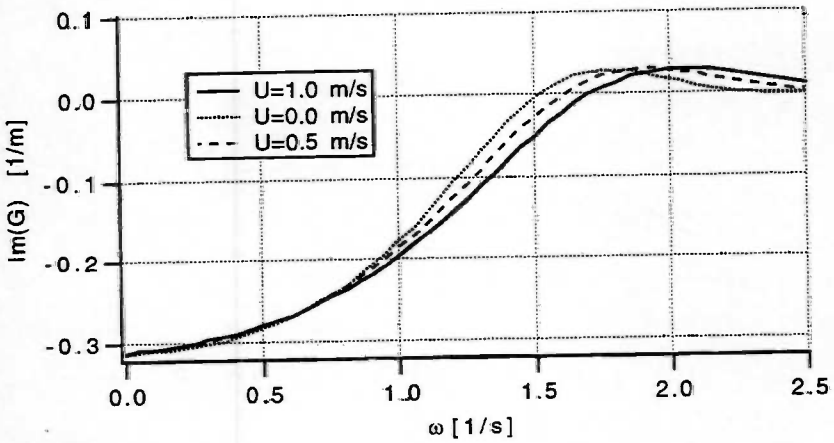

b) Imaginary part.

Figure 3.9: *Green's function as function of frequency. The infinite frequency Green's function gives* $G_{\omega\to\infty} = (0.04007, 0)[1/m]$ *and the zero frequency limit is given in section 3.1.3 as* $G_{\omega\to 0} = (\infty, -\frac{\pi}{h})[1/m]$ *(*$r = 10m$, $h = 10m$, $z = c = -5m$ *and* $\alpha = u = 0$*).*

Chapter 4

Hydrodynamic Forces

In this chapter we will look at quantities needed in calculating sea loads and wave induced motions of marine structures. That is: wave exciting forces, added mass and damping coefficient, mean drift forces and wave-drift damping. The analytic expressions will be presented and the results from the computer program MULDIF, now extended to include the effect of finite water depth, will be discussed. The basic method is described in Chapter 2.

It is necessary to distribute elements on both the free surface and control surface, as well as on the body surface. Figure 4.1 shows how the elements are obtained.

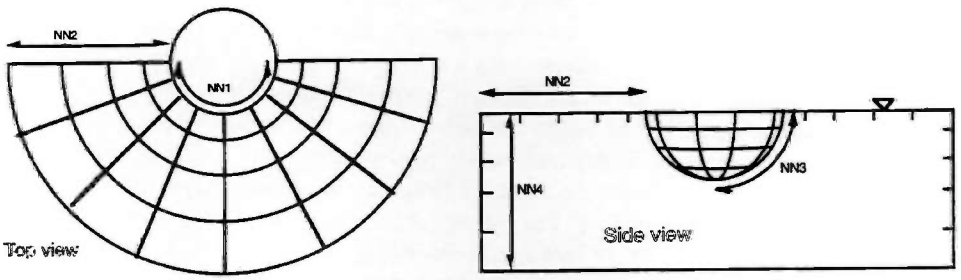

Figure 4.1: *Definitions of number of elements for a floating sphere.*

The lines surrounding the elements on the body surface have constant angular spacing, both horizontally and vertically, with the smallest elements against the sea floor. The angle definitions are given in figure 2.8 in chapter 2, and the element distribution on the body is illustrated in figure 2.7 under the name "element distribution 1". If we were considering an infinite water depth problem it would be natural to choose small elements close to the free surface. This is due to stronger flow variation on this upper part of the body. If we had a finite water depth case, where the steady potential was known analytically, it might also be natural to pick smaller elements close to the free surface, and not worry too much about the lower part of the body. The reason is that the m_j-terms (as discussed in section 2.2) are then known. In our case, however, the calculation of these terms, where we interpolate

back from some distance from the body, gets critical. Thus, handling m_j-terms give the main reason for requiring distribution of small elements on the lower part of the body surface. Of course, large flow variation on this lower part, is also a reason for choosing this distribution.

At the free surface the elements are smallest near the body, and at the control surface the elements are smallest close to the free surface. This is mathematically expressed as $L_n = factor^{n-1} L_1$, $1 \leq n \leq NN2$ or $1 \leq n \leq NN4$, where L_n is the length of an element. $NN2$ and $NN4$ are explained in figure 4.1. L_1 denotes the length of the element closest to the body when we consider element distribution at the free surface. At the control surface, L_1 denotes the length of the element closest to the free surface. Experience with MULDIF suggests that the *factor*'s are chosen as $factor_{S_F} = 1.1$ and $factor_{S_C} = 1.25$.

In most of the following examples the NNi-terms explained in figure 4.1 are set to $NN1 = 32$, $NN2 = 18$ and $NN3 = NN4$=16.

In order to calculate the m_j-terms the steady potential will be evaluated at distances 2.0, 2.2 and 2.4 times the diagonal of an element, along the normal vector. Why this procedure is necessary is explained in the discussion starting on page 15. With the preceding values for $NN1$ and $NN3$, these distances imply that the minimal z-value where derivatives of the steady potential are evaluated, is $z \approx -1.23R$. The symbol R still denotes the radius of the hemisphere. We are going to choose water depths that are more shallow than $1.23R$. This may or may not cause errors, as discussed on page 15 and illustrated in figure 2.6.

Zhao and Faltinsen [1989] investigated the radius of the control surface, R_C, in the deep water case. They reported less than 2% difference in results for a floating cylinder if the control surface was moved between $R_C = 3R$ and $R_C = 5R$. We therefore choose the control surface at four times the radius.

The velocity potential in the outer domain is approximated by multipoles inside the body. The locations of these multipoles are called singularity points. Our model is based on a Taylor series expansion, implying that quite few multipoles and singularity points are needed if the control surface is located far from the body. Likewise, more multipoles and singularity points are needed if the control surface and body surface are close. All details about this expansion procedure are given in Appendix A. For the sphere we first use only one singularity, situated on the z-axis at minus half the radius. The number of multipoles is set to 10. These choices are not wild guesses, they equal those of Zhao and Faltinsen [1989]. These authors found, again for a floating cylinder in deep water, that the results changed less than 1% when number of singularity points increased from one to two. Moreover, if number of multipoles increased from 10 to 16, their values varied less than 0.2%.

One should note that the infinite water depth results presented in this section are due to standard routines for the Green's functions, both in the steady and unsteady case. For finite water depth the control surface fills the gap between the sea floor and free surface, while for infinite water depth the control surface ends one wave length down in the fluid. In the deep water case it is all right to use such a short control surface when considering linear problems and mean forces, as we do. The flow then decays rapidly with respect to z. However, if we had solved the second order sum frequency problem, part of the solution

would decay like z^{-1}, and a deeper control surface would be necessary.

4.1 Linear forces

Here, we will look at the wave exciting forces and the added mass- and damping- coefficients.

4.1.1 Wave exciting forces

The linear wave exciting forces and moments, $\mathcal{F}_j = \Re\{F_j e^{i\omega t}\}$, $j \in \{1,..,6\}$, are obtained by integrating the pressure due to incident and diffracted waves over the body surface. Within linear theory this may be written

$$F_j = -\rho \iint_{S_B} [i\omega n_j - m_j](\phi_0 + \phi_7) ds, \qquad j \in \{1,..,6\}. \tag{4.1}$$

Here a theorem by Ogilvie and Tuck [1969], valid for wall-sided structures, has been applied to rewrite equation 2.21 in section 2.1.

Nossen et.al. [1991] presented the 3-D generalized Haskind relation, also valid for wall sided structures. The derivation was based on an idea of Zhao and Faltinsen [1988] (2-D case). They introduced a reversed flow, but let the frequency of encounter for the reversed flow equal that of the physical flow. An alternative way of writing the wave exciting forces, without solving the diffraction problem, was then established. In our setting their method gives

$$F_j = \rho \iint_{S_{C_0}} \left[\frac{\partial \psi_j}{\partial n} \phi_0 - \frac{\partial \phi_0}{\partial n} \psi_j \right] ds + 2i\tau\rho \int_{C_c} \phi_0 \psi_j \cos(\alpha - v) dl, \quad j \in \{1,..,6\}, \tag{4.2}$$

where ψ_j is the radiation potential due to a reversed current, and v denotes the coordinate angle from the positive x-axis.

A less sophisticated way of checking the accuracy in the calculations of the forces, is given by applying Green's second identity to ϕ_j and $(\phi_0 + \phi_7)$, resulting in

$$F_j = -2\rho \iint_{S_B} i\omega n_j (\phi_0 + \phi_7) ds - \rho f(\phi_j, \phi_7 + \phi_0), \qquad j \in \{1,..,6\}. \tag{4.3}$$

Here,

$$\begin{aligned} f(\phi_j, \phi_7 + \phi_0) &= \iint_{S_{C_0}} \left[\frac{\partial \phi_j}{\partial n} (\phi_0 + \phi_7) - \frac{\partial (\phi_0 + \phi_7)}{\partial n} \phi_j \right] ds \\ &\quad + \frac{2i\omega}{g} \iint_{S_F} [\nabla \phi_s \cdot \nabla \phi_j (\phi_0 + \phi_7) - \nabla \phi_s \cdot \nabla (\phi_0 + \phi_7) \phi_j] ds. \end{aligned} \tag{4.4}$$

By the same approach we also obtain

$$F_j = 2\rho \iint_{S_B} m_j (\phi_0 + \phi_7) ds + \rho f(\phi_j, \phi_7 + \phi_0), \quad j \in \{1,..,6\}. \tag{4.5}$$

So, we get a check on the relation between the diffraction potential and ϕ_j, $j \in \{1,..,6\}$ without having to run the program twice.

The above expressions all include m_j-terms, either directly or implicitly through ϕ_j or ψ_j ($j \in \{1,..,6\}$). If the intention is to examine what effect the m_j-terms have upon the forces we should compare with the original expression (eq. 2.21). On the other hand, if we do not want to include derivatives at the body surface at all, we should apply

$$F_j = -\rho \iint_{S_B} i\omega n_j(\phi_0 + \phi_7)ds - \rho \iint_{S_F+S_{C_0}} \frac{\partial \phi_s}{\partial x_j}\frac{\partial(\phi_0+\phi_7)}{\partial n}ds, \quad j \in \{1,2\}, \qquad (4.6)$$

which comes from applying Green's second identity to $(\phi_0 + \phi_7)$ and $\frac{\partial \phi_s}{\partial x_j}$ for $j \in \{1,2\}$. A smilar procedure also leads to a simple way of writing the yaw moment, without including m_j-terms. In heave, pitch and roll, however, this approach implies non-zero contributions from the sea floor surface (S_0) if water depth is regarded finite.

Discussion of results

In figure 4.2 through 4.6 the different methods are compared for four water depths.

The figures might need some explanation: The solid lines denote F_1 and F_3 as calculated with equation 4.1 (**Original F_j**), the dotted lines are due to the two alternative methods stated in equation 4.3 and 4.5 (**Alt. with m_j**), and the dashed lines denote horizontal wave exciting forces due to equation 4.6 (**Alt. without m_j**). The generalized Haskind relation (**Gen. Haskind**), written in equation 4.2, is presented in figure 4.4 and figure 4.5, only. Forces calculated by the different methods should of course agree.

In figure 4.2 through 4.5 a current has been included (Froude number $F_n = \frac{U}{\sqrt{gR}} = 0.04$). Incident waves and current propagate in opposite or same direction. The results for $h/R = 1.2$ and $h/R = \infty$ are compared with Grue and Biberg [1993] with satisfying agreement. The only exception is the horizontal force in the case of long waves ($KR <\approx 0.5$), with m_j-terms included and $h/R = 1.2$. For $h/R = 1.1$ the results differ more than 20% depending on whether or not m_j-terms have been included. We notice that all methods that involve m_j-terms give approximately the same results.

We will convince ourselves that this difference is due to errors in our calculations of the m_j-terms. That means, the dashed lines (Alt. without m_j), which represent results not involving the errors associated with calculations of m_j-terms, are most accurate whenever large differences occur.

By increasing $NN3$ from 16 to 22 the m_j-terms are calculated within the fluid in the case of $h/R = 1.2$. However, the results change very little. Next, we look at the dependency of the factors deciding how far out along the normal vector the differentiation is executed ($\vec{FFi}$). This is shown in figure 4.7 and 4.8 for frequency coefficient $\omega_0^2 R/g = 0.0917$ and $\omega_0^2 R/g = 0.5$, respectively. The horizontal wave exciting force is most sensitive to $\vec{FFi}$ for low frequencies, where the results change about 10% by varying between $\vec{FFi}$=(0.8,1.0,1.2) and $\vec{FFi}$=(2.0,2.2,2.4). For the vertical forces in both cases, and for the horizontal forces with frequency coefficient $\omega_0^2 R/g = 0.5$, the difference is less than 2%. It seems like we should have chosen $\vec{FFi}$=(1.2,1.4,1.6) for $h/R = 1.2$.

The same investigation ought to be performed for $h/R = 1.1$ to decide whether the vertical forces are correct when a current is present (we now conlude that the horizontal forces are inaccurate, unless written as in equation 4.6). The vertical forces are likely to also be more sensitive to $\vec{FFi}$ as the depth decreases. However, since such investigations are rather time-consuming we just say that they *may* be very inaccurate. That the alternative methods agree (also the generalized Haskind relation) gives no verification on good results at all.

The steady potential is not to blame for all inaccuracies in the results. For large wave numbers we notice a disagreement in the alternative methods of calculating the horizontal force (fig. 4.2, 4.4 and 4.6). This is independent of water depth, and the gap is also present when a current is not included. It seems like the error depends on the frequency of oscillation, and thereby the length of the diffracted waves. It is natural to suspect insufficient number of elements on part of the surfaces.

So, we look at the wave exciting forces at large wave number, deep water and head sea. For deep water the steady potential is easily expressed analytically, a procedure that is used in this part of the discussion.

First a convergence study is made, where $NN1$ varies between 20 and 40 ($NN2 = 1.1 \cdot NN3$ and $NN3 = NN4 = \frac{NN1}{2}$). But, the results change less than one per cent. Next, we try to increase the number of singularity points from one to three. Again, the results change less than one per cent. Eventually, when the control surface is put at three times the radius -instead of four- something happens: A gap of 10% between the methods calculating the horizontal force is reduced to less than one per cent. At the same time, for the method of pressure integration on the body surface, the results increase approximately 1%. However, the gap between the alternative ways of calculating vertical wave exciting force increases from 0.5% to 5%, while for the pressure integration method the result changes 2%. When the control surface is put at $3R$ we choose $NN1 = 26$ and $NN2 = NN3 = NN4 = \frac{NN1}{2}$.

We can explain the lack of sensitivity to number of elements as follows: The factor, $factor_{S_F}$, that relates the radial length of the elements on the free surface is chosen as $factor_{S_F} = 1.1$. This means for $R_C = 4R$ that the smallest radial length of an element is $0.05R$ when $NN2 = 22$, and $0.19R$ when $NN2 = 11$. The corresponding largest length is $0.41R$ and $0.53R$, respectively. If $R_C = 3R$ and $NN2 = 13$, the largest length is reduced to $0.37R$. The largest examined wave number ($KR = 1.25$) corresponds to a wave length of $\lambda = 5R$ for the incident wave. The upstream waves are even shorter. To describe these waves properly, and to evaluate derivatives by applying the potential at adjacent elements, small elements are needed also at some distance from the body. We should try to decrease $factor_{S_F}$ when $NN2$ is large. By the same argument also $factor_{S_C}$ should be reduced during convergence studies. The horizontal length of the elements on the control surface seems from the above to be less important. For $R_C = 4R$ and $NN1$ equal to 20 and 40, l_{elemS_C}=0.63R and l_{elemS_C}=0.31R, respectively. When the control surface is moved to $R_C = 3R$, l_{elemS_C}=0.36R.

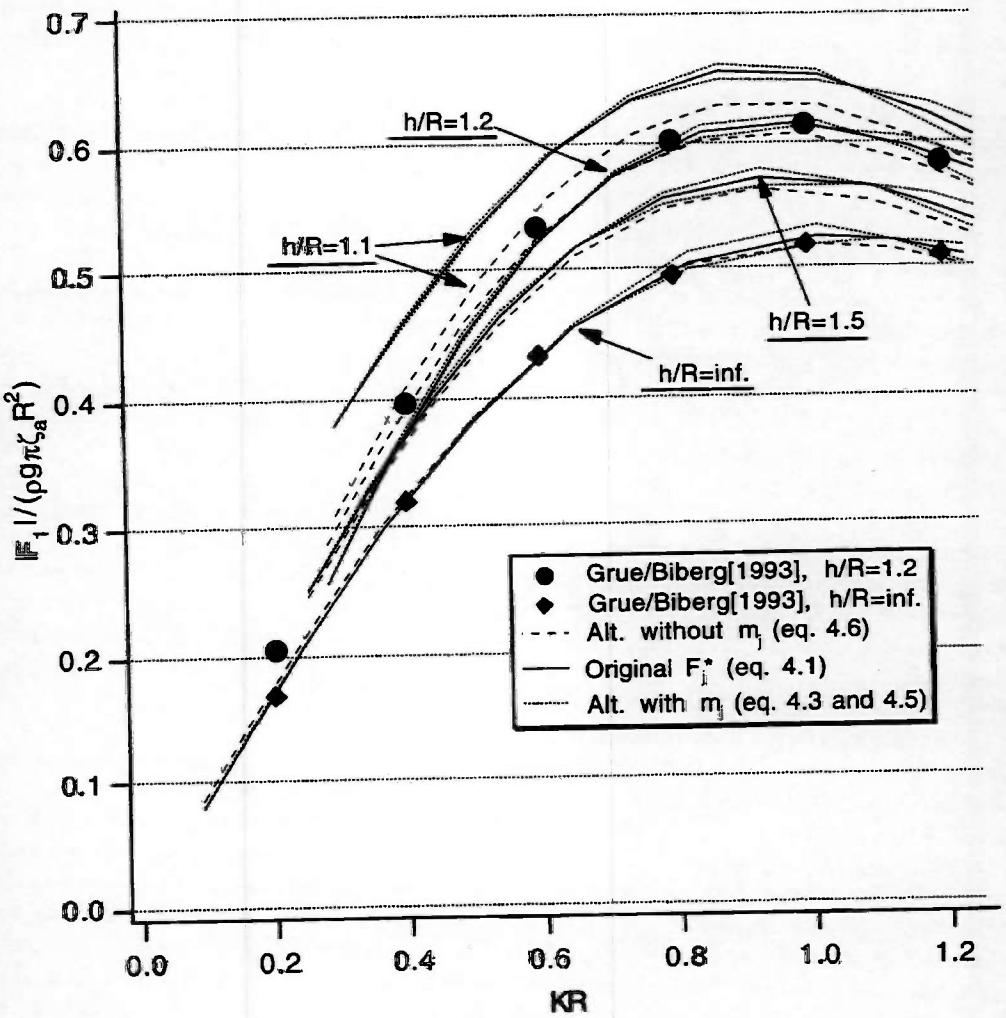

Figure 4.2: *Horizontal wave exciting forces for a half immersed sphere when current and incident wave propagate in opposite directions* ($\alpha = 0, \beta = \pi$). *Froude number:* $F_n = 0.04$. *(*$NN1 = 32, NN2 = 18, NN3 = NN4 = 16$. *1 singularity in* $(0, 0, -R/2)$. *Control surface at* $4R$. *10 multipoles.* $\vec{FFi} = (2.0, 2.2, 2.4)$. $factor_{S_F} = 1.1$ *and* $factor_{S_C} = 1.25$.*)*

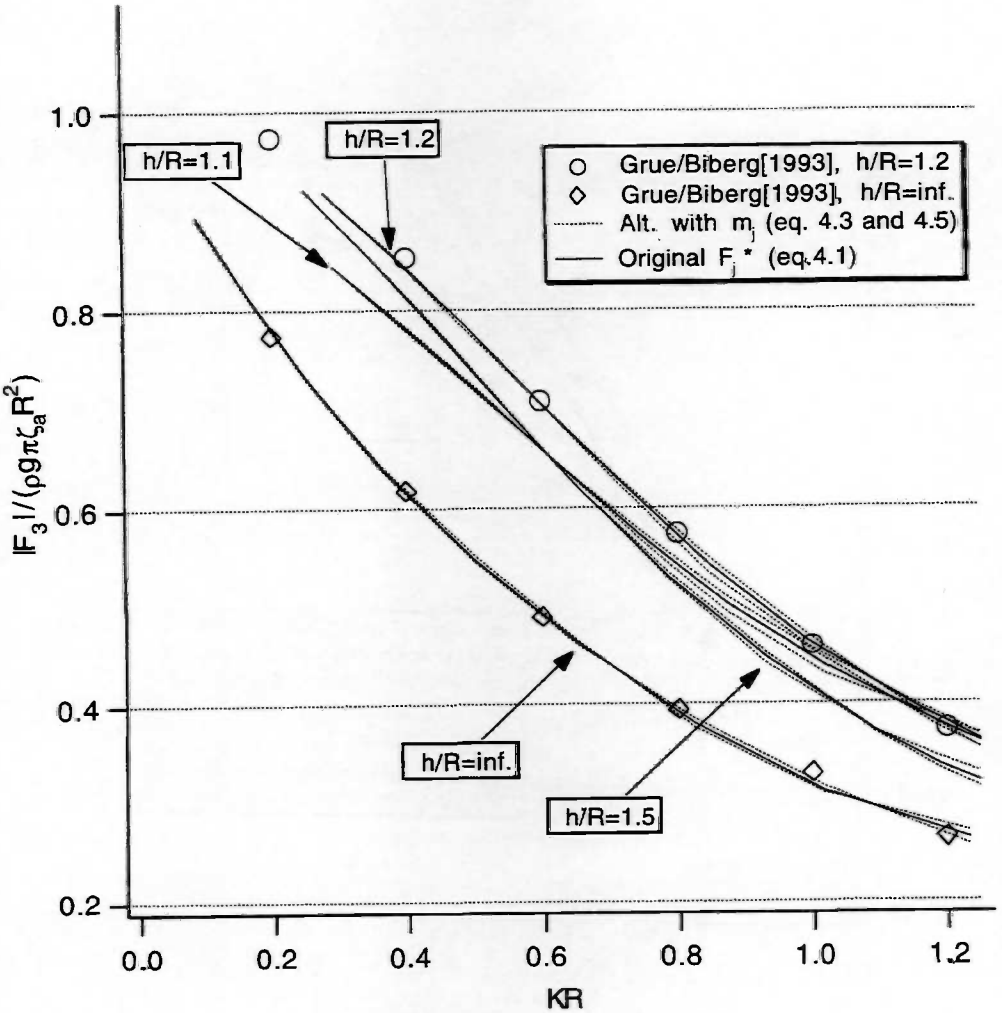

Figure 4.3: *Vertical wave exciting forces for a half immersed sphere when current and incident wave propagate in opposite directions* ($\alpha = 0, \beta = \pi$). *Froude number:* $F_n = 0.04$. *Note that the results for* h/R *=1.1 may be inaccurate.* ($NN1 = 32, NN2 = 18, NN3 = NN4 = 16$. *1 singularity in* $(0, 0, -R/2)$. *Control surface at* $4R$. *10 multipoles.* $\vec{FFi} = (2.0, 2.2, 2.4)$. $factor_{S_F} = 1.1$ *and* $factor_{S_C} = 1.25$.)

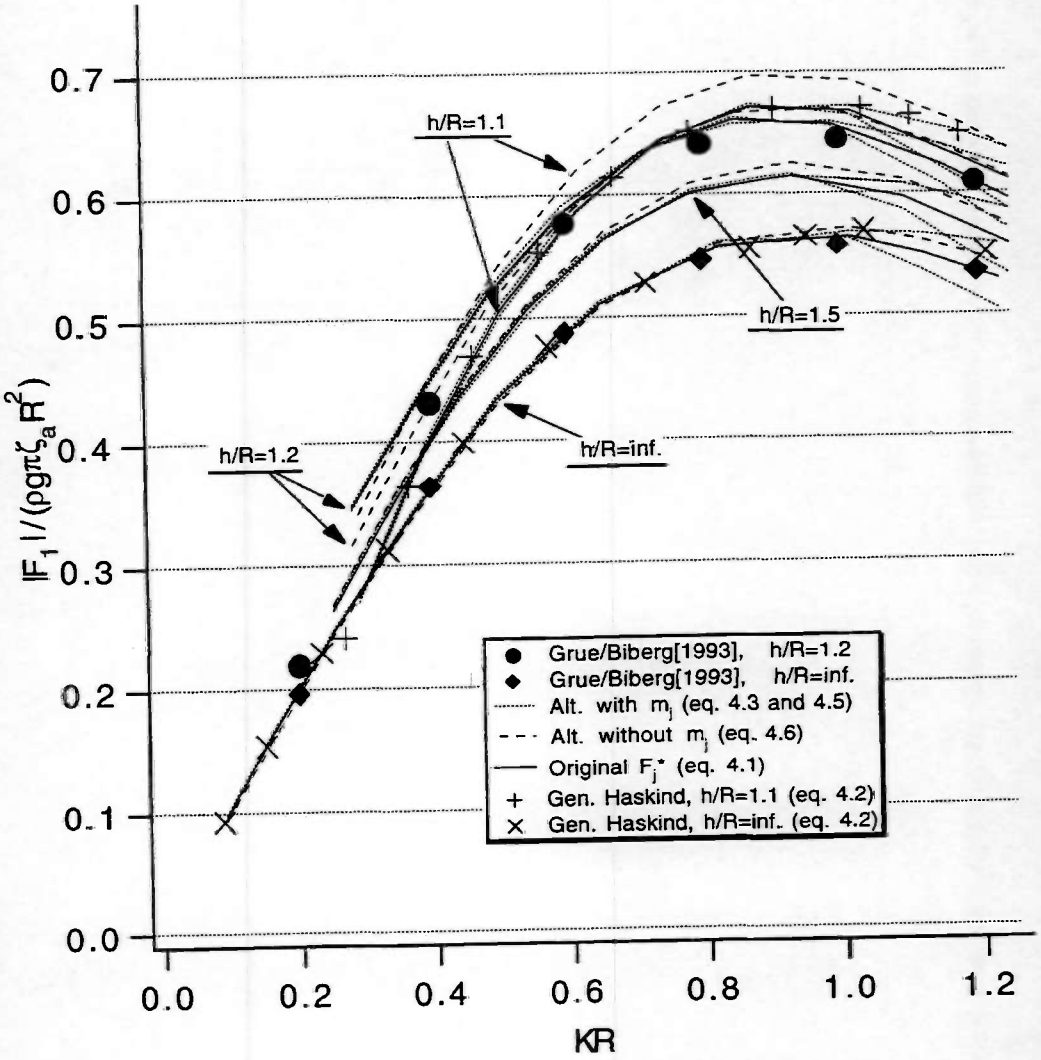

Figure 4.4: *Horizontal wave exciting forces for a half immersed sphere when current and waves propagate in the same direction* ($\alpha = 0, \beta = 0$). *Froude number:* $F_n = 0.04$. *(*$NN1 = 32, NN2 = 18, NN3 = NN4 = 16$. *1 singularity in* $(0, 0, -R/2)$. *Control surface at* $4R$. *10 multipoles.* $\vec{FFi} = (2.0, 2.2, 2.4)$. $factor_{S_F} = 1.1$ *and* $factor_{S_C} = 1.25$.*)*

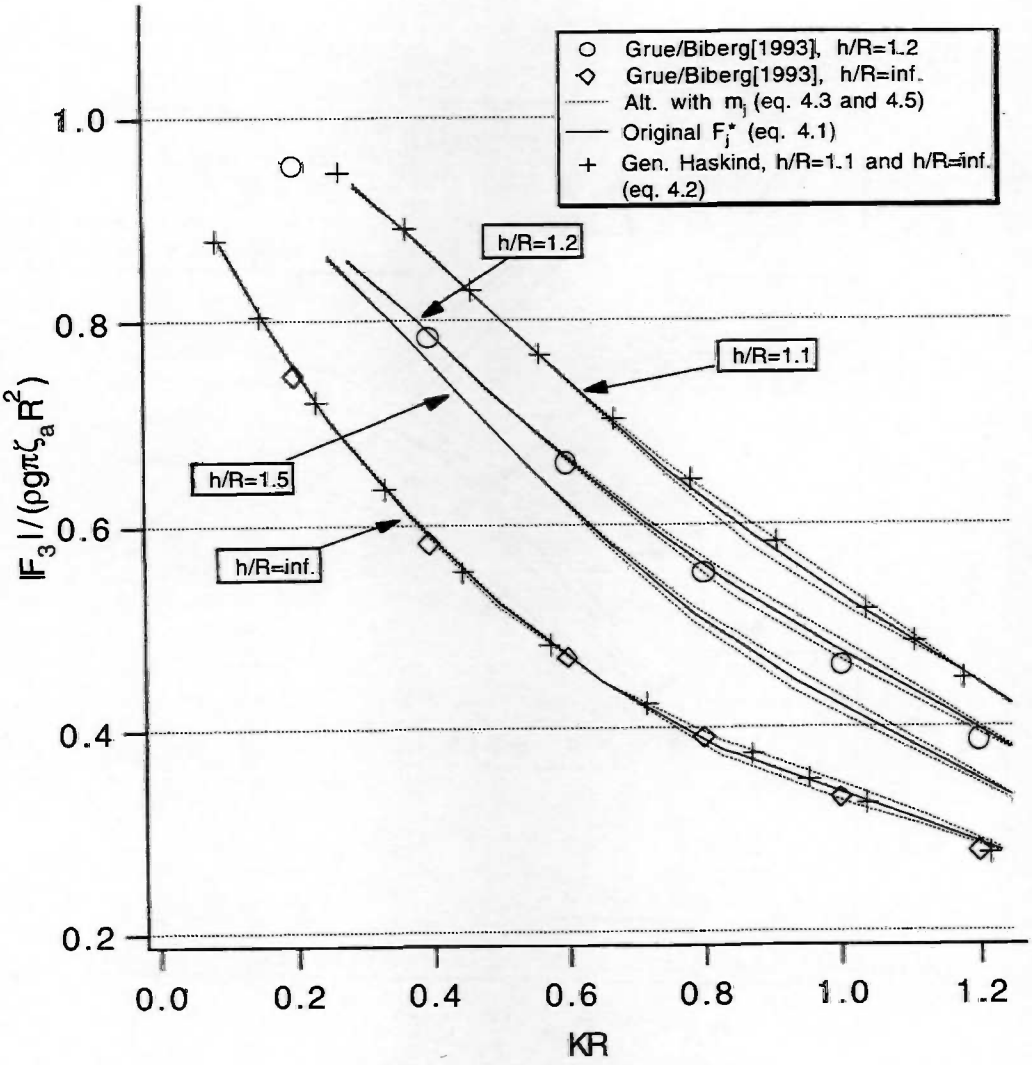

Figure 4.5: *Vertical wave exciting forces for a half immersed sphere when current and waves propagate in the same direction* ($\alpha = 0, \beta = 0$). *Froude number:* $F_n = 0.04$. *Note that the results for* h/R *=1.1 may be inaccurate.* ($NN1 = 32, NN2 = 18, NN3 = NN4 = 16$. *1 singularity in* $(0, 0, -R/2)$. *Control surface at* $4R$. *10 multipoles.* $\vec{FFi} = (2.0, 2.2, 2.4)$. $factor_{S_F} = 1.1$ *and* $factor_{S_C} = 1.25$.)

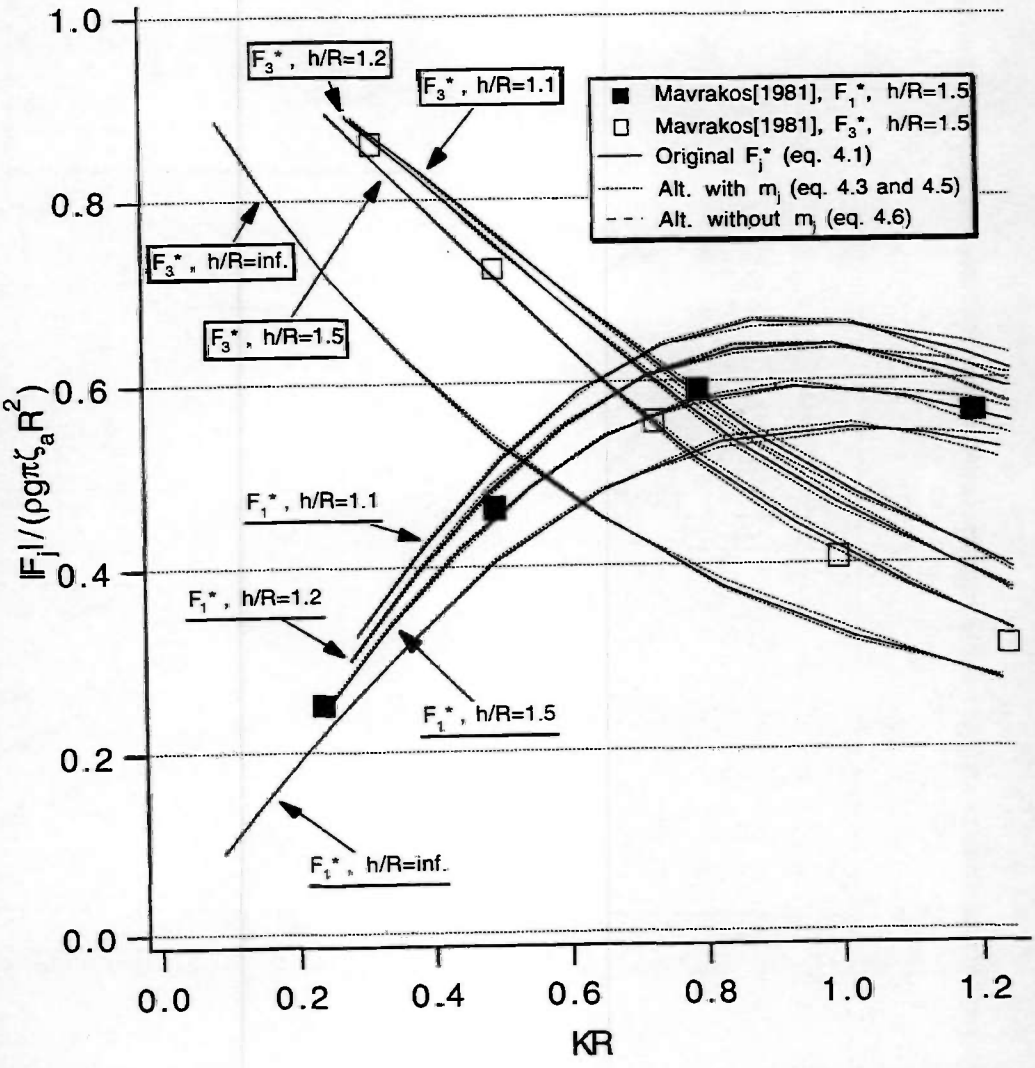

Figure 4.6: *Wave exciting forces for a half immersed sphere for zero current velocity,* $F_n = 0.0$ *(*$NN1 = 32, NN2 = 18, NN3 = NN4 = 16$*. 1 singularity in* $(0, 0, -R/2)$*. Control surface at* $4R$*. 10 multipoles.* $factor_{S_F} = 1.1$ *and* $factor_{S_C} = 1.25$*.)*

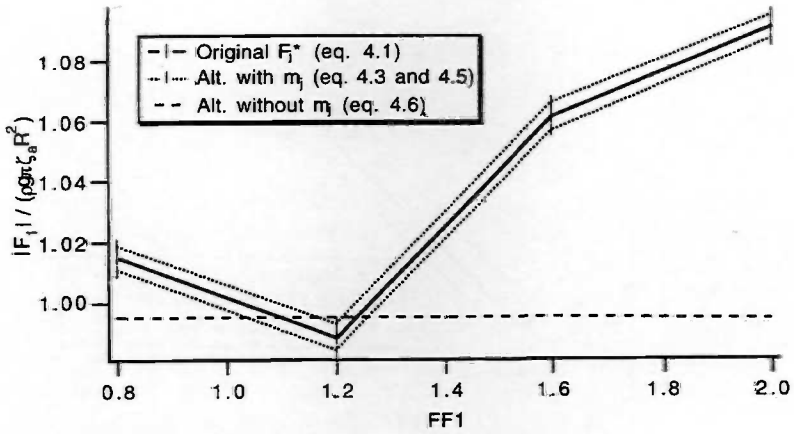

a) Horizontal wave exciting force.

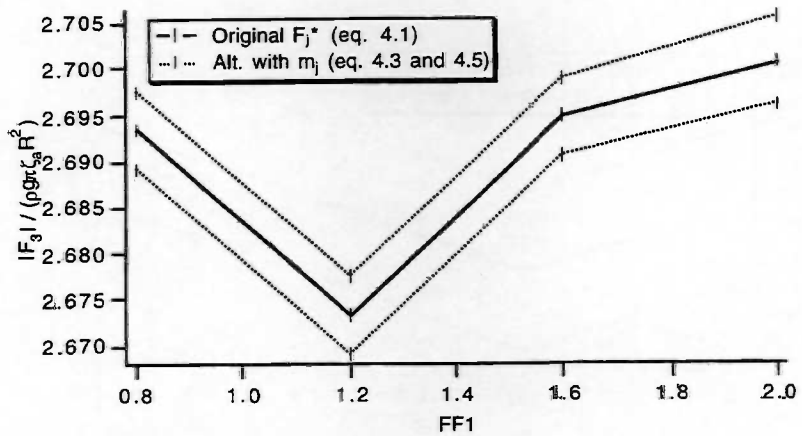

b) Vertical wave exciting force.

Figure 4.7: *Wave exciting force as function of* $\vec{FFi} = (FF1, FF1 + 0.2, FF1 + 0.4)$. $\omega_0^2 R/g = 0.0917$. $h/R = 1.2$ *(*$NN1 = 32, NN2 = 18, NN3 = NN4 = 16$. *1 singularity in* $(0, 0, -R/2)$. *Control surface at* $4R$. *10 multipoles.* $F_n = 0.04$. $\alpha = \beta = 0$. $factor_{S_F} = 1.1$ *and* $factor_{S_C} = 1.25$.*)*

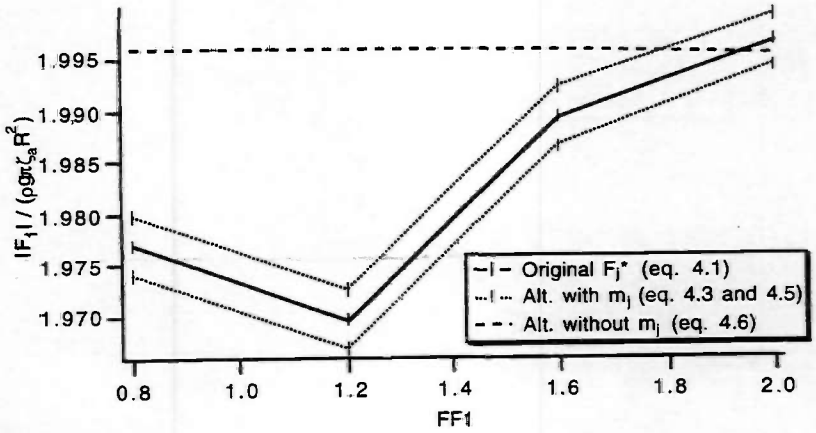

a) Horizontal wave exciting force.

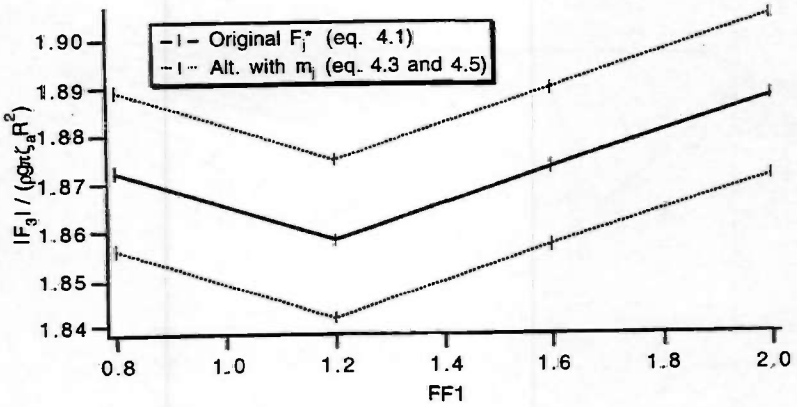

b) Vertical wave exciting force.

Figure 4.8: *Wave exciting force as function of* $\vec{FFi} = (FF1, FF1 + 0.2, FF1 + 0.4)$. $\omega_0^2 R/g = 0.5$. $h/R = 1.2$ *(*$NN1 = 32, NN2 = 18, NN3 = NN4 = 16$. *1 singularity in* $(0, 0, -R/2)$. *Control surface at* $4R$. *10 multipoles.* $F_n = 0.04$. $\alpha = \beta = 0$. *factor*$_{S_F} = 1.1$ *and factor*$_{S_C} = 1.25$.*)*

4.1.2 Added mass and damping coefficients

The added mass and damping coefficients are given by the equation

$$F_{km} = A_{km}\omega^2 - iB_{km}\omega = -\rho \iint_{S_B} (i\omega n_k - m_k)\phi_m ds \tag{4.7}$$

Nossen et. al [1991] presented the generalized Timman-Newman relation for small current velocities; $F_{km}(U,\omega) = F_{mk}(-U,\omega)$. They pointed out one important consequence of this symmetry relation: The diagonal terms, F_{kk}, do not depend on U as long as U is small, other than through the frequency of encounter. The same assumptions on the reversed flow as in section 4.1.1 were made.

Again, we want to check the relations between F_{km} and F_{mk} without introducing the reversed flow. Applying Green's second identity to ϕ_k and ϕ_m, the following alternative expressions for added mass and damping are established:

$$A_{km} = A_{mk} - \frac{\rho}{\omega^2}\Re\{g(\phi_k,\phi_m)\} \tag{4.8}$$

$$B_{km} = B_{mk} + \frac{\rho}{\omega}\Im\{g(\phi_k,\phi_m)\}, \tag{4.9}$$

where g can be chosen among one of the following:

$$g(\phi_k,\phi_m) = \begin{cases} 2i\omega \iint_{S_B}[n_k\phi_m - n_m\phi_k]ds + f(\phi_k,\phi_m) \\ -2\iint_{S_B}[m_k\phi_m - m_m\phi_k]ds - f(\phi_k,\phi_m) \end{cases} \tag{4.10}$$

and $f(\phi_k,\phi_m)$ is given by equation 4.4.

Conservation of energy gives a test on the diagonal damping coefficients. The following consideration has already been taken into account in MULDIF. Zhao and Faltinsen [1989] did not describe their procedure, however, so we take the opportunity to do it here:

The total energy, E, in a fluid volume, Ω, consists of both potential- and kinetic energy, written

$$E(t) = \rho \iiint_{\Omega} (\frac{1}{2}|\nabla\Phi|^2 + gz)d\tau, \tag{4.11}$$

and its time derivative says

$$\frac{dE(t)}{dt} = \rho \int\int_S \left[\frac{\partial\Phi}{\partial t}\frac{\partial\Phi}{\partial n} - \left(\frac{p-p_0}{\rho} + \frac{\partial\Phi}{\partial t}\right)U_n\right] ds \tag{4.12}$$

as given e.g in Newman [1977, page 260]. Here p is the total pressure, p_0 the atmospheric pressure and U_n is the normal velocity of the surface, S, enclosing the fluid volume. The time derivative of the energy averaged over a period is zero when no energy is removed from the system. That is, if the structure is restrained or freely floating but restrained from drifting. We choose as fluid volume the one enclosed by the surfaces in figure 2.3. Then $S = S_F + S_B + S_C + S_0$ and equation 4.12 becomes, at least after time-averaging (denoted by overline),

$$\overline{\int\int_{S_B}(p-p_0)U_n ds} = \rho\overline{\int\int_{S_C}\frac{\partial\Phi}{\partial t}\frac{\partial\Phi}{\partial n}ds}. \tag{4.13}$$

Next, force the body to oscillate in one specific direction and assume a situation with no incident waves. Then $\Phi = \phi_s + \Re\{\eta_i\phi_i\}$, $i \in \{1,..,6\}$. Following Faltinsen [1990, page 45] (zero current velocity) the diagonal terms of the damping coefficients are found from the above equation as

$$B_{ii} = \frac{\rho}{\omega}\int\int_{S_{C_0}}\Im\{\phi_i\frac{\partial\phi_i^*}{\partial n}\}ds - \frac{\rho}{g}\int_{C_c}\Re\{\phi_i\phi_i^*\}\frac{\partial\phi_s}{\partial n}dl, \tag{4.14}$$

where the star denotes complex conjugation and C_c is the water line curve of S_{C_0}.

Discussion of results

The off-diagonal coefficients are zero for a floating sphere when no current is present, and small otherwise. These terms are here evaluated in the infinite water depth case, both for numerical and analytical calculation of the steady potential. The difference is remarkable. For analytical ϕ_s-calculation the results agree rather well with Nossen et.al. [1991], while for numerical ϕ_s-calculation our values increase almost 100%. There is no significant variation between the three different methods used to calculate each of the two cases. For finite water depth we know that the error in the steady potential increases (see figure 2.9 in section 2.2), and that the m_j-terms are more difficult to evaluate. Thus, we expect even larger differences as the water depth decreases.

Although the wave exciting forces seem to be almost not at all influenced by $\vec{F}\vec{i}$ for infinite water depth, we ought to do a sensitivity analysis for the off-diagonal coefficients. However, the off-diagonal terms are not important in the further calculations, so we do not bother too much about it. The fact that the off-diagonal terms are sensitive is also expressed by Eatock-Taylor and Teng [1993]. They studied the effect of corner radius of a truncated cylinder, and found the off-diagonal added mass and damping terms to be affected by a small corner radius while the diagonal terms, the wave exciting forces and the drift forces were rather insensitive.

The diagonal damping coefficients are presented in figure 4.9. The agreement between the zero and non-zero current results is good. Because fewer multipoles are needed and the control surface may be situated closer to the body for $U = 0$ (see Appendix A), it indicates that our model works well with this respect. Besides, different expressions for the wave-current Green's function are applied in the two cases and we get a check of their relation. Also the results achieved by conservation of energy agree well. However, when comparing with Mavrakos [1981] for $h/R = 1.5$ we discover a maximum difference of approximately 4%.

In figure 4.10 the diagonal added mass and damping coefficients for zero current velocity are again compared with Mavrakos [1981]. Here, however, the number of multipoles is reduced to three without affecting the results. This agrees with the calculations in Appendix A.

In section 2.2 the "added mass"-coefficients for a steady problem was studied. The convergence, as a function of number of elements on the body surface, was found to be slow. In the steady case sources were distributed over the body surface. In order to indicate the convergence if both sources and dipoles were distributed for a steady problem, we look at the added mass coefficient for an unsteady case, and apply a small wave number. This is illustrated in figure 4.11. The convergence seems somewhat improved, relative to the results in section 2.2.

The same parameters as for the forces presented in subsection 4.1.1 have been used to find the coefficients in figure 4.9. Results like those in figure 4.6 show that not everything is satisfactory. Thus, due to the good agreement for the diagonal damping coefficients, both for zero and non-zero value of the m_j-terms, we conclude that the check-routine which comes from conserving the energy is not sufficient in this case.

Other check-routines are necessary to make MULDIF a more user-friendly tool. As pointed out in section 4.1.1: the horizontal wave exciting force has to be compared with the expression not containing m_j-terms in order to detect errors concerning these terms. Alternative expressions for the wave forces also detect probable inaccuracies due to panel distribution.

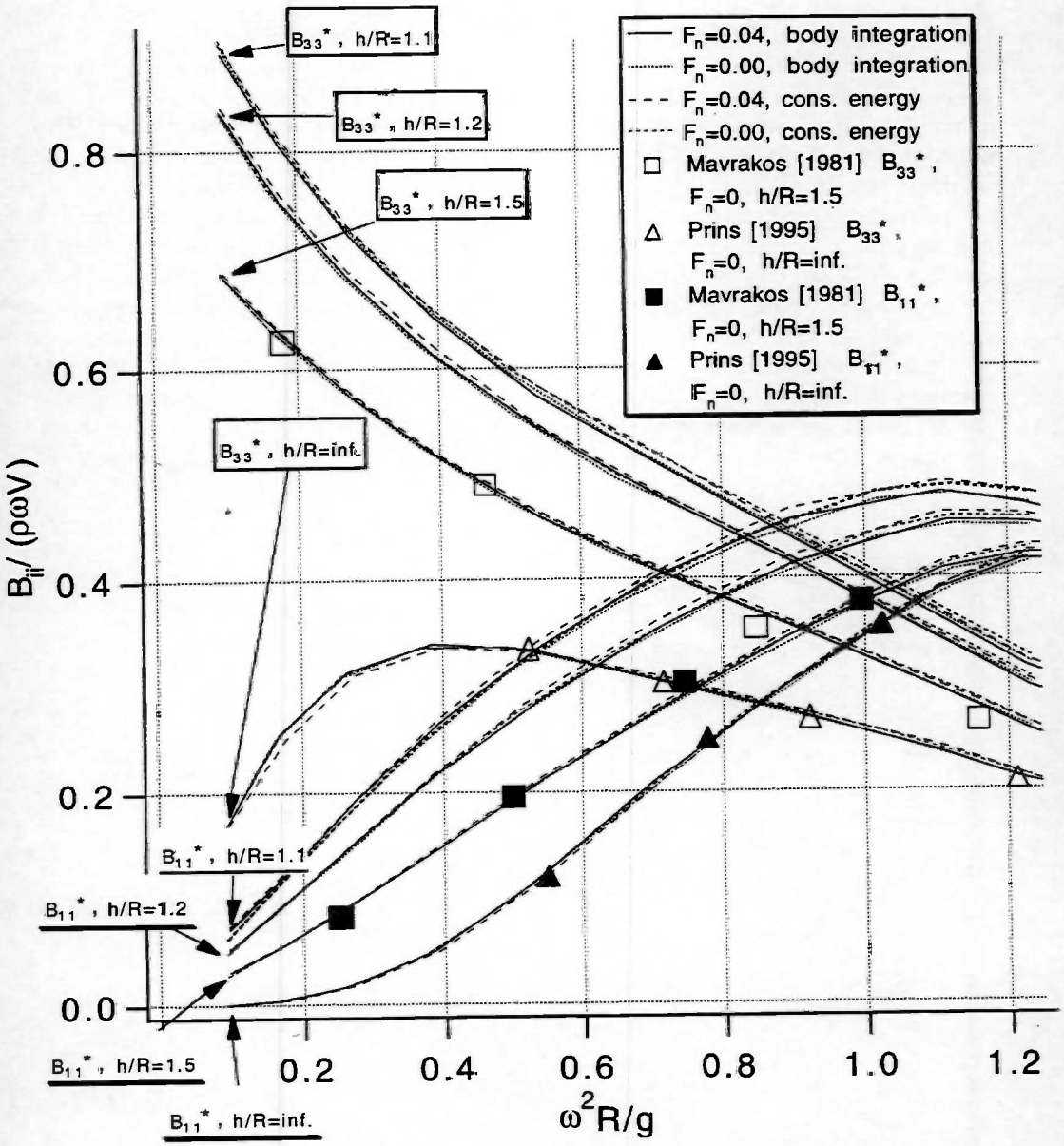

Figure 4.9: *Damping coefficients* $B_{11}^* = \frac{B_{11}}{\rho\omega\nabla}$ *and* $B_{33}^* = \frac{B_{33}}{\rho\omega\nabla}$ *calculated by direct body integration and by conservation of energy in the case of a half immersed sphere* ($NN1 = 32, NN2 = 18, NN3 = NN4 = 16$. *1 singularity in* $(0, 0, -R/2)$. *Control surface at* $4R$. *10 multipoles.* $\vec{FFi} = (2.0, 2.2, 2.4)$. $factor_{S_F} = 1.1$ *and* $factor_{S_C} = 1.25$.)

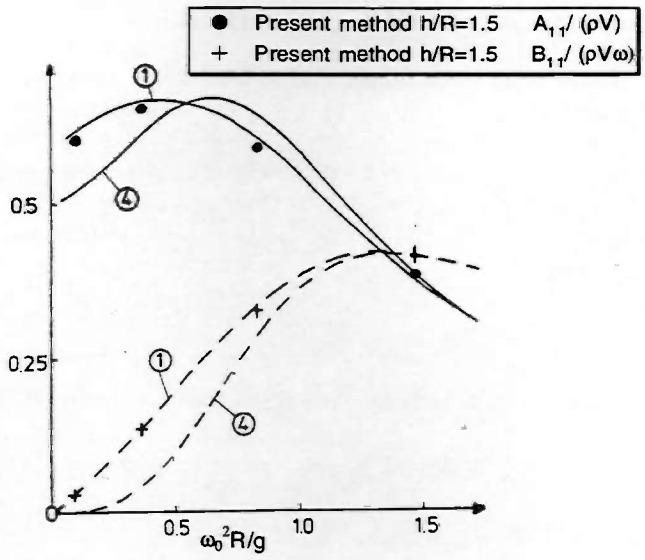

Figure 4.10: *Surge added mass and damping coefficient for a half immersed sphere compared to the results of Mavrakos[1981]. Zero current velocity.* **1** *points at* $h/R = 1.5$ and **4** *points at* $h/R = 10$. *The solid lines denote added mass- and the dashed lines denote damping coefficients* ($NN_1 = 34$ *and* $NN_2 = NN_3 = NN_4 = 17$. *Number of multipoles: 3. Number of points inside the body: 2, in (0,0,-0.1R) and (0,0,-0.5R). The control surface is here situated at* $3R$. $factor_{S_F} = 1.1$ *and* $factor_{S_C} = 1.25$.*)*

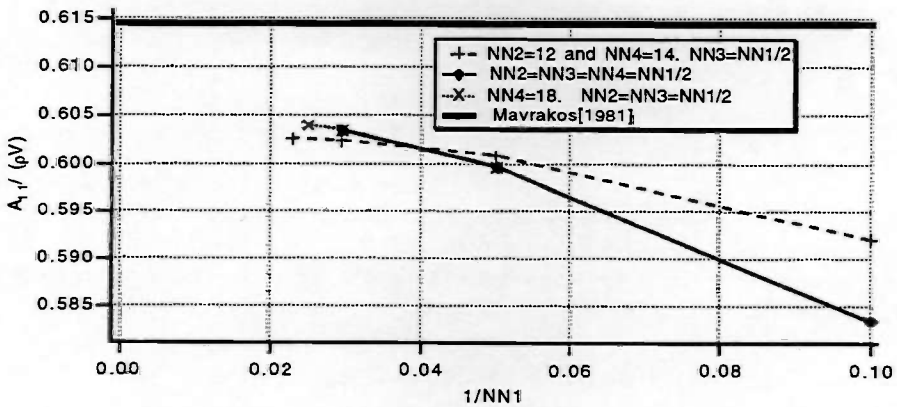

Figure 4.11: *Convergence test for surge added mass with the same properties as in the above figure.* $\frac{\omega_0^2}{g}R = 0.0917$. *(The result of Mavrakos[1981] is not function of number of elements)*

4.2 Mean second order potential

The drift forces are second order quantities. When evaluating these forces we have to keep terms to second order, writing $\Phi = \phi_s + \Phi_1 + \Phi_2$. For zero current velocity Φ_2 does not enter in the equations for the mean drift forces. This is no longer the case when a current is present, where it appears multiplied by ϕ_s. We will therefore look at the mean second order potential, by following a method given in Grue and Biberg [1993].

The mean second order potential fulfills the Laplace equation, and the free surface condition can be written

$$\frac{\partial \overline{\Phi}_2}{\partial z} = \frac{1}{g}\overline{\frac{\partial \Phi_1}{\partial t}\frac{\partial^2 \Phi_1}{\partial z^2}} \qquad \text{for } z = 0. \tag{4.15}$$

We may directly apply the body boundary condition given by Ogilvie [1983] for zero speed:

$$\frac{\partial \overline{\Phi}_2}{\partial n} = -\overline{\vec{n}\cdot[(\vec{\eta} + (\vec{\alpha}\times\vec{x})\cdot\nabla]\nabla\Phi_1} + \overline{(\vec{\alpha}\times\vec{n})\cdot[\frac{d}{dt}(\vec{\eta} + (\vec{\alpha}\times\vec{x}) - \nabla\Phi_1]}. \tag{4.16}$$

Here $\vec{\eta} = (\eta_1, \eta_2, \eta_3)$ and $\vec{\alpha} = (\eta_4, \eta_5, \eta_6)$.

A solution to this boundary value problem can be found through applying Green's second identity in the whole fluid domain to $\overline{\Phi}_2$ and the Green's function used in the steady problem, G_{ST}:

$$\iint_{S_{F\infty}+S_B+S_{C\infty}+S_0} \frac{\partial \overline{\Phi}_2}{\partial n} G_{ST} - \frac{\partial G_{ST}}{\partial n}\overline{\Phi}_2 ds = -4\pi\overline{\Phi}_2. \tag{4.17}$$

G_{ST} satisfies both the bottom condition and the zero normal flow condition at the mean free surface.

To be consistent with the method used in MULDIF we should apply Φ_1 as calculated earlier although $\overline{\Phi}_2$ only appears multiplied by ϕ_s. However, this leads to a more difficult task than if Φ_1 was calculated purely for $U = 0$. We will show why:

The free surface condition for the mean second order potential (eq. 4.15) may be written

$$\frac{\partial \overline{\Phi}_2}{\partial z} = \frac{\omega}{2g}\Im(\hat{\Phi}_1\frac{\partial^2 \hat{\Phi}_1^*}{\partial z^2}) \tag{4.18}$$

where $\Phi_1 = \Re\{\hat{\Phi}_1 e^{i\omega t}\}$. Now write $\hat{\Phi}_1$ as the sum of the complex incident wave potential and the complex radiation and diffraction potential, $\hat{\Phi}_1 = \phi_0 + \phi_{RD}$. We will look at the free surface equation at large distances from the body. Then $\phi_{RD} \sim G$ where G is the asymptotic Green's function from chapter 3 having wave number c_0. Thus,

$$\frac{\partial \overline{\Phi}_2}{\partial z} \to \frac{\omega}{2g}(K^2 - c_0^2)(\Re\{\phi'_{RD}\}\Im\{\phi_0\} - \Im\{\phi'_{RD}\}\Re\{\phi_0\}) + \mathcal{O}(\frac{1}{R}), \tag{4.19}$$

where $\phi_{RD} = \phi'_{RD} + \mathcal{O}(\frac{1}{R})$. We see that this term dies out like $\mathcal{O}(\frac{1}{\sqrt{R}})$. If a current is not present, the Green's function says (equation 3.49 slightly rewritten)

$$G_{U=0} \rightarrow \frac{2\pi i K^2 \cosh K(z+h)\cosh K(c+h)}{\nu \cosh^2 Kh + K^2 h} J_0(Kr) + \mathcal{O}(\frac{1}{R^2}). \tag{4.20}$$

Here, the free surface condition for the mean second order potential dies out like $\frac{\partial \overline{\Phi}_2}{\partial z} \rightarrow \mathcal{O}(\frac{1}{R^2})$. The integral over S_{F_∞} in the Fredholm equation

$$\iint_{S_B} \frac{\partial \overline{\Phi}_2}{\partial n} G_{ST} - \frac{\partial G_{ST}}{\partial n}\overline{\Phi}_2 ds + \iint_{S_{F_\infty}} \frac{\partial \overline{\Phi}_2}{\partial n} G_{ST} ds = -4\pi \overline{\Phi}_2 \tag{4.21}$$

is therefore simpler to evaluate if $\overline{\Phi}_2$ is found for zero Froude number. Numerical calculations will, however, not be performed here.

4.3 Drift forces

The drift forces are obtained by time-averaging the forces, correct to second order, over a period. They may be found in two different ways; either by conservation of momentum in the fluid domain, as given by Newman [1967] (zero speed), or by direct pressure integration.

Zhao and Faltinsen [1989] gave the horizontal drift forces by the method of conservation of momentum as

$$\begin{aligned} \overline{F_i^{cm}} &= -\rho \oint_{C_c} \overline{\left(\frac{\partial \Phi_1}{\partial t} + \nabla\phi_s \cdot \nabla\Phi_1\right)^2} n_i \, dl + \rho \iint_{S_{C_0}} \frac{1}{2}\overline{|\nabla\Phi_1|^2} n_i \, ds \\ &\quad -\rho \iint_{S_{C_0}} \overline{\frac{\partial \Phi_1}{\partial x_i}\frac{\partial \Phi_1}{\partial n}} \, ds - \rho \oint_{C_c} \overline{\frac{\partial \Phi_1}{\partial x_i}\zeta \frac{\partial \phi_s}{\partial n}} \, dl, \qquad i \in \{1,2\}, \end{aligned} \tag{4.22}$$

and by direct pressure integration as

$$\begin{aligned} \overline{F_i^{pi}} &= -\rho \iint_{S_{\overline{B}}} \left\{ \frac{1}{2}\overline{|\nabla\Phi_1|^2} n_i + \overline{(\vec{\eta} + \vec{\alpha} \times \vec{r}) \cdot \nabla\left(\frac{\partial \Phi_1}{\partial t} + \nabla\phi_s \cdot \nabla\Phi_1\right) n_i} \right. \\ &\quad \left. + \overline{(\vec{\alpha} \times \vec{n})_i \left(\frac{\partial \Phi_1}{\partial t} + \nabla\phi_s \cdot \nabla\Phi_1\right)} + \nabla\phi_s \cdot \nabla\overline{\Phi}_2 n_i \right\} ds \\ &\quad + \frac{1}{2}\rho g \oint_{C_B} \overline{[\zeta^2 - 2\zeta(\eta_3 + y\eta_4 - x\eta_5)]} n_i \, dl, \qquad i \in \{1,2\}. \end{aligned} \tag{4.23}$$

Here ζ denotes the free surface elevation. The expressions are valid for arbitrary depth.

We notice that equation 4.23 consists of first order quantities, only. The last term in the first integral in equation 4.24 contains the second order potential and will be rewritten:

We consider the relation given by Ogilvie and Tuck [1969] for wall-sided structures and use the fact that $\frac{\partial \phi_s}{\partial z} = 0$ on the free surface. Then

$$\iint_{S_{\overline{B}}} \nabla\phi_s \cdot \nabla\overline{\Phi}_2 n_i ds = -\iint_{S_{\overline{B}}} \overline{\Phi}_2 \vec{n} \cdot \nabla \frac{\partial \phi_s}{\partial x_i} ds, \tag{4.24}$$

and Greens second identity, $\iint_S \left(\overline{\Phi}_2 \frac{\partial}{\partial n}\frac{\partial \phi_s}{\partial x_i} - \frac{\partial \phi_s}{\partial x_i}\frac{\partial \overline{\Phi}_2}{\partial n}\right) ds = 0$, over the closed surface $S = S_{\overline{B}} + S_{\overline{F}} + S_{C_0} + S_0$ gives

$$\iint_{S_{\overline{B}}} \nabla\phi_s \cdot \nabla\overline{\Phi}_2 n_i ds = \iint_{S_{\overline{B}}+S_{\overline{F}}+S_{C_0}} \frac{\partial \phi_s}{\partial x_i}\frac{\partial \overline{\Phi}_2}{\partial n} ds. \tag{4.25}$$

At the body surface and at the free surface $\frac{\partial \overline{\Phi}_2}{\partial n}$ is rewritten according to equation 4.15 and 4.16, and at the control surface we apply Green's theorem, giving

$$\iint_{S_{C_0}} \frac{\partial \phi_s}{\partial x_i}\frac{\partial \overline{\Phi}_2}{\partial n} ds = \begin{cases} -U\cos\alpha \iint_{S_{\overline{B}}+S_{\overline{F}}} \frac{\partial \overline{\Phi}_2}{\partial n} ds & \text{if } i = 1 \\ -U\sin\alpha \iint_{S_{\overline{B}}+S_{\overline{F}}} \frac{\partial \overline{\Phi}_2}{\partial n} ds & \text{if } i = 2. \end{cases} \tag{4.26}$$

Thus,

$$\iint_{S_{\overline{B}}} \nabla\phi_s \cdot \nabla\overline{\Phi}_2 n_i ds = \iint_{S_{\overline{B}}+S_{\overline{F}}} \frac{\partial \phi_{sb}}{\partial x_i}\frac{\partial \overline{\Phi}_2}{\partial n} ds \tag{4.27}$$

and the horizontal drift forces obtained by the method of direct pressure integration are now written in terms of the linear potential. Grue and Palm [1993] studied the term, which in their setting corresponded to equation 4.27 for infinite water depth. They found this term to be negligible in all their examples.

Grue and Biberg [1993] developed the mean yaw moment for finite water depth without solving the mean second order potential. Their way is easily modified to the present method. To achieve results for mean force/moments in heave, roll and pitch it seems to be necessary to solve the mean second order potential. That was also the conclusion of Grue and Palm [1993].

Wave-drift damping

The drift force may for small current velocities be written

$$\overline{F}_1 = \overline{F}_{1|F_n=0} + F_n \frac{\partial \overline{F}_1}{\partial F_n}_{|F_n=0}, \tag{4.28}$$

where $\frac{\partial \overline{F}_1}{\partial F_n}$ denotes the wave-drift damping $\overline{B}_1$. In the numerical solution $\overline{B}_1$ is found by numerically differentiating the results for the drift forces.

Clark et.al [1992] have given a simple formula for the wave-drift damping, which only includes zero-current terms. This formula is not properly explained, but there has been shown excellent agreement with existing results for a restricted cylinder in both deep and finite water depth. It would of course be a tremendous simplification if the drift forces, as a function of current, may be evaluated the way suggested by Clark et.al [1992].

Discussion of results

The drift forces for a restrained, half-immersed sphere are presented in figure 4.12, 4.13 and 4.14, again for four different water depths. We notice that the drift forces increase almost 100% if we simultaneously impose a current and decrease the depth from infinity to $h/R = 1.1$. Current then propagate in the same direction as the incident waves and the Froude number is 0.04.

When inspecting equation 4.23 and 4.24 we realize that a larger accuracy is needed in evaluation of the drift forces, than of the linear forces. Because the drift forces found by the method of direct pressure integration are more difficult to evaluate numerically than by conservation of momentum, we will not compare these methods here. Instead we compare drift forces for $h/R = 1.2$ and $h/R = \infty$, with results by Grue and Biberg [1993]. Figure 4.12 and 4.14 show results with a current present. The current and incident waves propagate in the same and opposite direction, respectively. The agreement is satisfactory.

The point where a convergence test is performed is chosen when the wave number is $KR = 0.5$, the water depth infinite and incident waves and current propagate in the same direction. In figure 4.16 the situation is illustrated when the drift force is written as function of horizontal length of the elements on the control surface. This was to better compare the results for two locations of the control surface. Results due to both analytical and numerical ϕ_s-calculation are shown. The maximum difference resulting from evaluating the steady potential analytically and numerically, respectively, is approximately 6%. The difference which comes from putting the control surface at $3R$ and $4R$, respectively, is less than 3% if the steady potential is evaluated analytically in both cases. The same situation was investigated for $KR = 1.23$. Also there the difference was approximately 3%. In neither of the cases the factors that relates lengths of adjacent elements ($factor_{S_F}$ and $factor_{S_C}$) are adjusted while increasing number of elements.

The wave-drift damping for four water depths are shown is figure 4.15. These results are compared with Grue and Biberg [1993] for $h/R = 1.2$ and $h/R = \infty$. In figure 4.17 a comparison with Clark et.al [1992] is presented. Their formula involves a term ω_0^2/g which for finite depth here, with success, is replaced by the wave number K. The agreement is not excellent, opposite to the case for restricted cylinders presented in Grue and Biberg [1993]. However, we have previously seen rather large errors in the calculations. Besides, in real life viscous and higher order effects matter. A disagreement of maximum 10% is therefore acceptable.

For a structure restrained from oscillating the m_j-terms are not involved. So, here this error source is not present. If the structure is free to respond to waves this is no longer the case. Therefore, before proceeding to oscillating structures we should develop a more robust way of evaluating m_j-terms.

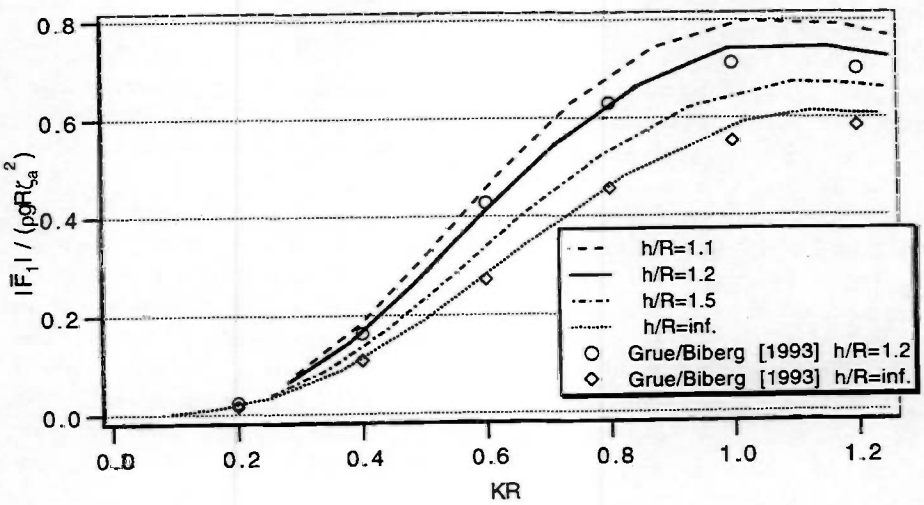

Figure 4.12: *Mean drift force for a restricted, half immersed sphere. Waves and current propagate in the same direction* ($\beta = 0$, $\alpha = 0$). *Froude number:* $F_n = 0.04$. ($NN1 = 32, NN2 = 18, NN3 = NN4 = 16$. *1 singularity in* $(0, 0, -R/2)$. *Control surface at* $4R$. *10 multipoles.* $factor_{S_F} = 1.1$ *and* $factor_{S_C} = 1.25$.)

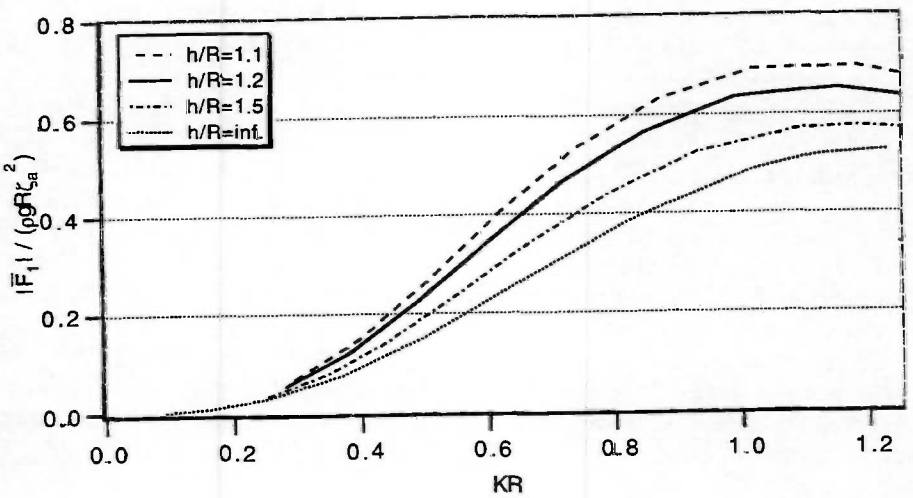

Figure 4.13: *Mean drift force for a restricted, half immersed sphere. Froude number:* $F_n = 0.0$. ($NN1 = 32, NN2 = 18, NN3 = NN4 = 16$. *1 singularity in* $(0, 0, -R/2)$. *Control surface at* $4R$. *10 multipoles.* $factor_{S_F} = 1.1$ *and* $factor_{S_C} = 1.25$.)

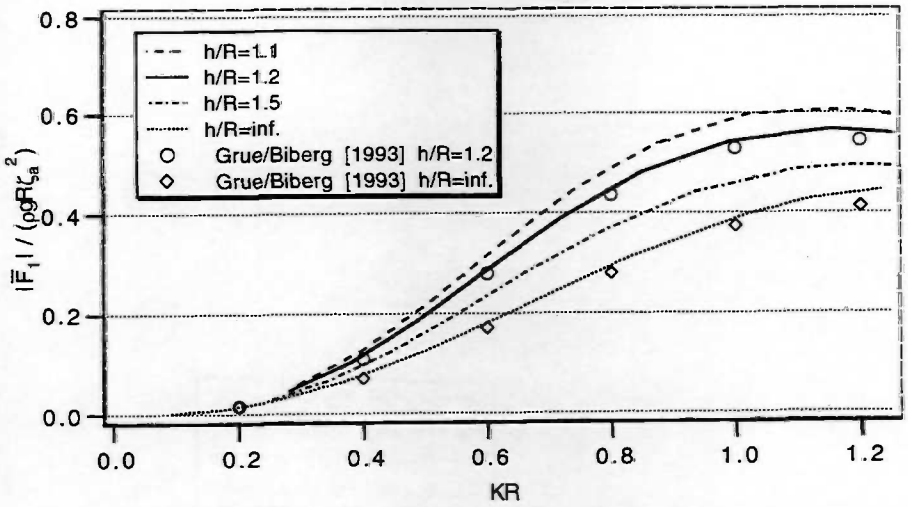

Figure 4.14: *Mean drift force for a restricted, half immersed sphere. Waves and current propagate in opposite directions ($\beta = \pi$, $\alpha = 0$). Froude number: $F_n = 0.04$. ($NN1 = 32, NN2 = 18, NN3 = NN4 = 16$. 1 singularity in $(0, 0, -R/2)$. Control surface at $4R$. 10 multipoles. $factor_{S_F} = 1.1$ and $factor_{S_C} = 1.25$.)*

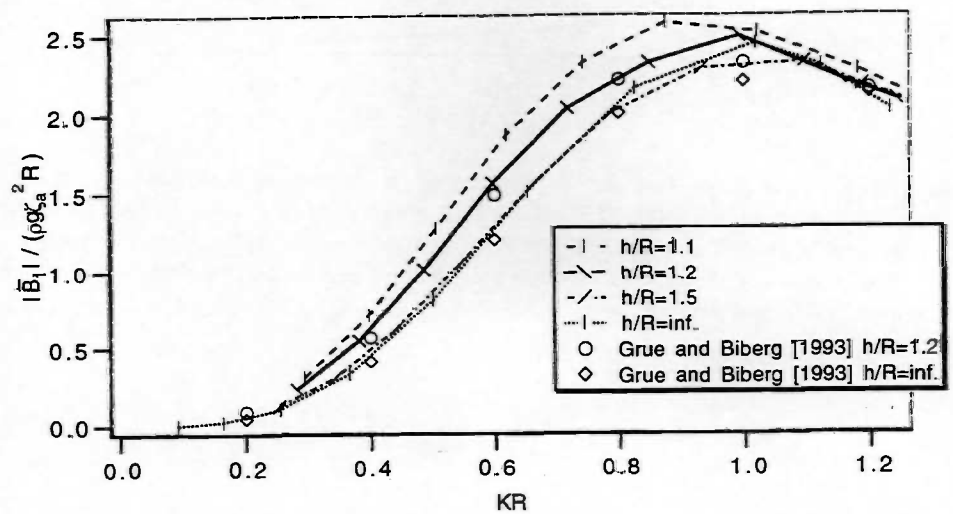

Figure 4.15: *Wave-drift damping coefficient for a restricted, half-immersed sphere ($NN1 = 32, NN2 = 18, NN3 = NN4 = 16$. 1 singularity in $(0, 0, -R/2)$. Control surface at $4R$. 10 multipoles. $factor_{S_F} = 1.1$ and $factor_{S_C} = 1.25$.)*

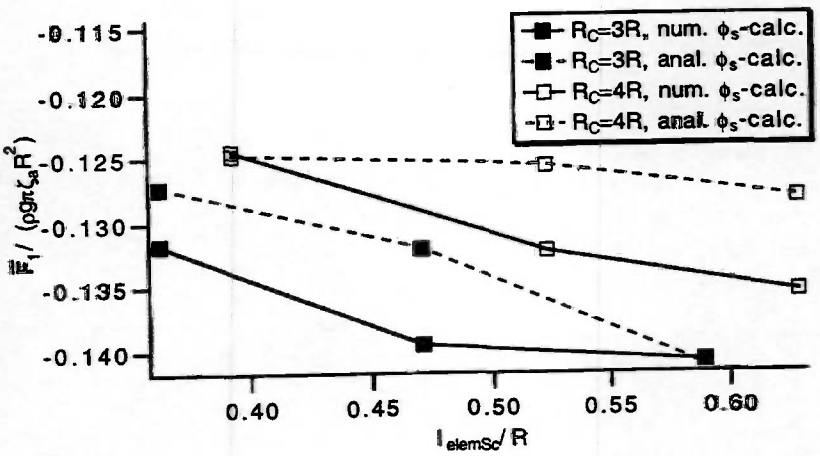

Figure 4.16: *Convergence test for drift force on a restrained half-immersed sphere. (F_n=0.04, Infinite water depth, $\omega_0^2 R/g = 0.5$, 1 singularity in $(0, 0, -R/2)$. 10 multipoles. $\alpha = 0$, $\beta = \pi$. $NN2 = NN3 = NN4 = NN1/2$ when control surface is situated at $3R$. $NN2 = NN4 = NN1/2$ and $NN2 = 1.1 \cdot NN3$ when control surface is situated at $4R$. $factor_{S_F} = 1.1$ and $factor_{S_C} = 1.25$.)*

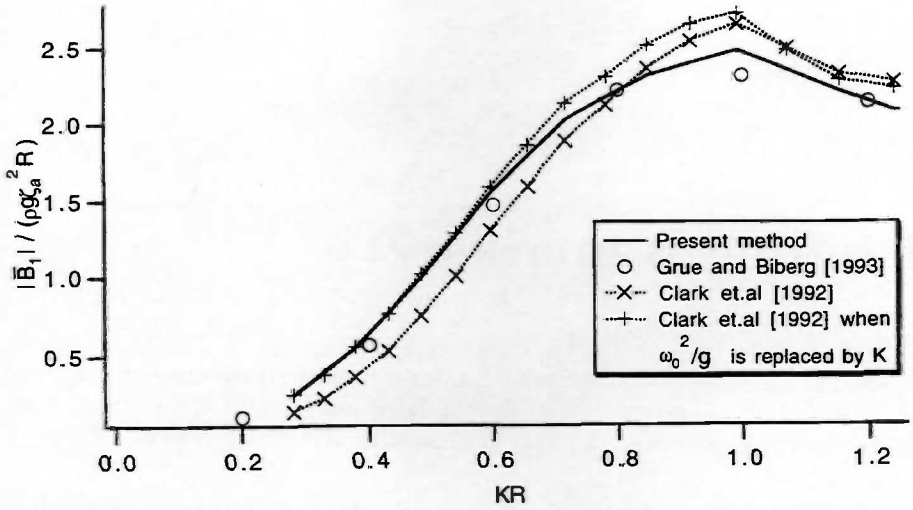

a) $h/R = 1.2$.

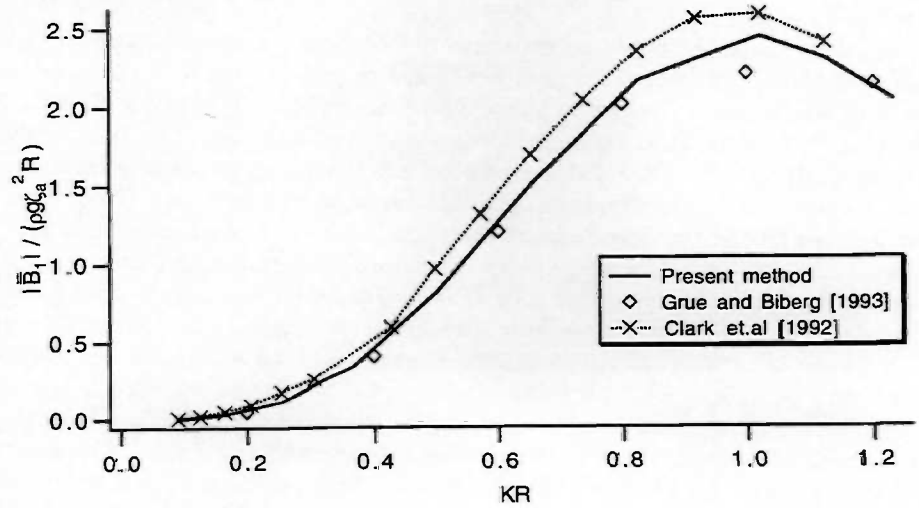

b) $h/R = \infty$.

Figure 4.17: *Comparison of wave-drift damping coefficient for a restrained half-immersed sphere with the simple formula of Clark et.al [1992]* ($NN1 = 32, NN2 = 18, NN3 = NN4 = 16$. *1 singularity in* $(0, 0, -R/2)$. *Control surface at* $4R$. *10 multipoles.* $factor_{S_F} = 1.1$ *and* $factor_{S_C} = 1.25$.)

Chapter 5

Concluding Remarks

In the previous chapters we have considered a floating large-volume structure in combined waves and current. Focus has been on the effect of finite water depth. Finite water depth represents the main difference from the work of Zhao et.al. [1988] and Zhao and Faltinsen [1989].

The steady flow problem was solved by distributing sources over the body surface. A Green's function was modified to satisfy the sea floor condition, by applying existing theory (Newman [1991]).

In the unsteady case the far-field potential due to a body was written as a sum of multipoles inside the body. The wave-current Green's function, which satisfies the free surface condition with wave-current interaction and the bottom condition, is initially given as a double integral. Two alternative expressions were established when analytically simplifying this integral. Both methods included expansion into infinite series before integrating. A way to increase speed of convergence of certain series was introduced. Good agreement was achieved for the two Green's functions in a broad range of parameter variations. Their higher order derivatives, however, were found to differ significantly when realistic parameters for the present problem were used. The multipoles for the chosen method were verified by applying the free surface condition. By letting parameters tend to limiting values and then comparing with calculated limiting Green's functions additional verification were performed.

A half-immersed sphere, restrained from oscillating, has been our test example. Moreover, the numerical calculations have been restricted to head and following sea. The results for wave exciting forces, added mass and damping coefficients, drift forces and wave-drift damping, have been compared with existing results. As Grue and Biberg [1993] we found that the drift forces may increase considerable when a current is present and water depth becomes shallow. The wave-drift damping, as given by Clark [1992], was found to represent a reasonable estimate compared to our results.

Although satisfactory results were achieved in most cases, some limitations for the computer program (MULDIF) were pointed out. The steady potential has slow convergence with respect to number of elements on the body surface. A new method should be applied, for instance the one given by Hiren [1995]. Due to the higher order element method he

also has the possibility of calculating m_j-terms directly at the surfaces.

Here, the m_j-terms were evaluated out in the fluid, and then extrapolated back to the body surface. This procedure was found to be more difficult as the water depth decreased. More generally: problems appear if two rigid surfaces are close.

Additional check-routines of the program have been implemented. This was done to get a better understanding of what parameters that caused problems. A new way of writing the horizontal linear wave exciting forces was found to be necessary in order to detect errors due to m_j-terms. In this way derivatives of the potentials at the body surface were avoided. The generalized Haskind relation, and also an alternative way of writing the diagonal damping coefficients, were in our case both found to be insufficient as objects of check-routines.

Bibliography

[1970] Abramowitz, M. and Stegun, I.A. : "Handbook of mathematical functions". Dover Publications inc.

[1984] Børresen, R. : "The unified theory of ship motions in water of finite depth". Dr.Ing-thesis. Norwegian Institute of Technology.

[1992] Clark, P.J., Malenica, S. and Molin, B. : "An heuristic approach to wave drift damping". Note.

[1981] Daubisse J.C. : "Some results on approximating by exponential series applied to hydrodynamic problems." Third Conference on Numerical Ship Hydrodynamics, Paris.

[1993] Eatock Taylor, R. and Teng, U. : "The Effect of Corners on Diffraction/Radiation Forces and Wave Drift Damping". Offshore Technol. Conf. (OTC), Vol.2, pp. 571-582.

[1990] Faltinsen, O. M. : "Sea loads on ships and offshore structures". Cambridge University Press.

[1974] Faltinsen, O. M. and Michelsen, F,C : "Motions of Large Structures in Waves at Zero Froude Number". Proceedings of the International Symposium on the Dynamics of Marine Vehicles and Structures in Waves. University College London, April 1-5.

[1981] Grekas, A. : "Contribution a l'etude theoretique et experimentale des efforts du second ordre et du comportement dynamique d'une structure marine solicitee par une houle reguliere et un courant". These de Docteur-Ingenieur, Ecole Nationale Superieure de Mechanique, Universite de Nantes.

[1993] Grue, J. and Biberg, D. : "Wave forces on marine structures with small speed in water of restricted depth". *Applied Ocean Research*, Vol.15, pp. 121-135.

[1985] Grue, J. and Palm, E. : "Wave radiation and wave diffraction from a submerged body in uniform current". *Journal of Fluid Mechanics*, Vol.151, pp. 257-278.

[1993] Grue, J. and Palm, E. : "The mean drift force and yaw moment on marine structures in waves and current". *Journal of Fluid Mechanics*, Vol. 250, pp.121-142.

[1974] Henrici, P. : "Applied and computational complex analysis". Wiley.

[1962] Hess, J.L. and Smith, A.M.O. : "Calculations of Non-lifting Potential flow about Arbitrary Three-dimensional Bodies". Report No. E.S 40622, Douglas Aircraft Division, Long Beach, California.

[1995] Hiren, D.M. : "A three dimensional higher order panel method based on B.splines". Ph.D-thesis. Massachusetts Institute of Technology.

[1990] Hoff, J.R. : "Three-dimensional Green function of a Vessel with forward speed in Waves." Dr.Ing-thesis. Norwegian Institute of Technology.

[1985] Huijsmans, R.H.M. and Hermans, A.J. : "A Fast Algorithm for Computations of 3-D Ship Motions at Moderate Forward Speed". 4th Internat. Conf. on Numerical Ship Hydrodynamics, Washington.

[1986] Huse, E. : "Influence of mooring line damping upon rig motions". Offshore Technol. Conf. (OTC), Vol. 2, pp. 433-38, Houston.

[1991] Håvie T. : "Numeriske beregninger". Tapir Forlag.

[1950] John, F. : "On the motion of floating bodies II". *Commun. Pure Appl. Math.* , Vol.3, pp.45-101.

[1992] Knudsen, F.F. : Personal communications.

[1945] Lamb, H. : "Hydrodynamics". New York: Dover Publications.

[1981] Mavrakos, S. :"Eine lineare Lösung des Oberflächenwellenproblems ausserhalb und innerhalb rotationssymmetrischer Körper mit vertikaler Achse". Dr.Ing-thesis. Technischen Hochschule Achen.

[1967] Newman, J.N. : "The drift force and moment on ships in waves". *Journal of Ship Research*, Vol.11, pp. 51-60.

[1974] Newman, J.N. : "Second order, slowly varying forces in irregular waves". Proc. Int. Symp. Dynamics of Marine Vehicles and Structures in Waves, ed. R.E.D. Bishop and W.G. Price, pp. 182-186.

[1977] Newman, J.N. : "Marine Hydrodynamics", Cambridge: The MIT Press.

[1978] Newman, J.N. : "The Theory of Ship Motions". *Advances in Applied Mechanics*, Vol.18, pp.221-283.

[1986] Newman, J.N. : "Distributions of sources and normal dipoles over a quadrilateral panel". *Journal of Engineering Mathematics*. pp. 113-126.

[1991] Newman, J.N. : "The approximation of free-surface Green functions". in: Wave asymptotics - Proc. of the Fritz Ursell Retirement Meeting, Camb. Univ. Press.

[1991] Nossen, J., Grue, J. and Palm, E. : "Wave forces on three-dimensional floating bodies with small forward speed". *Journal of Fluid Mechanics.* Vol. 227, pp. 135-160.

[1983] Ogilvie, T. F. : "Second-order hydrodynamic effects on ocean platforms". Proc. Int. Workshop on Ship and Platforms Motions. Univ. California, Berkeley.

[1969] Ogilvie, T.F. and Tuck, E.O. : "A rational strip theory of ship motions". The department of Naval Architecture and Marine Engineering, The University of Michigan, College of Engineering.

[1980] Pettersen, B : "Calculation of potential flow about ship hulls in shallow water with particular application to maneuvering". Dr.Ing-thesis. Norwegian Institute of Technology.

[1989] Press, W.H., Flannery B.P., Teukolsky S.A. and Vetterling W.T. : "Numerical Recepies. The art of scientific computations". Cambridge University Press.

[1995] Prins, H.J. : "Time-Domain Calculations of Drift Forces and Moments". Ph.D-thesis. Technische Universiteit Delft.

[1950] Whittaker, T.E. and Watson, E. : "Modern analysis". Cambridge University Press.

[1994] Zhao, R. : "Studies of Weak and Strong Non-Linear Sea Loads on Floating Marine Structures". Dr.Techn-thesis. Norwegian Institute of Technology.

[1988] Zhao, R. and Faltinsen, O.M. : "Interaction between waves and current on a two dimensional body in the free surface". *Applied Ocean res.*, Vol.10, pp. 87-98.

[1989] Zhao, R. and Faltinsen, O.M. : "Interaction between current, waves and marine structures". 5th International Confer. on Numerical ship Hydrodynamics, Hiroshima.

[1988] Zhao, R., Faltinsen, O.M., Krokstad, J.R. and Aanesland, V. : "Wave-current Interaction Effects on Large-Volume Structures". Int. Conf. BOSS, Trondheim.

Appendix A

Approximating the outer potential by a sum of multipoles inside the body

First, we would like to convince ourselves about the claim that ϕ_k actually can be found by distributing sources and dipoles over the body surface and the body near part of the free surface. This is already proven by Nossen et.al. [1991] for infinite water depth and found to be valid also for arbitrary depth by Grue and Biberg [1993].

We look at Green's second identity in the whole fluid domain on ϕ_k ($k \in \{1,..,7\}$) and the Green's function from chapter 3 having current angle $\alpha + \pi$:

$$-4\pi\phi_k(\vec{x}_0) = \iint_{S_{C_\infty}+S_B+S_{F_\infty}} \left(G(\vec{x},\vec{x}_0;\alpha+\pi)\frac{\partial\phi_k(\vec{x})}{\partial n(\vec{x})} - \phi_k(\vec{x})\frac{\partial G(\vec{x},\vec{x}_0;\alpha+\pi)}{\partial n(\vec{x})} \right) ds(\vec{x}) \quad \text{(A.1)}$$

The surfaces S_{C_∞}, S_B and S_{F_∞} are shown in figure A.1. Since both G and ϕ_k satisfies the bottom condition the integral over the sea floor vanish. The normal vector, $\vec{n}$, is still pointing out of the fluid.

The integral over the infinite free surface may be written (we apply equation 2.11 and equation 2.12 in section 2.1)

$$\begin{aligned} \iint_{S_{F_\infty}} \left(G^{\alpha+\pi}\frac{\partial\phi_k}{\partial n} - \phi_k\frac{\partial G^{\alpha+\pi}}{\partial n} \right) ds &= -2i\tau\int_{C_\infty}\cos(\alpha-v)\phi_k G^{\alpha+\pi}dl \\ &+\frac{2i\omega}{g}\iint_{S_{F_i}}\phi_k\left(\frac{1}{2}G^{\alpha+\pi}\nabla^2_{(2D)}\phi_{sb} + \nabla_{(2D)}\phi_{sb}\cdot\nabla_{(2D)}G^{\alpha+\pi}\right)ds \quad \text{(A.2)} \end{aligned}$$

if $k \in \{1,..,6\}$ and

$$\begin{aligned} \iint_{S_{F_\infty}} \left(G^{\alpha+\pi}\frac{\partial\phi_7}{\partial n} - \phi_7\frac{\partial G^{\alpha+\pi}}{\partial n} \right) ds &= -2i\tau\int_{C_\infty}\cos(\alpha-v)\phi_7 G^{\alpha+\pi}dl \\ +\frac{2i\omega}{g}\iint_{S_{F_i}}\left[\nabla_{(2D)}\phi_{sb}(\phi_7\nabla_{(2D)}G^{\alpha+\pi} - G^{\alpha+\pi}\nabla_{(2D)}\phi_0) + \frac{1}{2}G^{\alpha+\pi}\nabla^2_{(2D)}\phi_{sb}(\phi_7-\phi_0)\right]ds & \quad \text{(A.3)} \end{aligned}$$

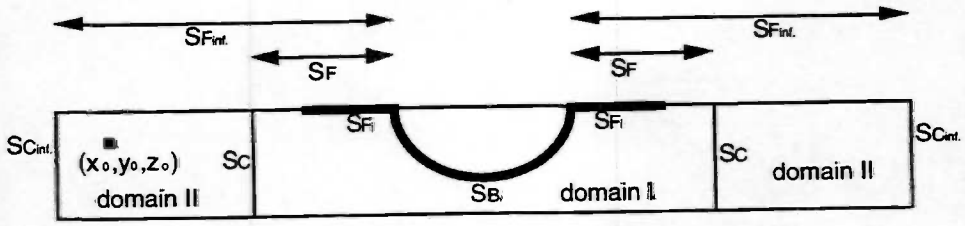

Figure A.1: *Surface and domain definitions.*

Here C_∞ is the line intersecting the mean infinite free surface, S_{F_∞}, and the infinite control surface, S_{C_∞}. We have used the short form $G^{\alpha+\pi}$ for $G(\vec{x},\vec{x}_0;\alpha+\pi)$ and $(x,y) = (R\cos v, R\sin v, z)$. The results are valid for structures that are wall-sided at the free surface.

The far field Green's function may be written (from page 34)

$$G(\vec{x},\vec{a};\alpha) \sim \frac{B(\vec{a},v)}{\sqrt{R}}\cosh[c_0(\alpha)(z+h)]e^{-ic_0(\alpha)R\sqrt{1-\frac{4\tau^2}{F(c_0)^2}\sin^2(v-\alpha)}}, \tag{A.4}$$

thus we may write the far field velocity potential as

$$\phi_k(\vec{x}) \sim \frac{A(v)}{\sqrt{R}}\cosh[c_0(\alpha)(z+h)]e^{-ic_0(\alpha)R\sqrt{1-\frac{4\tau^2}{F(c_0)^2}\sin^2(v-\alpha)}} \tag{A.5}$$

We insert the far field approximations in the integral over the infinite control surface, giving for $k \in \{1,..,7\}$

$$\begin{aligned}
&\iint_{S_{C_\infty}} G^{\alpha+\pi}\frac{\partial\phi_k}{\partial n} - \phi_k\frac{\partial G^{\alpha+\pi}}{\partial n}ds \;=\\
&i\iint_{S_{C_\infty}} G^{\alpha+\pi}\phi_k[\sqrt{1-\tfrac{4\tau^2}{F[c_0(\alpha+\pi)]^2\sin^2(v-\alpha)}}c_0(\alpha+\pi) - \sqrt{1-\tfrac{4\tau^2}{F[c_0(\alpha)]^2\sin^2(v-\alpha)}}c_0(\alpha)]ds\\
&= i\int_{C_\infty} G^{\alpha+\pi}\phi_k[\sqrt{1-\tfrac{4\tau^2}{F[c_0(\alpha+\pi)]^2\sin^2(v-\alpha)}}c_0(\alpha+\pi) - \sqrt{1-\tfrac{4\tau^2}{F[c_0(\alpha)]^2\sin^2(v-\alpha)}}c_0(\alpha)]\\
&\qquad\times\int_{-h}^{0}\frac{\cosh[c_0(\alpha+\pi)(z+h)]\cosh[c_0(\alpha)(z+h)]}{\cosh[c_0(\alpha+\pi)(h)]\cosh[c_0(\alpha)(h)]}dzdl\\
&= i\int_{C_\infty} G^{\alpha+\pi}\phi_k[\sqrt{1-\tfrac{4\tau^2}{F[c_0(\alpha+\pi)]^2\sin^2(v-\alpha)}}c_0(\alpha+\pi) - \sqrt{1-\tfrac{4\tau^2}{F[c_0(\alpha)]^2\sin^2(v-\alpha)}}c_0(\alpha)]\\
&\qquad\times\frac{\tanh[c_0(\alpha+\pi)h]c_0(\alpha+\pi) - \tanh[c_0(\alpha)h]c_0(\alpha)}{c_0^2(\alpha+\pi) - c_0^2(\alpha)}dl\\
&\qquad = 2i\tau\int_{C_\infty}\cos(\alpha-v)\phi_k G^{\alpha+\pi}dl + \mathcal{O}(\tau^2).
\end{aligned} \tag{A.6}$$

From the third to the fourth step a Taylor expansion in τ has been used. This term cancels the first term in equation A.2 and equation A.3 to first order in τ. Thus, ϕ_k may be written

$$-4\pi\phi_k(\vec{x}_0) \;=\; \iint_{S_B} G^{\alpha+\pi}\frac{\partial\phi_k}{\partial n} - \phi_k\frac{\partial G^{\alpha+\pi}}{\partial n}ds \tag{A.7}$$

$$+\begin{cases} \frac{2i\omega}{g}\iint_{S_{F_i}} \phi_k \left(\frac{1}{2}G^{\alpha+\pi}\nabla^2_{(2D)}\phi_{sb} + \nabla_{(2D)}\phi_{sb}\cdot\nabla_{(2D)}G^{\alpha+\pi}\right) ds & \text{if } k\in\{1,..,6\} \\ \frac{2i\omega}{g}\iint_{S_{F_i}} \nabla_{(2D)}\phi_{sb}(\phi_7\nabla_{(2D)}G^{\alpha+\pi} - G^{\alpha+\pi}\nabla_{(2D)}\phi_0) + \frac{1}{2}G^{\alpha+\pi}\nabla^2_{(2D)}\phi_{sb}(\phi_7-\phi_0)ds & \text{if } k=7. \end{cases}$$

If $\vec{x}_0$ is far from the body we may make a Taylor expansion in $\vec{x}$ to any point $\vec{a}_m$ inside the body (according to Newman [1977, page 143] who considered a steady problem) . The Green's function is then

$$\begin{aligned} G(\vec{x},\vec{x}_0;\alpha+\pi) &= \sum_{m=1}^{M} G(\vec{a}_m,\vec{x}_0;\alpha+\pi) + \left((\vec{x}-\vec{a}_m)\cdot\nabla_{\vec{x}}\right) G(\vec{x},\vec{x}_0;\alpha+\pi)_{|\vec{x}=\vec{a}_m} \\ &\quad + \left((\vec{x}-\vec{a}_l)\cdot\nabla_{\vec{x}}\right)^2 G(\vec{x},\vec{x}_0;\alpha+\pi)_{|\vec{x}=\vec{a}_m} + \cdots \end{aligned} \tag{A.8}$$

and the normal derivative satisfies

$$\begin{aligned} \frac{\partial G(\vec{x},\vec{x}_0;\alpha+\pi)}{\partial n(\vec{x})} &= \vec{n}\cdot\Big[\nabla_{\vec{x}}G(\vec{x},\vec{x}_0;\alpha+\pi)_{|\vec{x}=\vec{a}_m} \\ &\quad + \left((\vec{x}-\vec{a}_m)\cdot\nabla_{\vec{x}}\right)\nabla_{\vec{x}}G(\vec{x},\vec{x}_0;\alpha+\pi)_{|\vec{x}=\vec{a}_m} + \cdots\Big]. \end{aligned} \tag{A.9}$$

We apply

$$\nabla_{\vec{x}}G(\vec{x},\vec{x}_0;\alpha+\pi)_{|\vec{x}=\vec{a}_m} = \nabla_{\vec{a}_m}G(\vec{x}_0,\vec{a}_m;\alpha) \tag{A.10}$$

and the velocity potential in the outer domain, ϕ_k^{II} $k\in\{1,..,6\}$, can be written as

$$\begin{aligned} \phi_k^{II}(\vec{x}_0) &= -\frac{1}{4\pi}\sum_{m=1}^{M}\left[\iint_{S_B}\frac{\partial\phi_k}{\partial n}ds + \frac{2i\omega}{g}\iint_{S_{F_i}}\frac{1}{2}\phi_k\nabla^2_{(2D)}\phi_{sb}\right] G(\vec{x}_0,\vec{a}_m;\alpha) \\ &+\left[\iint_{S_B}\left(\frac{\partial\phi_k}{\partial n}(x-a_m) - \phi_k n_1\right)ds + \frac{2i\omega}{g}\iint_{S_{F_i}}\frac{1}{2}\phi_k\nabla^2_{(2D)}\phi_{sb}(x-a_m) + \frac{\partial\phi_{sb}}{\partial x}ds\right]\frac{\partial G(\vec{x}_0,\vec{a}_m;\alpha)}{\partial a_m} \\ &+\left[\iint_{S_B}\left(\frac{\partial\phi_k}{\partial n}(y-b_m) - \phi_k n_2\right)ds + \frac{2i\omega}{g}\iint_{S_{F_i}}\frac{1}{2}\phi_k\nabla^2_{(2D)}\phi_{sb}(y-b_m) + \frac{\partial\phi_{sb}}{\partial y}ds\right]\frac{\partial G(\vec{x}_0,\vec{a}_m;\alpha)}{\partial b_m} \\ &\quad + \cdots. \end{aligned} \tag{A.11}$$

By the same method ϕ_7^{II} is found, and we reach equation 2.19 in section 2.1:

$$\phi_k^{II}(\vec{x}) = \sum_{l=1}^{L}\sum_{m=1}^{M} A_{lm}G^l(\vec{x};\vec{a}_m), \text{ for } k\in\{1,..,7\}. \tag{A.12}$$

The preceding calculations indicates that the control surface, S_C, has to be placed further away from the body in the presence of a current. Alternatively we have to include more terms in the Taylor series.

Appendix B

Details from Chapter 3

B.1 Location of the poles far from origo

(ref. pg. 21)
We want to find the asymptotic solutions to

$$c_n \sinh c_n h = (\nu + 2\tau c_n \cos\theta) \cosh c_n h. \tag{B.1}$$

That is find the c_n's for $|n|$ large. Since the c_n's are isolated, $|c_n|$ tends to infinity. Hence the magnitude of the real part of c_n, the imaginary part of c_n, or both, tend to infinity as n tends to infinity.

Writing c_n as $c_n = a_n + id_n$, equation B.1 is

$$\begin{aligned}(a_n + id_n)[\sinh a_n h \cos d_n h + i \cosh a_n h \sin d_n h] = [\nu + (a_n + id_n)2\tau \cos\theta] \\ \times [\cosh a_n h \cos d_n h - i \sinh a_n h \sin d_n h].\end{aligned} \tag{B.2}$$

By simple considerations we find that $\cos d_n h = 0$ is not a solution if n is large. Thus we may divide by $\cosh a_n h \cos d_n h$. The real part then equals

$$a_n \tanh a_n h - d_n \tan d_n h = \nu + a_n 2\tau \cos\theta + d_n 2\tau \cos\theta \tanh a_n h \tan d_n h \tag{B.3}$$

and the imaginary part looks like

$$d_n \tanh a_n h + a_n \tan d_n h = -(\nu + a_n 2\tau \cos\theta) \tanh a_n h \tan d_n h + d_n 2\tau \cos\theta. \tag{B.4}$$

The poles are plotted for the first n's. It seems reasonable to assume that $|d_n| \gg |a_n|$ for $|n|$ large. However, all cases will be examined:

- a_n bounded

  The real part gives

$$d_n \tan d_n h = \frac{a_n \tanh a_n h - \nu - a_n 2\tau \cos\theta}{2\tau \cos\theta \tanh a_n h + 1}. \tag{B.5}$$

As $|d_n|$ grows, $\tan d_n h \to 0$, or $d_n \to \frac{m\pi}{h}$. Assuming $[a_n \tanh a_n h - \nu - a_n 2\tau \cos\theta]$ having a constant sign in n

$$d_n = \begin{cases} \frac{n\pi}{h} & \text{if } [a_n \tanh a_n h - \nu - a_n 2\tau \cos\theta] < 0 \\ \frac{(n+1)\pi}{h} & \text{if } [a_n \tanh a_n h - \nu - a_n 2\tau \cos\theta] > 0 \end{cases} \tag{B.6}$$

Inserting $\tan d_n h = 0$ in equation B.4, we find

$$\tanh a_n h = 2\tau \cos\theta \tag{B.7}$$

which gives the real part of asymptotic poles:

$$a_n = \frac{1}{2h} \ln \left[\frac{1 + 2\tau \cos\theta}{1 - 2\tau \cos\theta} \right], \tag{B.8}$$

and in turn

$$d_n = \frac{n\pi}{h}. \tag{B.9}$$

- a_n unbounded

When $|a_n|$ tends to infinity, ν is negligible in the calculations and $\tanh |a_n| h$ tends to 1. If $a_n > 0$ we have

$$a_n - d_n \tan d_n h = a_n 2\tau \cos\theta + d_n 2\tau \cos\theta \tan d_n h \tag{B.10}$$

$$d_n + a_n \tan d_n h = -a_n 2\tau \cos\theta \tan d_n h + d_n 2\tau \cos\theta, \tag{B.11}$$

and if $a_n < 0$

$$-a_n - d_n \tan d_n h = a_n 2\tau \cos\theta - d_n 2\tau \cos\theta \tan d_n h \tag{B.12}$$

$$-d_n + a_n \tan d_n h = a_n 2\tau \cos\theta \tan d_n h + d_n 2\tau \cos\theta. \tag{B.13}$$

In both cases this gives

$$a_n^2 = -d_n^2, \tag{B.14}$$

and since we seek real solutions, we conclude that there are no poles for $|a_n|$ large.

Thus, all asymptotic poles are represented by

$$c_n \to \frac{1}{2h} \ln \left[\frac{1 + 2\tau \cos\theta}{1 - 2\tau \cos\theta} \right] + i \frac{n\pi}{h} \qquad n \text{ large.} \tag{B.15}$$

B.2 Residues

(ref. pg. 22)
We will find the residues in $k = c_n$ for

$$p(k,\theta) = \frac{\cosh k(z+h)[k(1+2\tau\cos\theta)+\nu]}{k\sinh kh - [\nu + 2\tau\cos\theta k]\cosh kh}. \tag{B.16}$$

The residue in c_n of the function $p(k,\theta) = \frac{r(k,\theta)}{q(k,\theta)}$ is $b_n = r(c_n,\theta)/\frac{\partial q(k,\theta)}{\partial k}_{|k=c_n}$. Thus,

$$b_n = \frac{\cosh c_n(z+h)[c_n(1+2\tau\cos\theta)+\nu]}{\sinh c_n h + c_n h\cosh c_n h - 2\tau\cos\theta\cosh c_n h - h(\nu+2\tau c_n\cos\theta)\sinh c_n h}. \tag{B.17}$$

We remove the $\cos\theta$ terms by applying $2\tau\cos\theta = \tanh c_n h - \frac{\nu}{c_n}$:

$$b_n = \frac{\cosh c_n(z+h)c_n(1+\tanh c_n h)}{\sinh c_n h + c_n h\cosh c_n h - h(\tanh c_n h - \frac{\nu}{c_n})\cosh c_n h}. \tag{B.18}$$

Multiplying by $c_n\cosh c_n h$ in numerator and denominator gives

$$b_n = \frac{c_n^2 e^{c_n h}\cosh c_n(z+h)}{c_n^2 h + \nu\cosh^2 c_n h}. \tag{B.19}$$

B.3 Convergence of the infinite series

(ref. pg. 22)
Approximating the function $p(z)$ by the sum $\sum_{n=1}^{\infty} p_n(z)$, the sum converges uniformly in a region if

$$|p(z) - p_N(z)| < \epsilon \tag{B.20}$$

for all z in that region and all $n > N(\epsilon)$.
Here we have

$$|p(k,\theta) - p_N(k,\theta)| = \left|\sum_{n=N+1}^{\infty} 2\Re\{\frac{b_n}{k-c_n}\}\right|. \tag{B.21}$$

Choosing N large, we approximate c_n with $c_n = a + \frac{in\pi}{h}$. Thus,

$$|p(k,\theta) - p_N(k,\theta)| = 2\left|\sum_{n=N+1}^{\infty} \frac{\Re\{b_n\}(k-a) - \Im\{b_n\}\frac{n\pi}{h}}{(k-a)^2 + \left(\frac{n\pi}{h}\right)^2}\right|. \tag{B.22}$$

We have

$$b_n = \frac{c_n^2 e^{c_n h}\cosh c_n(z+h)}{c_n^2 h + \nu\cosh^2 c_n h}. \tag{B.23}$$

It is immediately seen that b_n is of order 1 in n. Thus, we have to make a closer study of b_n for large n.

Inserting the limiting value of c_n we get

$$b_n = \frac{1}{2h(1-2\tau\cos\theta)^2} \times \left\{ \left[\frac{1+2\tau\cos\theta}{1-2\tau\cos\theta}\right]^{\frac{z}{2h}} (1+2\tau\cos\theta)[\cos\frac{n\pi z}{h} + i\sin\frac{n\pi z}{h}] + \left[\frac{1-2\tau\cos\theta}{1+2\tau\cos\theta}\right]^{\frac{z}{2h}} (1-2\tau\cos\theta)[\cos\frac{n\pi z}{h} - i\sin\frac{n\pi z}{h}] \right\}. \tag{B.24}$$

Writing $b_n = f\cos\frac{n\pi z}{h} + ig\frac{n\pi z}{h}$ and inserting this in equation B.22, we get

$$|p(k,\theta) - p_N(k,\theta)| = 2\left| \sum_{n=N+1}^{\infty} \frac{f\cos\frac{n\pi z}{h}(k-a)}{(k-a)^2 + \left(\frac{n\pi}{h}\right)^2} - \frac{g\sin\frac{n\pi z}{h}\frac{n\pi}{h}}{(k-a)^2 + \left(\frac{n\pi}{h}\right)^2} \right|. \tag{B.25}$$

Uniform convergence of the first term is shown by applying Weierstrass' M-test:

$$\left| f \sum_{n=N+1}^{\infty} \frac{(k-a)\cos\frac{n\pi z}{h}}{(k-a)^2 + \left(\frac{n\pi}{h}\right)^2} \right| \leq |f|\frac{h^2}{\pi^2} \sum_{n=N+1}^{\infty} \frac{|k-a|}{n^2} \leq |f|G\frac{h^2}{\pi^2} \sum_{n=N+1}^{\infty} \frac{1}{n^2}, \tag{B.26}$$

where G denotes the largest $|k-a|$ in the region.

The second term represents a series which is not absolutely convergent. We will then use the fact that a series is convergent if it is the sum of two convergent series. $\sum_{n=1}^{\infty} \frac{\sin n\pi a}{n}$ is the Fourier series of the odd expansion of $f(a) = \frac{\pi}{2}(1-a)$ with half period 1, and thus converges. Hence,

$$\left| \sum_{n=N+1}^{\infty} -\frac{g\sin\frac{n\pi z}{h}\frac{n\pi}{h}}{(k-a)^2 + \left(\frac{n\pi}{h}\right)^2} + \sum_{n=N+1}^{\infty} \frac{g\sin\frac{n\pi z}{h}\frac{n\pi}{h}}{\frac{n\pi}{h}} \right| = \left| \sum_{n=N+1}^{\infty} \frac{g\sin\frac{n\pi z}{h}(k-a)^2}{(k-a)^2 + \left(\frac{n\pi}{h}\right)^2} \right|, \tag{B.27}$$

and by the same argument as above this series converges.

So far we have neglected the fact that c_n never really reaches $a + \frac{in\pi}{h}$. Since the convergence is slow and there is no such thing as intuition when it comes to infinite series, it is necessary to check the effect this will have upon the convergence. We will concentrate on the term which is not absolutely convergent. Writing b_n as $b_n = \left[\frac{1}{h} - \frac{\nu\cosh^2 c_n h}{c_n^2 h + \nu\cosh^2 c_n h}\right] e^{c_n h}\cosh c_n(z+h)$, we see that this term is

$$-\frac{2}{h}\left| \sum_{n=N+1}^{\infty} \frac{\Im\{e^{c_n h}\cosh c_n(z+h)\}\Im\{c_n\}}{(k-\Re\{c_n\})^2 + \Im\{c_n\}^2} \right|. \tag{B.28}$$

Writing $c_n = a + \epsilon_n^a + i\left[\frac{n\pi}{h} + \epsilon_n^d\right]$ this gives

$$-\frac{1}{h}\left|\sum_{n=N+1}^{\infty}\frac{[f_n(z)+f_n(z+2h)]\left(\frac{n\pi}{h}+\epsilon_n^d\right)}{(k-a-\epsilon_n^a)^2+\left(\frac{n\pi}{h}+\epsilon_n^d\right)^2}\right|, \tag{B.29}$$

where

$$f_n(z)=e^{(a+\epsilon_n^a)z}\left[\sin\frac{n\pi z}{h}\cos\epsilon_n^d z+\cos\frac{n\pi z}{h}\sin\epsilon_n^d z\right]. \tag{B.30}$$

We will need an estimate for the errors ϵ_n^a and ϵ_n^d. For small errors the approximations $\tanh(a+\epsilon_n^a)h=\frac{2\tau\cos\theta+\epsilon_n^a h}{1+2\tau\cos\theta\epsilon_n^a h}$ and $\tan(\frac{n\pi}{h}+\epsilon_n^d)h=\epsilon_n^d h$ may be used in the equations B.3 and B.4 in section B.1. This produces two simple equations with two unknowns with solutions

$$\epsilon_n^a = \frac{\left[\nu 2\tau\cos\theta+\frac{1}{2h}\ln\left[\frac{1+2\tau\cos\theta}{1-2\tau\cos\theta}\right](1+4\tau^2\cos^2\theta)\right]\nu}{(1+4\tau^2\cos^2\theta)\pi^2}\frac{1}{n^2}+\text{higher order of }\frac{1}{n} \tag{B.31}$$

$$\epsilon_n^d = -\frac{\nu}{(1+4\tau^2\cos^2\theta)\pi h}\frac{1}{n}+\text{higher order of }\frac{1}{n} \tag{B.32}$$

Using the above,we are convinced that the series $\sum_{n=-\infty}^{\infty}\frac{b_n}{k-c_n}$ converges uniformly in k, in every interval $[0,A]$ with the exception of the poles.

B.4 Integration of the remaining integral

(ref. pg. 30)
We want to simplify the double integral

$$RI^A=\frac{1}{2\pi}\int_0^{2\pi}\int_{\sigma_3}^{\infty}e^{-\beta k}\frac{k(1+2\tau\cos\theta)+\nu}{k(1-2\tau\cos\theta)-\nu}dkd\theta \tag{B.33}$$

where $\beta=-[z+c+i\tau\cos(\theta-u+\alpha)]$. It is noticed that

$$\frac{k(1+2\tau\cos\theta)+\nu}{k(1-2\tau\cos\theta)-\nu}=\frac{1+2\tau\cos\theta}{1-2\tau\cos\theta}+\frac{2\nu}{(1-2\tau\cos\theta)^2}\frac{1}{k-\frac{\nu}{1-2\tau\cos\theta}}. \tag{B.34}$$

Inserting this in the integral above, we get

$$\begin{aligned}RI^A = {} & \frac{1}{2\pi}\int_0^{2\pi}\frac{1+2\tau\cos\theta}{1-2\tau\cos\theta}\int_{\sigma_3}^{\infty}e^{-\beta k}dkd\theta+\\ & \frac{1}{2\pi}\int_0^{2\pi}\frac{2\nu}{(1-2\tau\cos\theta)^2}\int_{\sigma_3}^{\infty}\frac{e^{-\beta k}}{k-\frac{\nu}{1-2\tau\cos\theta}}dkd\theta.\end{aligned} \tag{B.35}$$

Evaluation of the first integral in k is straight forward. The second results in, when substituting $t=\beta(k-\frac{\nu}{1-2\tau\cos\theta})$,

$$\int_{\sigma_3}^{\infty}\frac{e^{-\beta k}}{k-\frac{\nu}{1-2\tau\cos\theta}}dk=e^{-\beta(\frac{\nu}{1-2\tau\cos\theta})}\int_{\beta(\sigma_3-\frac{\nu}{1-2\tau\cos\theta})}^{\infty}\frac{e^{-t}}{t}dt. \tag{B.36}$$

Since σ_3 is chosen larger than σ_2, and $\sigma_2 = \frac{\nu}{\tanh\sigma_2 h - 2\tau\cos\theta} > \frac{\nu}{1-2\tau\cos\theta}$, the real part of $\beta(\sigma_3 - \frac{\nu}{1-2\tau\cos\theta})$ is larger than zero, and the integral represent an exponential integral. Thus,

$$RI^A = \frac{1}{2\pi}\int_0^{2\pi}\left[\frac{1}{\beta}\frac{1+2\tau\cos\theta}{1-2\tau\cos\theta} + \frac{2\nu}{(1-2\tau\cos\theta)^2}G[\beta(\sigma_3 - \frac{\nu}{1-2\tau\cos\theta})]\right]e^{-\beta\sigma_3}d\theta, \quad \text{(B.37)}$$

where $G[\beta(\sigma_3 - \frac{\nu}{1-2\tau\cos\theta})] = e^{[\beta(\sigma_3 - \frac{\nu}{1-2\tau\cos\theta})]}E_1[\beta(\sigma_3 - \frac{\nu}{1-2\tau\cos\theta})]$ and E_1 is the exponential integral.

B.5 Derivatives

(ref. pg. 26 and 31)
We look at the integral part of $G_{Alt.1}$; G_{1_B} given by

$$G_{1_B} = \frac{1}{2\pi}\int_0^{2\pi}\sum_{i=1}^{2}\left[\sum_{n=-N(\theta)}^{N(\theta)} b_n\left\{\frac{1}{(\beta_i c_n)} + e^{-\beta_i c_n}\int_{-\beta_i c_n}^{\infty}\frac{e^{-t}}{t}dt\right\}\right.$$
$$\left. + \sum_{j=1}^{L}\left[\left(\sum_{n=-N(\theta)}^{N(\theta)}\frac{b_n}{c_n^{j+1}}\right) - \frac{1}{j!}\frac{\partial^j p(k,\theta)}{\partial k^j}_{|k=0}\right]\frac{j!}{\beta_i^{j+1}}\right]d\theta.$$

The derivatives of G_{1_B} are

$$\frac{\partial^M G_{1_B}}{\partial a^{M_1}\partial b^{M_2}\partial c^{M_3}} = \frac{1}{2\pi}\int_0^{2\pi}\sum_{i=1}^{2}\left[\sum_{n=-N(\theta)}^{N(\theta)} b_n c_n^M\left\{\sum_{m=0}^{M}\frac{m!}{(\beta_i c_n)^{m+1}} + e^{-\beta_i c_n}\int_{-\beta_i c_n}^{\infty}\frac{e^{-t}}{t}dt\right\}\right.$$
$$\left. + \sum_{j=1}^{L-M}\left[\left(\sum_{n=-N(\theta)}^{N(\theta)}\frac{b_n}{c_n^{j+1}}\right) - \frac{1}{j!}\frac{\partial^j p(k,\theta)}{\partial k^j}_{|k=0}\right]\frac{(M+j)!}{\beta_i^{M+j+1}}\right]$$
$$\times\frac{\partial^{M_1}\beta_i}{\partial a^{M_1}}\frac{\partial^{M_2}\beta_i}{\partial b^{M_2}}\frac{\partial^{M_3}\beta_i}{\partial c^{M_3}}d\theta,$$

where $M = M_1 + M_2 + M_3$ and the derivatives of β_i are:

$$\frac{\partial^{M_1}\beta_1}{\partial a^{M_1}} = \frac{\partial^{M_1}\beta_2}{\partial a^{M_1}} = [i\cos(\theta+\alpha)]^{M_1}$$
$$\frac{\partial^{M_2}\beta_1}{\partial b^{M_2}} = \frac{\partial^{M_2}\beta_2}{\partial b^{M_2}} = [i\sin(\theta+\alpha)]^{M_2}$$
$$\frac{\partial^{M_3}\beta_1}{\partial c^{M_3}} = (-1)^{M_3}$$
$$\frac{\partial^{M_3}\beta_2}{\partial c^{M_3}} = 1.$$

For the second alternative method we look at the integral parts of $G^A_{Alt.2}$:

$$\begin{aligned} G_1 &= -2\int_0^{\sigma_3} \frac{C^{(0)}(k)\cosh k(z+h)e^{-kh}}{\cosh kh} g_0^{(0,0)}(k)dk \qquad \text{(B.38)} \\ &\quad -2\int_0^{\sigma_1} C^{(0)}(k)F(k)[g_0^{(0,0)}(k) + 2\sum_{n=1}^{\infty}(i\rho_{s_1})^n g_n^{(0,0)}(k)]dk \\ &\quad +2\int_{\sigma_1}^{\sigma_3} C^{(0)}(k)F(k)[g_0^{(0,0)}(k) + 2\sum_{n=1}^{\infty}(i\rho_{s_2})^n g_n^{(0,0)}(k)]dk \\ &\quad +\frac{1}{2\pi}\int_0^{2\pi} e^{-\beta\sigma_3}\left[\frac{1}{\beta}\frac{1+2\tau\cos\theta}{1-2\tau\cos\theta} + \frac{2\nu}{(1-2\tau\cos\theta)^2} G[\beta(\sigma_3 - \frac{\nu}{1-2\tau\cos\theta})]\right] d\theta \end{aligned}$$

The derivatives satisfy

$$\begin{aligned} \frac{\partial^{(M_1+M_2+M_3)}G_1}{\partial a^{M_1}\partial b^{M_2}\partial c^{M_3}} &= -2\int_0^{\sigma_3} \frac{k^{(M_1+M_2+M_3)}}{2^{(M_1+M2)}} \frac{C^{(M_3)}(k)\cosh k(z+h)e^{-kh}}{\cosh kh} g_0^{(M_1,M_2)}(k)dk \qquad \text{(B.39)} \\ &\quad -2\int_0^{\sigma_1} \frac{k^{(M_1+M_2+M_3)}}{2^{(M_1+M2)}} C^{(M_3)}(k)F(k)[g_0^{(M_1,M_2)}(k) + 2\sum_{n=1}^{\infty}(i\rho_{s_1})^n g_n^{(M_1,M_2)}(k)]dk \\ &\quad +2\int_{\sigma_1}^{\sigma_3} \frac{k^{(M_1+M_2+M_3)}}{2^{(M_1+M2)}} C^{(M_3)}(k)F(k)[g_0^{(M_1,M_2)}(k) + 2\sum_{n=1}^{\infty}(i\rho_{s_2})^n g_n^{(M_1,M_2)}(k)]dk \\ &\quad +\frac{1}{2\pi}\int_0^{2\pi} e^{-\beta\sigma_3}\left\{\frac{2\nu}{(1-2\tau\cos\theta)^2}\left[\left(\frac{\nu}{1-2\tau\cos\theta}\right)^M G[\beta(\sigma_3 - \frac{\nu}{1-2\tau\cos\theta})]\right.\right. \\ &\qquad \left. + \sum_{m=1}^{M}\left(\frac{\sigma_3}{\beta}\right)^m \sum_{l=m}^{M}\frac{(l-1)!}{(l-m)!}\left(\frac{\nu}{\sigma_3(1-2\tau\cos\theta)}\right)^{M-l}\right] \\ &\quad \left. + \frac{1+2\tau\cos\theta}{1-2\tau\cos\theta} M!\sum_{m=0}^{M}\frac{\sigma_3^{M-m}}{\beta^{m+1}}\frac{1}{(M-m)!}\right\}[i\cos(\theta+\alpha)]^{M_1}[i\sin(\theta+\alpha)]^{M_2}(-1)^{M_3}d\theta \end{aligned}$$

where

$$\begin{aligned} \beta &= -[c+z+ir\cos(\theta+u-\alpha)] \\ F(k) &= \frac{k\cosh k(z+h)}{\cosh^2 kh\sqrt{(k\tanh kh-\nu)^2 - 4\tau^2k^2}} \\ \rho_{s_1} &= \frac{k\tanh kh - \nu + \sqrt{(k\tanh kh-\nu)^2-4\tau^2k^2}}{2\tau k} \\ \rho_{s_2} &= \frac{k\tanh kh - \nu - \sqrt{(k\tanh kh-\nu)^2-4\tau^2k^2}}{2\tau k} \end{aligned}$$

$$C^{M_3}(k) = \begin{cases} \cosh k(c+h) & \text{if } M_3 = 0,2,4,6 \\ \sinh k(c+h) & \text{if } M_3 = 1,3,5 \end{cases},$$

and introducing the short forms

$$gco(n,m) = J_{n+m}(kr)\cos[n\alpha - (n+m)u]$$
$$gsi(n,m) = J_{n+m}(kr)\sin[n\alpha - (n+m)u],$$

we find

$$\begin{aligned}
g_n^{(0,0)}(k) &= gco(n,0)\\
g_n^{(1,0)}(k) &= gco(n,-1) - gco(n,1)\\
g_n^{(0,1)}(k) &= gsi(n,-1) - gsi(n,1)\\
g_n^{(2,0)}(k) &= gco(n,-2) - 2gco(n,0) + gco(n,2)\\
g_n^{(1,1)}(k) &= gsi(n,-2) - gsi(n,2)\\
g_n^{(0,2)}(k) &= -gco(n,-2) - 2gco(n,0) - gco(n,2)\\
g_n^{(3,0)}(k) &= gco(n,-3) - 3gco(n,-1) + 3gco(n,1) + gco(n,3)\\
g_n^{(2,1)}(k) &= gsi(n,-3) - gsi(n,-1) + gsi(n,1) + gsi(n,3)\\
g_n^{(1,2)}(k) &= -gco(n,-3) - gco(n,-1) + gco(n,1) + gco(n,3)\\
g_n^{(0,3)}(k) &= -gsi(n,-3) - 3gsi(n,-1) - 3gsi(n,1) - gsi(n,3)\\
g_n^{(4,0)}(k) &= -gco(n,-4) - 4gco(n,-2) + 6gco(n,0) - 4gco(n,2)\\
&\quad +gco(n,4)\\
g_n^{(3,1)}(k) &= gsi(n,-4) - 2gsi(n,-2) + 2gsi(n,2) - gsi(n,4)\\
g_n^{(2,2)}(k) &= -gco(n,-4) + 2gco(n,0) - gco(n,4)\\
g_n^{(1,3)}(k) &= -gsi(n,-4) - 2gsi(n,-2) + gsi(n,2) + gsi(n,4)\\
g_n^{(0,4)}(k) &= gco(n,-4) + 4gco(n,-2) + 6gco(n,0) + 4gco(n,2)\\
&\quad +gco(n,4)\\
g_n^{(5,0)}(k) &= gco(n,-5) - 5gco(n,-3) + 10gco(n,-1) - 10gco(n,1)\\
&\quad +5gco(n,3) - gco(n,5)\\
g_n^{(4,1)}(k) &= gsi(n,-5) - 3gsi(n,-3) + 2gsi(n,-1) + 2gsi(n,1)\\
&\quad -3gsi(n,3) + gsi(n,5)\\
g_n^{(3,2)}(k) &= -gco(n,-5) + gco(n,-3) + 2gco(n,-1) - 2gco(n,1)\\
&\quad -gco(n,3) + gco(n,5)\\
g_n^{(2,3)}(k) &= -gsi(n,-5) - gsi(n,-3) + 2gsi(n,-1) + 2gsi(n,1)\\
&\quad -gsi(n,3) - gsi(n,5)\\
g_n^{(1,4)}(k) &= gco(n,-5) + 3gco(n,-3) + 2gco(n,-1) - 2gco(n,1)\\
&\quad -3gco(n,3) - gco(n,5)\\
g_n^{(0,5)}(k) &= gsi(n,-5) - 5gsi(n,-3) + 10gsi(n,-1) - 10gsi(n,1)\\
&\quad +5gsi(n,3) - gsi(n,5)\\
g_n^{(6,0)}(k) &= gco(n,-6) - 6gco(n,-4) + 15gco(n,-2) - 20gco(n,0)\\
&\quad +15gco(n,2) - 6gco(n,4) + gco(n,6)
\end{aligned}$$

$$
\begin{aligned}
g_n^{(5,1)}(k) &= gsi(n,-6) - 4gsi(n,-4) + 5gsi(n,-2) - 5gsi(n,2) \\
&\quad +4gsi(n,4) - gsi(n,6) \\
g_n^{(4,2)}(k) &= -gco(n,-6) + 2gco(n,-4) + gco(n,-2) - 4gco(n,0) \\
&\quad +gco(n,2) + 2gco(n,4) - gco(n,6) \\
g_n^{(3,3)}(k) &= -gsi(n,-6) + 3gsi(n,-2) - 3gsi(n,2) + gsi(n,6) \\
g_n^{(2,4)}(k) &= gco(n,-6) + gco(n,-4) + gco(n,-2) - 4gco(n,0) \\
&\quad -gco(n,2) + gco(n,4) + gco(n,6) \\
g_n^{(1,5)}(k) &= gsi(n,-6) + 4gsi(n,-4) + 5gsi(n,-2) - 5gsi(n,2) \\
&\quad -4gsi(n,4) - gsi(n,6) \\
g_n^{(0,6)}(k) &= -gco(n,-6) - 6gco(n,-4) - 15gco(n,-2) - 20gco(n,0) \\
&\quad -15gco(n,2) - 6gco(n,4) - gco(n,6).
\end{aligned}
$$

B.6 Green's function in terms of non dimensional parameters

(ref.pg. 36)
To better see what parameters are important in the numerical evaluation, we express the Green's function in terms of non-dimensional parameters:

$$
\begin{aligned}
G_1 &= \frac{\nu}{\pi}\int_0^{2\pi}\int_0^{\infty} e^{iKR\cos(\theta-u+\alpha)}e^{-KH}\cosh K(Z+H)\cosh K(C+H) \\
&\quad \times \frac{[K(1+2\tau\cos\theta)+1]}{K\sinh KH - [1+2\tau\cos\theta K - \overline{\mu i}(1+\tau K\cos\theta)]\cosh KH} dK\,d\theta,
\end{aligned} \tag{B.40}
$$

and the new non-dimensional parameters are:

$$
\begin{array}{llll}
K = k/\nu & Z = z\nu & C = c\nu \\
R = r\nu & H = h\nu & \overline{\mu} = \frac{\mu}{\omega}
\end{array}
$$

The integral part of $G_{Alt.2}$ is then

$$
\begin{aligned}
G_1 &= -2\nu\int_0^{\Sigma_3} \frac{\cosh K(Z+H)\cosh K(C+H)e^{-KH}}{\cosh KH} J_0(KR)dK \\
&\quad -2\nu\int_0^{\Sigma_2} F(K)[J_0(KR) + 2\sum_{n=1}^{\infty}(i\Gamma_{s_1})^n J_n(KR)\cos n(\alpha-u)]dK \\
&\quad +2\nu\int_{\Sigma_2}^{\Sigma_3} F(K)[J_0(KR) + 2\sum_{n=1}^{\infty}(i\Gamma_{s_2})^n J_n(KR)\cos n(\alpha-u)]dK \\
&\quad +\frac{\nu}{2\pi}\int_0^{2\pi}\left[\frac{1}{B}\frac{1+2\tau\cos\theta}{1-2\tau\cos\theta}e^{-B\Sigma_3} + e^{-B\Sigma_3}\frac{2}{(1-2\tau\cos\theta)^2}G[B(\Sigma_3 - \frac{1}{1-2\tau\cos\theta})]\right]d\theta,
\end{aligned} \tag{B.41}
$$

where $B = -[Z+C+iR\cos(\theta-u+\alpha)]$ and $G[B(\Sigma_3-\frac{1}{1-2\tau\cos\theta})]$ is $e^{[B(\Sigma_3-\frac{1}{1-2\tau\cos\theta})]}E_1[\beta(\Sigma_3-\frac{1}{1-2\tau\cos\theta})]$, and

$$
\begin{aligned}
F(K) &= \frac{K\cosh K(Z+H)\cosh K(C+H)}{\cosh^2 KH\sqrt{(K\tanh KH-1)^2-4\tau^2K^2}} \\
\Gamma_{s_1} &= \frac{K\tanh KH-1+\sqrt{(K\tanh KH-1)^2-4\tau^2K^2}}{2\tau K} \\
\Gamma_{s_2} &= \frac{K\tanh KH-1-\sqrt{(K\tanh KH-1)^2-4\tau^2K^2}}{2\tau K},
\end{aligned}
$$

and Σ_1 and Σ_2 are given by the equations

$$
\begin{aligned}
\Sigma_1\tanh\Sigma_1 H-1 &= -2\tau\Sigma_1 \\
\Sigma_2\tanh\Sigma_2 h-1 &= 2\tau\Sigma_2.
\end{aligned}
$$

The integral part of $G_{Alt.1}$ may be written

$$
\begin{aligned}
G_1 &= -\frac{\nu}{\sqrt{C^2+R^2}}-\frac{\nu}{\sqrt{(2H+C)^2+R^2}} \\
&\quad +\frac{\nu}{2\pi}\int_0^{2\pi}\sum_{n=-\infty}^{\infty}Res_n\sum_{i=1}^{2}\left\{\frac{1}{C_nB_i}+e^{-B_iC_n}\int_{-B_iC_n}^{\infty}\frac{e^{-t}}{t}dt\right\}d\theta
\end{aligned}
\tag{B.42}
$$

where

$$B_1 = -C - iR\cos(\theta - u + \alpha)$$

$$B_2 = 2H + C - iR\cos(\theta - u + \alpha)$$

$$Res_n = \frac{C_n^2 e^{C_nH}\cosh C_n(Z+H)}{C_n^2H+\cosh^2 C_nH}.$$

and the C_n's are given by

$$[1+2\tau\cos\theta C_n-\overline{\mu}i(1+\tau\cos\theta C_n)]\cosh C_nH = C_n\sinh C_nH. \tag{B.43}$$

PREVIOUS DR.ING. THESES

Department of Marine Hydrodynamics

Løtveit, Magne	:	A Study of Pressure- and Velocity Relations in the Slip-Stream of Propellers of Single Screw Ships to clarify the Propeller Action behind the Hull. 1963. (in Norwegian)
Dahle, Emil Aall	:	A Study of the Coefficients in the Differential Equations for the Rolling Motion of a Vessel. 1971. (in Norwegian)
Langfeldt, Jan N.	:	A Theoretical and Experimental Study of the Feasibility of Two-Phase (Gas-Water) Jet Propulsion of Craft. 1972.
Berg, Tor Einar	:	Manoeuvring of Vessels. 1978. (in Norwegian)
Skjærdal, Svein O.	:	Wave Induced Oscillations of Ship Hulls. 1978.
Nielsen, Finn G.	:	Hydrodynamic Relations of Oil Booms. 1980.
Liapis, Nicolas	:	Hydrodynamic Analysis of the Ship-Buoy System. 1980.
Pettersen, Bjørnar	:	Calculation of Potential Flow about Ship Hulls in Shallow Water with Particular Application to Manoeuvring. 1980.
Rye, Henrik	:	Ocean Wave Groups. 1981.
Utnes, Torbjørn H.	:	Forward-Speed Effects on the Hydrodynamic Motion Coefficients of a Surface-Piercing Body. 1982
Børresen, Rolf	:	The unified theory of ship motions in water of finite depth. 1984.
Aarsnes, Jan Vidar	:	Current Forces on Ships. 1984.
Skomedal, Nere	:	Application of a Vortex Tracking Method to Three-Dimensional Flow Past Lifting Surfaces and Blunt Bodies. 1985.
Løken, Arne Edvin	:	Three-dimensionl second order hydrodynamic effects on ocean structures in waves. 1986.
Aanesland, Vidar	:	A Theoretical and Numerical Study of Ship Wave Resistance. 1986.
Sortland, Bjørn	:	Force Measurements in Oscillating Flow on Ship Sections and Circular Cylinders in a U-Tube Water Tank. 1986.
Falch, Sigurd	:	A numerical study of slamming of two-dimensional bodies. 1986.
Lian, Walter	:	A numerical study of two-dimensional separated flow past bluff bodies at moderate KC-numbers. 1986.
Braathen, Arne	:	Application of a vortex tracking method to the prediction of roll damping of a two-dimensional floating body. 1987.

Gang Miao	:	Hydrodynamic Forces and Dynamic Responses of Circular Cylinders in Wave Zones. 1989.
Greenhow, Martin	:	Linear and Non-Linear Studies of Waves and Floating Bodies. Part I and Part II. 1989.
Chang Li	:	Force Coefficients of Spheres and Cubes in Oscillatory Flow with and without Current. 1989.
Jæger, Arild	:	Seakeeping, Dynamic Stability and Performance of a Wedge Shaped Planing Hull. 1989.
Hoff, Jan Roger	:	Three-dimensional Green function of a vessel with forward speed in waves. 1990.
Rong Zhao	:	Slow-Drift of a Moored Two-Dimensional Body in Irregular Waves. 1990.
Løland, Geir	:	Current Forces and Flow through Fish Farms. 1991.
Krokstad, Jørgen R.	:	Second-order Loads in Multidirectional Seas. 1991.
Mørch, Hans J. B.	:	Aspects of Hydrofoil Design; with Emphasis on Hydrofoil Interaction in Calm Water. 1992.
Steen, Sverre	:	Cobblestone Effect on SES. 1993.
Kvålsvold, Jan	:	Hydroelastic Modelling of Wetdeck Slamming on Multihull Vessels. 1994.
Ulstein, Tore	:	Nonlinear Effects of a Flexible Stern Seal Bag on Cobblestone Oscillations of an SES. 1995.
Solaas, Frøydis	:	Analytical and Numerical Studies of Sloshing in Tanks. 1995.
Herfjord, Kjell	:	A Study of Two-dimensional Separated Flow by a Combination of the Finite Element Method and Navier-Stokes Equations. 1996.